Failure of CPVC Pipes – Study of Mechanical Properties

by

Bingjun Chen

A thesis submitted in partial fulfillment of the requirements for the degree of

Master of Science

Department of Mechanical Engineering

University of Alberta

Abstract

Premature failure occurred in the chlorinated polyvinyl chloride (CPVC) pipes from manufacturer A at the solvent-welded joints, while pipes from manufacturer B work normally under similar working conditions. Through characterization of mechanical properties and residual stresses in CPVC pipes this thesis seeks to test two hypotheses for pipe failure: (1) primer used in the solvent welding process, and (2) possible differences in mechanical properties between the two brands of CPVC pipes.

Firstly, the effects of primer on the mechanical properties of CPVC pipe material were studied through D-split tensile testing on three types of coupon specimens: round notched pipe ring (NPR) with notch radii ranging from 1 mm to 3.18 mm, flat NPR specimens, and ring specimens. All tests were conducted after 1-min exposure to primer and a half day of drying. Results show that exposure to primer deteriorates the mechanical properties of CPVC pipe material, with the main effect on reducing the material ductility, of which the extent of decrease is related to the specimen geometry and notch radius. To further investigate the changes of the CPVC pipe material in terms of drying time, mechanical properties, cross sectional surface morphology and fracture behavior of ring specimens were examined after 30-min exposure to primer, followed by eight different periods of drying time, ranging from a half-day to 113 days. Results show that the exposure to primer caused swelling of the cross section and generated a core-shell structure. The results also show that both the material strength and ductility decreased after exposure to primer. Although the drying process can recover some of the strength, up to 63% of the virgin material, ductility remains low, of at least 57% reduction from the virgin material. Fractography analysis indicates that the permanent loss of ductility is due to multiple sites

for crack initiation along the border between the core and shell regions.

Distribution of residual hoop stress in 2-inch CPVC pipe was characterized by the slit-one-ring method. The results suggest that the commercial CPVC pipes contain a noticeable level of residual stress, with the maximum tensile residual stress above 2 MPa on the pipe inner surface. In addition, a refined slit-one-ring method was proposed to estimate the residual stress distribution on the cross section with core-shell structure that has different mechanical properties. Finite element simulation, by introducing a temperature field in the model, was conducted to simulate the diametral deformation of the slit-ring due to the release of residual stress. Good agreement was found between the analytical and simulation results. The refined slit-ring method was then employed to study the effect of primer on residual stress in CPVC pipes that have been dried in air for different lengths of time. The results suggest that residual hoop stress was decreased by the exposure to primer, with the variation of residual stress with drying time mainly occurring within the first 30 days.

Finally, the mechanical properties and residual hoop stresses of CPVC pipes with different nominal pipe size (NPS), from two manufacturers, were characterized and compared. Though mechanical strength and Young's modulus are quite consistent among different types of CPVC pipes, material ductility decreases significantly after being in service for a long time, suggesting that strain-based criteria should be considered in the specification of CPVC pipes, in addition to results from the stress-based standard tests. Higher levels of residual stress were found in CPVC pipes from one specific manufacturer, which is believed to be caused by the cooling rate used in the manufacturing process.

The thesis concludes that exposure to primer weakens the mechanical properties of CPVC pipe material, with the main effect on the permanent loss of ductility. Therefore, primer should be carefully applied to CPVC pipe to avoid unnecessary contact with pipe surfaces, especially if surfaces will not be covered by cement. On the other hand, the main differences in mechanical properties among commercial CPVC pipes from different manufacturers are material ductility and residual hoop stress. It is suggested that ductility and residual hoop stress in both CPVC pipes and their joints should properly be characterized to ensure their satisfactory long-term performance.

Preface

This thesis is an original work by Bingjun Chen under the supervision of Professors P.-Y. Ben Jar and Pierre Mertiny. The main body of the thesis is composed of one published conference paper, one paper being considered for publication in *Journal of Pressure Vessel Technology*, and two manuscripts to be submitted to technical journals later.

Chapter 2 is based on the conference paper published in ANTEC proceedings: B. Chen, P.-Y. Ben Jar, P. Mertiny and R. Prybysh, 2018, "Effects of primer on mechanical behavior of CPVC pipe" , SPE, ANTEC 2018, Orlando, USA. I was responsible for data collection and analysis and all of the experimental work, as well as the manuscript composition. Drs. Jar and Mertiny were the supervisory authors and involved in the experimental design and manuscript editing. Mr. Prybysh provided the test materials.

Chapter 3 is based on one paper submitted to *Journal of Pressure Vessel Technology*: B. Chen, P.-Y. Ben Jar, P. Mertiny and R. Prybysh, 2018, "Ductility loss of CPVC pipe material due to exposure to primer". I was responsible for data collection and experimental work, as well as the manuscript composition. Drs. Jar and Mertiny were the supervisory authors and involved in the experimental design and manuscript editing. Mr. Prybysh assisted with preparation of materials used for the testing.

Chapter 4 is based on one paper to be submitted to a technical journal later: B. Chen, P.-Y. Ben Jar, P. Mertiny and R. Prybysh, 2018, "A refined one-slit-ring method to quantify residual hoop stress in CPVC pipe – application to specimens after immersion in primer". I was responsible for data collection and analysis and all of the experimental and

simulation work, as well as the manuscript composition. Drs. Jar and Mertiny were the supervisory authors and involved in the experimental design and manuscript editing. Mr. Prybysh assisted with the materials preparation.

Chapter 5 is based on one manuscript to be submitted to a technical journal later: B. Chen, P.-Y. Ben Jar, P. Mertiny and R. Prybysh, 2018. "Characterization of mechanical properties and residual stress of CPVC pipes." I was responsible for all the experimental and simulation work, as well as the data collection, analysis and the manuscript composition. Drs. Jar and Mertiny were the supervisory authors and involved in the experimental design and manuscript editing. Mr. Prybysh assisted with the materials preparation.

Acknowledgement

After an intensive period of two years, today is the day. I really appreciate what I have learned during my graduate study, not only in the scientific arena, but also on a personal level. Having the graduate study overseas has had a profound influence on me. And I would like to express my sincere appreciation to individuals and organizations that have supported and helped me so much throughout this period.

I would first like to thank my supervisor Dr. Jar for his expertise and invaluable guidance through my master's study. I would not have acquired so much without his inspiration and encouragement. I would like to thank my co-supervisor Dr. Mertiny for his support on my project and I really appreciate those occasional group activities. I would also like to extend my thanks to Mr. Prybysh for providing the test materials, to Mr. Faulkner for fabrication of the extensometers and machine shop staff Mr. Marchand, Mr. Mooney, Mr. Campbell, Mr. Bubenko and Mr. Maccagno for machinery training and specimen preparation.

This project would have been impossible without the support of Master's Recruitment Scholarship and Engineered Air Endowment Fund at University of Alberta, as well as the Mitacs Globalink Fellowship.

My thanks and appreciation also go to all the friends I meet at University of Alberta, without their companion, I would not be able to overcome the difficulties during my graduate life. Last but not the least, I would like to express my deep gratitude to my parents and sister for their unconditional love and support, and Yingtao for his unlimited encouragement.

Table of contents

List of tables

List of figures

Nomenclature

A_{shell}	Cross section area of the shell region, m^2
A_{total}	Area of the overall cross section, m^2
a	Thickness of the shell region, mm
C_1, C_2, C_{A1}, C_{A2}, C_{C1}, C_{C2}, C_{i1}, C_{i2}, C_{o1}, C_{o2}, C_{co1}, C_{co2}	Coefficients of the residual hoop stress distribution
D_o	Original outer diameter of the pipe, mm
D	Outer diameter of the pipe ring specimen, mm
E	Young's modulus, MPa
E_c	Young's modulus of the core region, MPa
E_s	Young's modulus of the shell region, MPa
F	Load recorded by the tensile machine, N
F_t	Total force applied to specimen at S=4.15 mm, N
i, o	Number of layers removed
k	Exponent in the expression for residual stress distribution
l_1, l_2, l_3, l_4	Dimension of the core-shell structure, mm
M, M_t, M_w	Bending moment, N·mm
N	Constant in the expression for temperature field
r, r_1, r_2, r_3, r_4, r_{1d}, r_{2d}, r_{3d}, r_{4d}	Radii of different layers, mm
R, R_d, R_w, R_{wd}, R'_{wd}	Radii of the neutral planes, mm
S	Stroke, mm
t, h	Wall thickness, mm
t_f	Final wall thickness measured by extensometer, mm

t_o , h_o	Original wall thickness, mm
W	Width of specimen, mm
W_f	Final width measured by extensometer, mm
W_o	Original specimen width, mm
x	Relative coordinate
x_1, x_2	Normalized location of the interfaces
x_n , $x_n^{'}$	Normalized neutral position
ΔD	Diametrical change, mm
$\Delta\theta$	Change of the central angle, radian
ε_{area}	Area strain
ε_m	Maximum measured area strain
θ	Original central angle, radian
ν	Poisson's ratio
σ_{core}	Engineering stress in the core region, MPa
σ_{eng}	Engineering stress, MPa
σ_{res}	Residual hoop stress, MPa
σ_{shell}	Engineering stress in the shell region, MPa
σ_{true}	True stress, MPa
AASHTO	American Association of State Highway and Transportation Officials
ABS	Acrylonitrile-butadiene-styrene
ASTM	American Society for Testing and Materials
CPVC	Chlorinated polyvinyl chloride
EDS	Energy dispersive spectroscopic

EPDM	Ethylene propylene diene monomer
ESC	Environmental stress cracking
FE	Finite element
HDB	Hydrostatic design basis
LTHS	Long-term hydrostatic strength
MDPE	Medium-density polyethylene
MEK	Methyl ethyl ketone
NPR	Notched pipe ring
NPS	Nominal pipe size
PDB	Pressure design basis
PE	Polyethylene
PMMA	Poly(methyl methacrylate)
PP	Polypropylene
PVC	Polyvinyl chloride
SAZ	Solvent-affected zone
SCG	Slow crack growth
SEM	Scanning electron microscope
THF	Tetrahydrofuran
UV	Ultraviolet

Chapter 1: Introduction

1.1 Background and motivation

Chlorinated polyvinyl chloride (CPVC) pipes have widely been used due to their good mechanical properties, easy installation and low cost [1, 2]. CPVC is a variant of polyvinyl chloride (PVC) that is produced by reacting suspension PVC resin with chlorine using either high heat or ultraviolet (UV) radiation [3]. The effect of adding more chlorine to the PVC, from 57% to 63%-68%, is to raise the glass transition temperature of the base resin from about 90℃ to 115-135℃ [4, 5]. CPVC produced in this manner has the same good mechanical properties of PVC and retains them at significantly higher temperature, therefore CPVC pipe is suitable for hot water transportation [6, 7]. Though well-known for low failure rates [8], PVC and CPVC pipes still fail occasionally within the design lifetime, and it is therefore important to conduct failure analysis to prevent the unpredicted failure.

This thesis presents a study of CPVC pipe failure based on a real case, in terms of mechanical properties. There were two buildings that use CPVC pipes for hot water service. Each building was built with a similar system with CPVC pipes from different manufacturers, namely, building 1 used pipes from manufacturer A while building 2 used pipes from manufacturer B. Around 10 years after pipe installation, severe failure started in building 1, causing considerable economic loss, but not in the other building. The manufacturers identified the failures as being an installation issue, caused by exposure to excessive solvent during the solvent welding process. But the observation that the entire building has problems with all the pipes would suggest it is more than some bad joints.

Failed parts were received from that building and carefully examined. Cracks were

found on the inner surfaces of CPVC pipes. Figure 1.1 shows some examples of cracks observed from the examination.

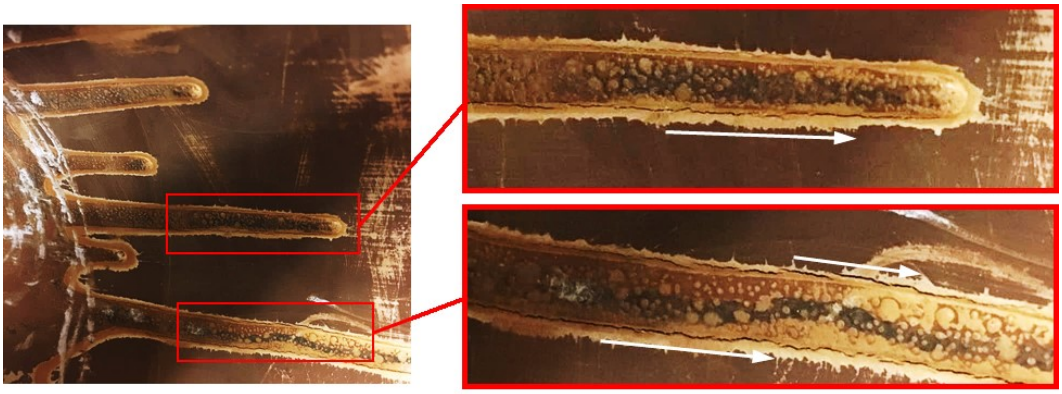

(a) Solvent flow (b) Cracks

Fig. 1.1 Solvent dribbles on inner surfaces of CPVC pipe with cracks found around the outer edge of the dribbles

Figure 1.1 shows clearly that cracks are located within the areas covered by solvents and close to the outer edge of the dribbles. Solvent welding is the most popular joining method for CPVC pipes, which involves the application of primer to soften the pipe surfaces and solvent cement with dissolved polymers to fill the gap between pipe fittings. It is because of the amorphous morphology of CPVC polymer that makes the pipes easy to be joined by solvent welding, but the relatively large free volume in the amorphous morphology also makes CPVC pipes more likely to be attacked by solvents than semi-crystallized polymers [9]. Premature failure of CPVC pipes at the solvent welded joints has been reported and the solvents used in the solvent welding process have been suspected to be responsible for leakage [10, 11]. Besides, it is suggested that primer used for solvent welding may lead to environmental stress cracking (ESC) of CPVC piping systems, especially when temperatures are below 0^{o}C [12], though the relevant mechanism

is yet to be fully understood. Thus, it is necessary to study the possible effects of solvents used for pipe installation on the mechanical behaviors of CPVC pipes, and most importantly, to understand the mechanisms responsible for the ESC in order to prevent future failures.

Since not all pipes but only those produced by manufacturer A failed prematurely, it is a possibility that certain differences exist between pipe products produced by the two manufacturers. Although all pipes passed the standard tests, it is conceivable that the standard test results do not appropriately reflect long-term performance of CPVC pipes. It is also possible that material degradation occurred during service [13, 14]. Based on the above speculations, it is worth comparing fundamental mechanical properties of those two brands of CPVC pipes. In addition, it is well-known that residual stress, originating from a non-uniform cooling process, exists in extruded pipes, which may also play an important role in the long-term performance of plastic pipes [15–18]. The evaluation of residual stress and effects thereof on the estimated lifetime of polyethylene (PE) pipes [19–22] have been widely studied. However, research on the same topic for PVC pipes [23, 24] is limited, and even less for CPVC pipes.

The present study focuses on the mechanical properties of CPVC pipe, in order to understand their roles on premature pipe failure, including characterization of tensile properties and residual stress of CPVC pipes, and discussion of the effects of the primer used in the solvent welding process on the mechanical properties.

1.2 Failure analysis of PVC and CPVC pipes

PVC and CPVC pipes are one of the most popular thermoplastic pipe materials and

have been successfully used for decades [10]. Compared to metallic piping, PVC and CPVC materials offer significant advantages including ease of installation and very low failure rates. However, as with all plumbing products, including metal piping, PVC or CPVC pipe may fail occasionally [25, 26].

Unexpected failures may be caused by a number of factors, such as improper system installation [10, 27], inappropriate operation, external and internal contamination, manufacturing defects, resin defects, abuse by distributor, and so on. Overall, as summarized by Priddy [10], improper installation is generally regarded as the most common cause when PVC and CPVC pipes fail. Bad joints may occur due to either excessive cement or insufficient cement, with the former causing swelling, reducing the load-carrying capacity of pipe and leading to final blowout, and the latter usually resulting in leakage. In addition to that, failure can be caused by contact of CPVC pipes with other materials that contain non-compatible plasticizers [28], such as various antifreezes, cleaners, sealants, caulks, spray on coatings, etc. Moreover, extensive crazing in PVC and CPVC pipes can be resulted from residual stress, creating weak points and increasing their vulnerability to ESC [10].

Failure analysis of PVC and CPVC piping material has also been studied by Knight [29], with particular emphasis on cracking phenomena. Four modes of failure, including softening, degradation, erosion, and cracking were discussed. Parts failed by softening usually have swollen or distorted appearance, which may be caused by a temperature or stress condition in excess of the recommended values, or the absorption of solvents or plasticizers. Degradation of PVC or CPVC pipe material occurs when excessively exposed to high heat, UV or strong chemicals, alternating or destroying the

vinyl resin or other compounding ingredients. Merah et al. [30, 31] studied the effect of both natural and artificial weathering on CPVC pipe materials and found that tensile strain at break or fracture strain was decreased most significantly among all tensile properties. Knight [29] also implied three main possible forms of fracture in PVC and CPVC pipes, which include ESC featured with smooth and glassy fracture surface, brittle fracture identified by typically smooth and dull appearance, as well as ductile fracture characterized by rough and dull surface and possible stress whitening. Knight [29] also provided the analysis on crack propagation to identify the crack initiation site and determine the reasons for failures of PVC and CPVC piping material.

Hauser [32] investigated the effects of single and of mixed glycols causing ESC of CPVC pipes by four different manufacturers from two different resin suppliers. The results show that a mixture of ethylene glycol and propylene glycol is more detrimental to CPVC pipes than either of the glycols by itself in the same relative concentration in water. Though all CPVC resins are not created equal, it was concluded that all commercial CPVC pipes must be considered to be at risk when exposed to the wrong chemicals and mixture thereof. Scott et al. [33] examined a premature failure of an unplasticized PVC sewer after 34 years of use and revealed that failure initiated at an inherent defect in the pipe wall that was attributed to the original manufacture.

Overall, premature failure in PVC and CPVC pipes can result from quite a few reasons, and it is important to study the corresponding mechanisms in order to prevent future failures. Compared with traditional water pipeline materials, such as cast iron and asbestos cement, PVC and CPVC piping materials are much newer, thus only limited historical failure data are available for reference during the failure diagnosis [23, 34], which increases

the difficulty to conduct a failure analysis [35].

1.3 Literature review on PVC and CPVC pipes

This section reviews studies on PVC and CPVC pipes, with respect to two parts: (1) popular joining methods for PVC and CPVC pipes, and (2) mechanical properties characterization of PVC and CPVC pipe material inclusive of tensile properties and residual stresses.

1.3.1 Joining methods

Joining methods of thermoplastic pipes can generally be categorized into nonpermanent joining and permanent joining [36]. Nonpermanent-joint techniques often create joints that can be disassembled through mechanical couples, including threading, flanging, bell-ring-gasket joint, compression-insert joint and grooved-end mechanical joints, etc. The biggest disadvantage of these methods is the low resistance to leakage, which limits their applications when good sealing is required. On the other hand, permanent joints usually provide much better leak resistance than nonpermanent joining methods [36, 37]. Two methods most widely used to form permanent joints in thermoplastic pipes are solvent welding and heat fusion.

The principle of heat fusion joining is to heat two prepared surfaces to a designated temperature until they soften, then fuse them together by application of a sufficient force [38]. Two basic types of heat fusion joints are butt fusion joint and socket fusion joint. Heat fusion is usually used in PE [39], polypropylene (PP) and polybutylene piping systems [36]. PVC pipes can also be heat-fused, but mainly in fields such as trenchless construction and rehabilitation [37].

Solvent welding, on the other hand, is the most popular joining method for PVC and CPVC pipes. During the joining process, primer [40] is first applied to soften and dissolve part of the pipe surfaces so that mobile polymer chains in the wet and semi fluidic layers can diffuse across the joint surfaces. Then solvent cement with dissolved polymer [41] is applied to fill the gap between the pipe and the fittings [2, 9, 42]. The typical thickness of the solvent-affected zone (SAZ) on either side of the weld by solvent welding is in the range of 50-500 μm [43]. It is said that the joint strength develops with the full evaporation of the solvents [1]. Work in literature indicates that after the primer is fully evaporated, strength in the welded region can reach up to 70% of the parent material [1].

Primer used in the solvent welding process is a blend of solvents, usually including methyl ethyl ketone (MEK), acetone, cyclohexanone and tetrahydrofuran (THF). As required by the ASTM standard F656 [40], a suitable primer for solvent welding of PVC or CPVC pipes should have the ability to dissolve at least 10 wt% of PVC or CPVC resin at room temperature within one hour. On the other hand, the cement should be able to dissolve an additional 3 wt% of PVC or CPVC compound or the equivalent PVC or CPVC resin at room temperature without evidence of gelation [41, 44]. Note that except for at least 10 wt% of CPVC resin, commercial cement for CPVC pipes generally contains solvents similar to those in the primer, such as THF and cyclohexanone, in order to meet the specific requirements [41, 45].

Solvent welding is a simple and inexpensive joining process for PVC and CPVC pipes that can produce durable and hermetic joints. Compared with those non-permanent joining techniques with additional mechanical components, the joint by solvent welding has the advantages of being light in weight, and low in cost. However, it is indicated that some

residual solvents usually remain in the SAZ [43]. Titow et al. [46, 47] reported that primer is usually present in the bonding zone for a joining process conducted at room temperature, which may reduce the mechanical properties of polymer in the SAZ [43].

As amorphous polymers, PVC and CPVC material is more likely to be attacked by solvents than semi-crystalline polymers [9]. Though the application of primer and solvent cement is widely accepted for joining PVC and CPVC pipes, premature failure sometimes occurred at the solvent-welded joint, and solvents used in the joining process have been suspected to be responsible for premature leakage that occurred in PVC piping [11]. Besides, a study [10] showed that both excessive and insufficient cement can be the root causes of failure in PVC and CPVC pipes. As a compounding effect, if the welded components contain residual stresses, then there is a risk of cracking or crazing when the solvents are applied [43]. So far, to the author's knowledge, the exact effect of solvents used in the solvent welding process on the mechanical behavior of those pipes is yet to be fully understood.

1.3.2 Mechanical properties

This session reviews studies on the mechanical properties of PVC and CPVC pipes, including tensile mechanical properties and residual stresses.

1.3.2.1 Tensile properties

PVC and CPVC pipes are mostly manufactured by extrusion, of which the mechanical properties are highly dependent on the manufacturing process. During pipe extrusion, the polymer compound in its powder form is first converted by heating into a viscous plastic mass, and then extruded into the pipe-forming die, followed by the final cooling process [48]. The mechanical properties of extruded pipes can be altered by changing the manufacturing parameters to facilitate the polymer chain entanglement during the melt processing and increase the degree of gelation or fusion [49–51]. Therefore, optimization is conducted on parameters such as extrusion temperature and screw speed, etc. to achieve good mechanical properties of extruded pipes. Summers [52] suggested that higher processing temperature usually improved the impact strength and stress rupture levels of pipes. Moghri et al. [50] found that the elongation at break [53] of rigid PVC pipes was more sensitive to the level of fusion than its yield strength.

In addition to the manufacturing parameters, the service time may also affect the mechanical properties of PVC or CPVC pipes. Hucks and Robert [54] studied the change in mechanical performance of pressurized PVC pipe with time, through testing strip samples prepared by longitudinal cutting of rigid PVC pipes, which had been subjected to burst testing for 10 years. Results showed that the elastic modulus was unaltered, while the tensile strength increased compared with that of new pipes, which was demonstrated as a result of preferential orientation of the polymer molecules in the stress field. Similarly,

Rabinovitch et al. [13] found that the tensile strength and elastic modulus increased slightly while the elongation at break decreased after a physical aging test at elevated temperature below the glass transition temperature. On the other hand, according to the mechanical properties recommended in the Design Manual, by the American Association of State Highway and Transportation Officials (AASHTO) [55], the value of the minimum 50-year tensile strength of PVC drainage pipes is 65% smaller than the value of its initial strength, and the modulus is about 47% smaller, which indicates the possible degradation of mechanical properties of PVC material.

As mechanical behavior of extruded pipes can be affected by both the manufacturing process and the service time, quality control testing is mandatary to ensure full compliance with the applicable product standard [48]. Extruded PVC or CPVC pipes are usually certificated using pressurized pipe tests. The resistance of pipes to hydraulic pressure in a short time is determined by ASTM D1599 [56], during which the specimen is loaded to failure or a predetermined minimum level in short-time by means of continuously increasing internal hydraulic pressure. On the other hand, ASTM D1598 [57] provides the method to determine the time-to-failure of pipes under constant internal pressure. ASTM D2837 [58] and ISO 9080 [59] describe the procedure to determine the hydrostatic design basis (HDB) and pressure design basis (PDB). HDB is a material property and is obtained by evaluating the long-term hydrostatic strength (LTHS) derived from testing pipe made from the subject material. LTHS is the critical value that causes failure of the pipe at 100,000 hours when applied continuously, and is determined through the intercept of the stress regression line with the 100,000-hour coordinate [58]. On the other hand, PDB is a product specific property that reflects not only the properties of the material from which

the product is made, but also the influence on product strength by product design, geometry, and dimensions and by the specific method of manufacture. Usually an HDB/PDB is one of the series of preferred long-term strength values.

Note that above standards mainly focus on the assessment of strength-based properties. While some standards with strain-based criteria have been established for steel pipelines to prevent rupture and buckling [60–62], limited attention has been put on the evaluation of material ductility of extruded PVC or CPVC pipes.

To evaluate the circumferential mechanical properties of plastic pipes, ring tests are popular and useful [63]. ASTM D2290 [64] provides a standard to measure the apparent hoop strength of plastic pipes using split disks and ring segments. Full-diameter, full-thickness rings cut from thermoplastic pipes with reduced sections, also named notched pipe ring (NPR) specimens, are suggested for testing. The comparison of the mechanical response between full ring and NPR specimens was discussed [63]. Full rings have the advantages that they are easy to produce and easy to test while there are bending effects on the cross section, leading to high values of strain at failure. In contrast, though NPR specimens have complex stress states, the bending effect is reduced significantly. Considering the advantages and disadvantages, both NPR and full ring specimens were used in the D-split tensile tests for the circumferential tensile properties characterization in this thesis.

1.3.2.2 Residual stress

Residual stress exists in the absence of external forces or thermal gradients and can arise in a material that is at equilibrium with its surroundings when subjected to heat

treatment or machining [15, 65]. It is well known that when manufacturing plastic pipes by extrusion, non-uniform solidification during the cooling process can cause residual stress in the pipe wall [66–69]. In traditional extrusion processes, the pipe outer surface is cooled by water while the inner surface is exposed to almost stationary air, thus the inner surface cools down slower than the outer parts. When the outer pipe surface is already frozen, the inner material still contracts due to the thermal gradient, resulting in a compression of the outer pipe material. During this process, tensile residual stress is formed in the inner pipe region. Therefore, the character of residual stress distribution in extruded pipes is usually tensile on the pipe inner surface and compressive on the pipe outer surface [16, 19, 69, 70]. The presence of residual stress is sometimes desirable, as it can be beneficial to product performance. For example, compressive residual stress is intentionally introduced to pressure vessels to enhance their pressure bearing capacity and fatigue life. On the other hand, research has shown that tensile residual stress can cause an increase of stress from the applied pressure, and may lead to premature failure, thus shortening the service life of the component [15–18].

Many studies have been conducted to characterize residual stress in extruded pipes and to investigate the effect of residual stress on their fracture behavior as well as lifetime. Poduška et al. [19] carried out a lifetime estimation of PE pipes by calculating the time of slow crack growth (SCG) from an initial crack size to a final damage. They found that when considering residual stress, the obtained time was significantly lower than in the case without residual stress. Hutař et al. [20] incorporated a non-homogenous distribution of residual stress into a numerical model of cracked pipes and concluded that when residual hoop stress acting on the inner surface of pipe exceeds half of the hoop stress induced by

the inner pressure, it has a significant effect on the crack shape and stress distribution. Krishnaswamy [21] studied the influence of residual stress on the performance of extruded PE pipes in terms of fracture through creep rupture testing, and indicated that the existence of residual stress played an important role in accelerating the ductile fracture process, but exerted insubstantial influence on brittle fracture which may due to the dissipation of the residual stress in the slit formation process as well as the crack growth process. Chaoui et al. [22] compared the propagation of cracks initiated from either the inner or outer surface of medium-density polyethylene (MDPE) pipe and concluded that MDPE pipes exhibit better resistance to inbound crack propagation, caused by residual stress and morphological gradients introduced in the manufacturing process. Though many studies have been conducted to investigate residual stress effects in PE pipes, the conducted review of the technical literature indicates that research on residual stresses of PVC and CPVC pipes are limited. Davis et al. [23] included through-wall residual hoop stress with the value of 3 MPa acting on the pipe inner surface into a physical probabilistic model to predict the failure rate in PVC pipeline, and Yu [24] showed that the increase of maximum residual stress from 3 MPa to 6 MPa caused a significant increase in failure rate of PVC pipes. Thus, it is important to quantify the residual stress accurately so that long-term performance of the components can be properly assessed to meet service requirements. Though fracture analyses on PVC or CPVC pipes [10, 35] indicate that residual stress caused by an uneven cooling rate can contribute to premature failure, not much research has been conducted to systematically quantify residual hoop stress distribution in PVC or CPVC pipes.

Various methods have been developed to measure residual stress, among which

mechanical methods are popular for plastic materials. The principle of the mechanical methods is to monitor deformation incurred from removing some material in a load-free state [65, 71]. Common mechanical methods include the hole drilling method [72], layer removal method [73] and slitting method [74]. The traditional hole drilling method is simple and quick, which determines the residual stress from measuring the strain introduced by the drilling near the surface. Because the hole drilling only affects a local area, this method is often classified as a semi-destructive method [75]. Considering that in most cases the residual stresses are not uniform with depth, the incremental hole drilling method was developed, during which the drilling process is carried out in a series of small steps [76]. The modified version of the basic drilling method improves the versatility of the method and enables better measurement of through-thickness stress [65]. Though working as the most popularly used semi-destructive methods of residual stress evaluation, the major limitation of the hole drilling method is the measurement accuracy, which is easily affected by local temperature fluctuations introduced either from connecting the strain gauge to the signal amplifier or from the drilling process [77].

On the contrary, the layer removal method is a destructive method for assessing the residual stress distribution across the specimen thickness. It involves the successive removal of material layers to monitor the corresponding strain change in the surrounding area [78]. This method is straightforward and suited to both flat plate and cylindrical specimens. For hollow cylindrical specimen, after annular layers are removed, the deformation measurement can be made on either the outer or inner surface. However, the requirement of consecutive removal of materials is not only time-consuming but may also cause accumulation of errors, thus reducing the methods accuracy [79–81].

The slitting method is similar to the hole drilling method, but rather than using a hole, a long slit is created. Basically, it uses a cut of progressively increasing depth to release the residual stress while the deformation is recorded. This method enables the evaluation of the residual stress profile over the entire specimen depth, providing both a near surface and through-thickness measurement [65, 71]. Besides, it is much faster to carry out than the layer removal method. The slitting method was originally introduced by Vaidyanathan and Finnie in 1971 [82] and developed by Cheng et al. [79, 80, 83, 84]. In order to obtain a reliable measurement of residual stresses by this method, attention must be paid to the generation of the slot and measurement of strain changes [85]. Considering the difficulty to measure the small displacement change and application of strain gauges to plastic pipes in practice, William et al. [66, 86] determined the residual stress in plastic pipes by layer removal and subsequent slitting, by which the gap displacement after release of residual stress is magnified by the ring distortion and easy to be measured. For a more detailed and realistic analysis of the residual stress without assumption of linear or symmetrical distribution of residual hoop stress, Poduška et al. [70, 87] proposed a methodology to determine the residual hoop stress distribution by measuring the deflection of axially slit ring specimens with 13 different wall thickness, which is referred to as 13-slit-ring method in this thesis. Since the residual stress is generated from an inhomogeneous cooling process, where the temperature gradient probably has an exponential nature [70], it is assumed that the residual stress variation across the wall thickness follows an exponential distribution as shown in Eq. (1.1).

$$\sigma_{\text{res}} = C_1 + C_2 e^{kx} \tag{1.1}$$

where σ_{res} is the residual hoop stress, x the normalized position along the wall thickness direction, with 0 being the inner surface and 1 the outer surface, and C_1, C_2 and k constants.

Deflections of each type of ring specimens were used to build up the equilibrium systems, of which the solutions were then used to perform curve fitting and determine the residual stress distribution through the pipe wall thickness. Though good results were obtained from extruded PP and PE pipes by the13-slit-ring method, considering the main drawback of the time-consuming process for specimen preparation, a further simplified method [19, 88] was developed, which enables the measurement of residual stress distribution by only a single ring specimen prepared from pipes, and is referred to as the one-slit-ring method in this thesis. The derivation is based on the validity of the above exponential function as shown in Eq. (1.1) to describe the residual stress distribution, with a fixed value of k. Work in references. [19, 70] showed that the k value can be fixed as 3.2 for both PP and PE pipes. Using the conditions that the total normal force on a given cross section of a slit ring specimen equals zero and that the diametrical change caused by the release of residual stress can be regarded as the result of a pure bending moment acting on the slit-ring specimen, C_1 and C_2 in Eq. (1.1) were explicitly expressed as Eqs. (1.2a) and (1.2b) [19]:

$$C_2 = \frac{[(D_o - h)/2 - R](\Delta D/2)E}{[R - (\Delta D/2)][-0.004R + 0.004(D_o/2 - h) - 1.68h]} \tag{1.2a}$$

$$C_1 = -\frac{C_2}{(e^{3.2} - 1)} = -7.35C_2 \tag{1.2b}$$

where D_o is the outer diameter of the pipe, h is the wall thickness, E is Young's modulus, ΔD is the measured diametrical change and R is the neutral surface radius.

In comparison to other residual stress measuring techniques, the above one-slit-ring method provides a quick and reliable tool to estimate the residual stress in extruded pipes and therefore was selected to characterize the residual stress distribution in CPVC pipes in this thesis. However, the application of this method requires homogenous material properties. It is problematic to directly evaluate the residual stress distribution in structures when nonuniform material properties are involved. To improve the versatility of this method, the work presented in this thesis proposes a refinement on this method so that it can be used to evaluate the residual hoop stress distribution in pipes, with a core-shell structure on the cross section. This refined one-slit-ring method was employed to quantify the residual stress distribution in CPVC pipe ring specimen after 30-min exposure to primer, which generates a core-shell structure on the cross section of ring specimen. The validity of this refined one-slit-ring method was evaluated also using finite element (FE) modelling.

1.4 Objectives and outline of this study

The overall objectives of this research project are to investigate the influence of primer used in the solvent welding process on mechanical properties of CPVC pipes, including tensile strength, material ductility and residual stress, as well as to study the possible differences in mechanical properties among commercial CPVC pipes produced by different manufacturers.

CPVC 4120 Schedule 80 pipes produced from two manufacturers A and B, with three types of nominal pipe sizes (NPSs), 1.25-inch (32-mm), 2-inch (50-mm) and 4-inch (100-mm), were selected as sample materials for the experimental work. To evaluate the effect of primer used in the solvent welding process on the mechanical behavior of CPVC pipes, a commercial primer product for the CPVC pipe joining was used.

The specific objectives of this thesis are:

(1) To test and compare the mechanical properties of CPVC pipes by different types of coupon specimens, with and without exposure to primer.

(2) To investigate the effect of drying time on the mechanical behavior of CPVC pipes after exposure to primer, in terms of mechanical properties, surface morphology and fracture behavior.

(3) To quantify the residual stress distribution in CPVC pipes by the ring slitting method and to propose the required modifications so that the refined method is applicable to pipes with core-shell structure on the cross section with different mechanical properties. Afterwards, the effect of primer on the residual stress distribution in CPVC pipes was

evaluated, using drying time as the parameter for the evaluation. Results from the FE modelling were also used in the evaluation.

(4) To study the possible differences between previously mentioned CPVC pipes, with emphasis on their tensile mechanical properties and residual hoop stress distribution.

The remainder of this thesis is divided into five chapters. Chapters 2 to 5 correspond to the four specific objectives mentioned above, and the final chapter provides summary of the thesis and future work.

Chapter 2 studies the mechanical properties of 2-inch CPVC pipes from manufacturer A through three types of coupon specimens, including round NPR, flat NPR and ring specimens. The chapter also compares mechanical behavior of CPVC pipe material with and without one-minute exposure to primer.

Chapter 3 further investigates the effect of drying time on the ductility of CPVC pipe material caused by exposure to primer. The exposure time of ring specimen was prolonged to be 30 minutes, and eight different drying periods, ranging from a half day to 113 days, were selected. The mechanical behavior, cross section morphology and fracture surfaces of specimens with different drying time were examined, to study possible reasons for mechanical property changes of CPVC pipe material by the exposure to primer.

In Chapter 4, the original one-slit-ring method from the technical literature was first applied to measurement of the residual hoop stress in dry ring specimens of CPVC pipes, and then a refined one-slit-ring method was proposed to quantify the residual hoop stress in CPVC pipes with a core-shell structure of different material properties on the cross section, caused by immersion in primer. In addition to that, FE simulation was conducted

to verify the validity of the refined one-slit-ring method.

Work presented in Chapter 5 characterizes and compares the tensile mechanical properties and residual hoop stress in CPVC pipes from two different manufacturers, named A and B, with three different NPSs of 1.25-, 2- and 4-inch. CPVC pipes in both pristine and used conditions are studied. The evaluation of residual hoop stress distribution along the wall thickness is accomplished by the one-slit-ring method.

Chapter 6 gives the summary of the main contributions of this work and recommendations on future work.

Chapter 2: Effects of primer on mechanical behavior of CPVC pipe

This chapter is concerned with the change of mechanical properties for CPVC pipe due to the exposure to primer that is commonly used for surface treatment before joining pipe sections. In this study, coupon specimens of different geometries, including round notched pipe ring (NPR) specimens with notch radii from 1 to 3.18 mm, flat NPR specimens and ring specimens, were used to measure mechanical properties in order to examine differences in mechanical properties due to the immersion in primer. The results suggest that although immersion in primer has a strong influence on the mechanical behavior of CPVC, the level of influence depends on the specimen geometry. Typically, round NPR specimens with the largest notch radius suffer the greatest reduction in tensile strength and fracture strain due to the immersion in primer. The study also suggests that influence on the latter is stronger than that on the former.

2.1 Introduction

Chlorinated polyvinyl chloride (CPVC) is produced by post-chlorination of PVC to increase the chlorine content from around 57% up to 68% [4]. The increase in chlorine content increases the temperature resistance, thus making CPVC an attractive material for hot water distribution [25]. As an amorphous polymer, CPVC has a microstructure without any long-range order [9], thus being less resistant to solvents than semi-crystalline polymers. This characteristic enables the use of solvent-welding to join pipe sections. In the solvent welding process, a primer is used to soften the pipe surface in order to facilitate diffusion of polymeric chains across the interface at the joint [42]. Although solvent welding is the easiest and most economical bonding method for CPVC [2], the primer may also weaken the mechanical properties of the CPVC. Work published in the technical

literature has shown that even after the primer is fully evaporated, the strength of the CPVC pipe in the welded region can only reach up to 70% of that of the parent material [1]. It is well known [2] that when a solvent with some level of compatibility is applied to the polymer surface where residual stress exists, crazing or micro-cracks can be generated and lead to premature failure.

Many research works published in the literature have been directed towards understanding the interaction between chemicals and plastic pipes. Beren et al. [89] investigated the permeation of organic chemicals through PVC pipe, including chlorinated and aromatic hydrocarbons. Interaction parameters for the PVC-organic liquid systems were determined from the level of swelling of PVC in different environments. These studies indicated that the nearly undiluted solvents, such as methylene chloride, acetone, EDC, and toluene, can soften and permeate PVC pipe quite significantly, even though rigid PVC is considered to be an effective barrier against organic solvents with solvent activities less than 0.25. It has also been pointed out that a minute quantity of organic pollutants with activities greater than 0.25 may lead to premature failure of PVC pipes. Rehab-Bekkouche et al. [90], who conducted a study on the influence of the environment on the degradation of mechanical properties of high-density polyethylene (HDPE) pipe, concluded that crude oil and toluene-methanol cause a decrease in yield stress, while sulfuric acid reduces the maximum strain. Exposure to any of these environments also has a negative influence on the Young's modulus. On the other hand, distilled water, methanol, ethanol, and acetone have been shown to reduce the degree of incompatibility between PVC and poly(methyl methacrylate) (PMMA) in friction welding, and using these solvents for surface treatment can eliminate residual stress in the welded zone between the two

polymers, thus improving their bonding strength. However, the presence of residual solvents (such as 0.03% distilled water, 0.3% methanol, 2% ethanol or 6% acetone) can decrease the level of improvement in bond strength [91].

In addition to the application for pipe joining, solvents are also used as surfactants to decontaminate plastic components. A recent study [92] examined the effects of the following solutions, Alconox detergent, Dawn soap and MAG-IT DG100, which are often used in the pipe cleaning process, on the integrity of plastic plumbing pipes. The study found that the exposure to MAG-IT DG100 solution can cause a significant drop in ultimate tensile strength of EPDM rubber (ethylene propylene diene monomer), and reduce the oxidative resistance of HDPE pipes by 15%, while effects of Alconox and Dawn solutions were limited.

In the context of CPVC pipe, a significant portion of the published studies were focused on the leaching and migration of organic compounds [93–97] and their influence on mechanical properties and failure [7, 30, 98]. To our knowledge, little attention has been paid to the effect of primer used in the solvent welding process on the mechanical properties of CPVC pipes.

The objective of the study presented in this chapter is to understand the influence of primer on the deformation and fracture behavior of CPVC pipe. Following some of the works available in the technical literature [99, 100], round notched pipe ring (NPR) specimens with five different notch radii were used to examine the influence of various stress states on the mechanical properties of CPVC pipe. In addition, flat NPR and ring specimens, prepared from the same CPVC pipe, were also used for the testing, to provide benchmark for the comparison purpose.

2.2 Experimental details

2.2.1 Specimen preparation and primer

Three types of specimens were prepared from commercial 2-inch CPVC pipes with nominal outer diameter of 60 mm and wall thickness of 5.5 mm. Geometries for the round and flat NPR specimens were modified from those specified in ASTM-2290 [64]. Figures 2.1(a) and (b) present dimensions for NPR specimens, and Fig. 2.1(c) for ring specimens.

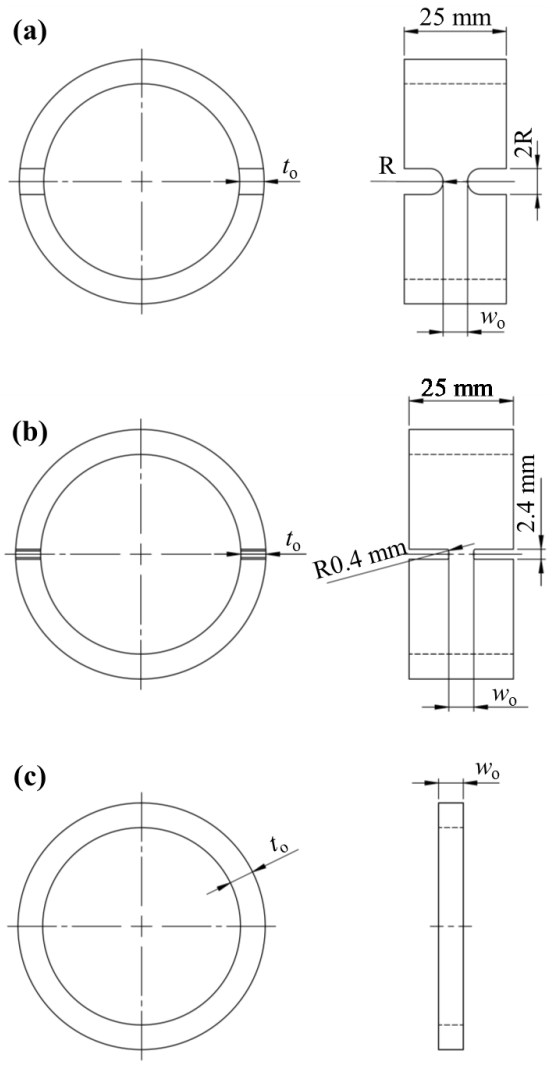

Fig. 2.1 Dimensions for (a) round NPR, (b) flat NPR and (c) ring specimens

Five notch radii of 3.18, 2.38, 1.98, 1.59 and 1.00 mm were used for the round NPR

specimens. Data from these specimens are denoted with prefix "R" followed by the notch radius, such as R3.18 for round NPR specimens with notch radius of 3.18 mm. On the other hand, data for the flat NPR specimens are denoted as flat NPR. Note that each of the round and flat NPR specimens has the same cross sectional width (w_o) and thickness (t_o) in the smallest gauge section so that aspect ratio of the cross section is unity. Likewise, width of each ring specimen is equal to its pipe wall thickness to have the aspect ratio of 1 for the cross section.

The primer used for this study is a commercial primer recommended for joining the CPVC pipe, which consists of mainly acetone, cyclohexanone, tetrahydrofuran and methyl-ethyl-ketone. In this chapter, "wet" specimens are referred to those having been immersion-treated in the primer for 1 minute and then dried in air (in the fume hood) for half a day before being tested. Data from specimens having the prefix "dry," as opposed to "wet," are from specimens without any exposure to the primer.

In view that after the immersion in the primer some residual primer might aggregate at the corners of the gauge section, making the actual exposure time at the corners longer than 1 minute. To examine the possible effect of the prolonged exposure time on the test results, surface of gauge section for some wet specimens were wiped with paper towel after the immersion in the primer, to make sure that the exposure time was exactly 1 minute.

2.2.2 Tensile test

All tensile tests were conducted using a Qualitest Quasar 100 universal testing machine at a crosshead speed of 1 mm/min. Two in-house-made extensometers were used to record the change in gauge section width and thickness during the tests. Figure 2.2 depicts the arrangement of the two extensometers in a tensile test. The specimen shown in the figure

is a flat NPR specimen. A similar arrangement was made for round NPR and ring specimens.

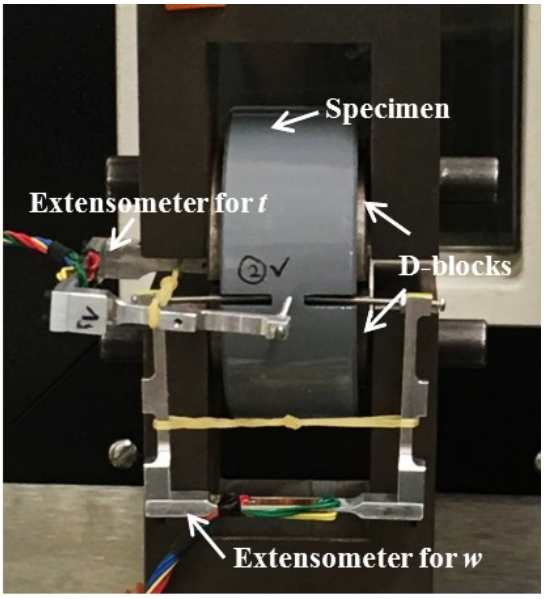

Fig. 2.2 Arrangement of extensometers in a tensile test

Note that for all types of specimens, the extensometers were mounted around the section with the minimum cross-sectional area so that a change in width and thickness could be recorded till the moment when fracture was about to occur. For each type of specimens of a given dimension, at least three tests were conducted to ensure repeatability of the test results. The test results were then used to calculate engineering stress (σ_{eng}), true stress (σ_{true}) and area strain ($\varepsilon_{\text{area}}$) based on Eqs. (2.1) to (2.3).

$$\sigma_{\text{eng}} = \frac{F}{2 \cdot w_{\text{o}} \cdot t_{\text{o}}} \tag{2.1}$$

$$\sigma_{\text{true}} = \frac{F}{2 \cdot w \cdot t} \tag{2.2}$$

$$\varepsilon_{\text{area}} = \ln\left(\frac{w_{\text{o}} \cdot t_{\text{o}}}{w \cdot t}\right) \tag{2.3}$$

where F stands for applied load, and w and t for specimen width and thickness, respectively, as measured by the two extensometers. w_{o} and t_{o} represent correspondingly

the original width and thickness of the specimen before the test.

2.3 Results and discussion

Figure 2.3 summarizes typical engineering stress-stroke curves from the tensile tests for dry ring and NPR specimens, i.e., without any exposure to primer.

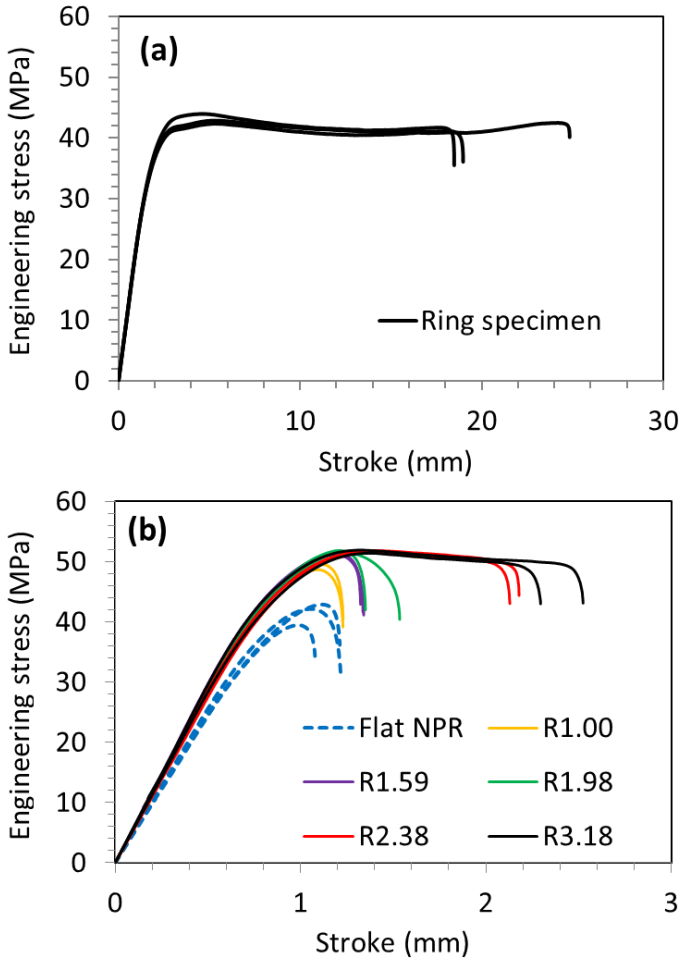

Fig. 2.3 Typical tensile test results for (a) ring and (b) NPR specimens without any exposure to primer

As shown in Fig. 2.3(a), ring specimens exhibited excellent ductility, with stroke at fracture being at least 18 mm, at which point significant necking was generated in the gauge section. For NPR specimens, on the other hand, fracture occurred at a much shorter stroke of less than 3 mm, as shown in Fig. 2.3(b), and only round NPR specimens with

notch radii of 3.18 mm and 2.38 mm exhibited necking before fracture. Figure 2.3(b) also suggests that a higher peak engineering stress occurred in round NPR specimens, compared to flat NPR specimens. Interestingly, as shown in Fig. 2.3(b), the initial slope for curves of round NPR specimens seems to be independent of the notch radius and is always higher than that of the flat NPR specimens. Curves for the flat NPR specimens also have a smaller peak engineering stress than their round counterparts. Fig. 2.3(b) indicates that among the round NPR specimens, a decrease in notch radius tends to decrease the stroke at fracture, which in turn reduces the peak engineering stress for specimens with notch radii smaller than 2 mm. Overall, peak engineering stress for the round NPR specimens is in the range from 49 MPa to 52 MPa, which is higher than that for the flat NPR specimens of 40 MPa to 43 MPa and ring specimens of 43 MPa to 44 MPa.

It should be noted that mechanical testing on notched specimens was also performed by Ognedal et al. [100], using axisymmetric PVC bar specimens, prepared from extruded plates. Their results suggest that peak engineering stress increases slightly with the decrease of notch radius, which is inconsistent with results presented in Fig. 2.3(b). While the difference in strain rate may be the cause for the inconsistency [101], the intrinsic difference between extruded pipe and plates is also believed to play a role. Therefore, further study is needed to clarify the inconsistency.

Figure 2.4 presents the difference in test results for round NPR specimens, caused by the immersion in primer for 1 minute. The curves in solid lines are for dry specimens, red curves in dashed line for wet specimens, and one blue curve in dashed line for wet specimens with primer wiped off after 1-minute immersion. In view of the small variation between the red curves in dashed line and the blue curve in dashed line, it is believed that

wiping off the residual primer from the specimen surface is not a critical aspect for controlling the time of primer exposure.

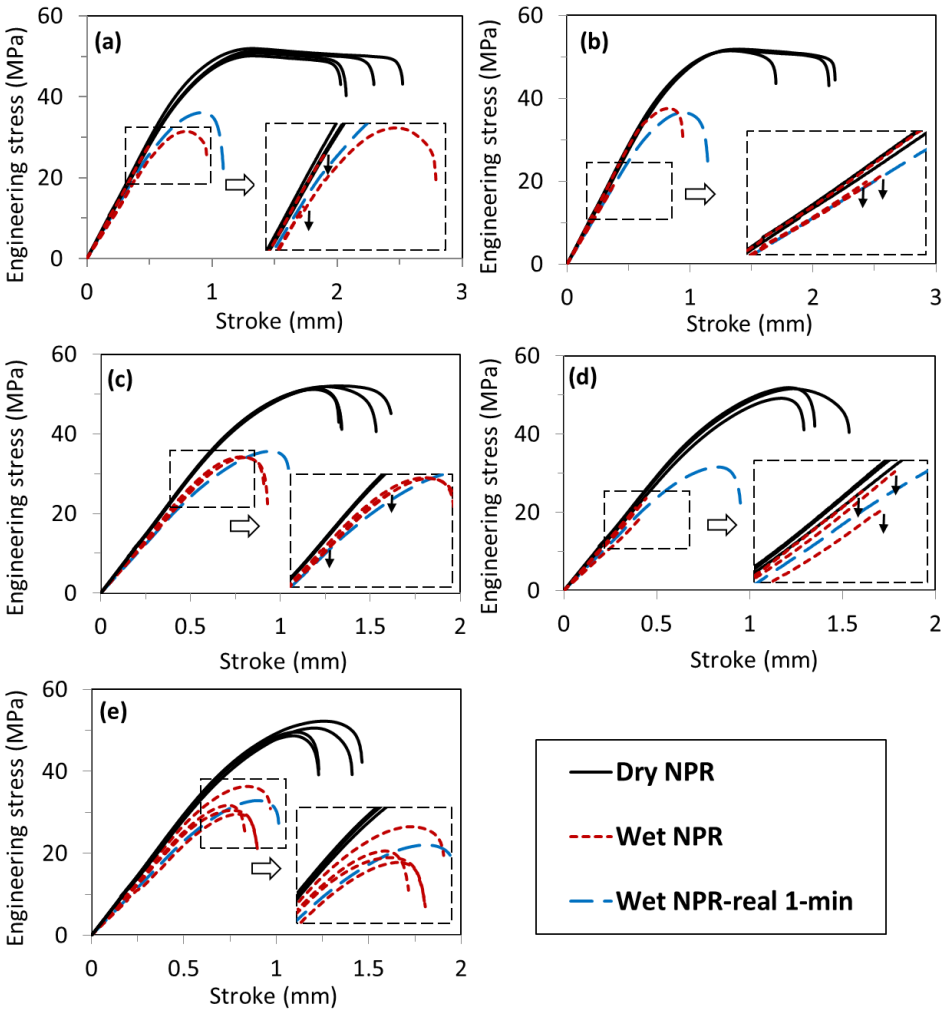

Fig. 2.4 Engineering stress-stroke curves for round NPR specimens without (solid black) and with (dashed red or blue) 1-min immersion in primer: (a) R3.18, (b) R2.38, (c) R1.98, (d) R1.59 and (e) R1.00

Figure 2.4 suggests that immersion in the primer, even just for a period of 1 minute, is sufficient to reduce dramatically elongation at fracture and peak engineering stress. Note that black arrows are used in the inserts in Fig. 2.4 to indicate the stroke at fracture for the wet specimens. The stroke values indicated by the black arrows suggest that the residual primer on the specimen surface, if not wiped out after 1 minute, can actually further reduce

the stroke at fracture. Therefore, the main effect of primer is believed to be a ductility reduction of CPVC pipe, though further study is needed to support this hypothesis.

Figure 2.5 compares area strain at fracture between dry round NPR specimens and their wet counterparts, in which open symbols represent all data obtained experimentally and solid symbols their averaged values. Arrows in the figure indicate the vertical axis (left or right) corresponding to the data.

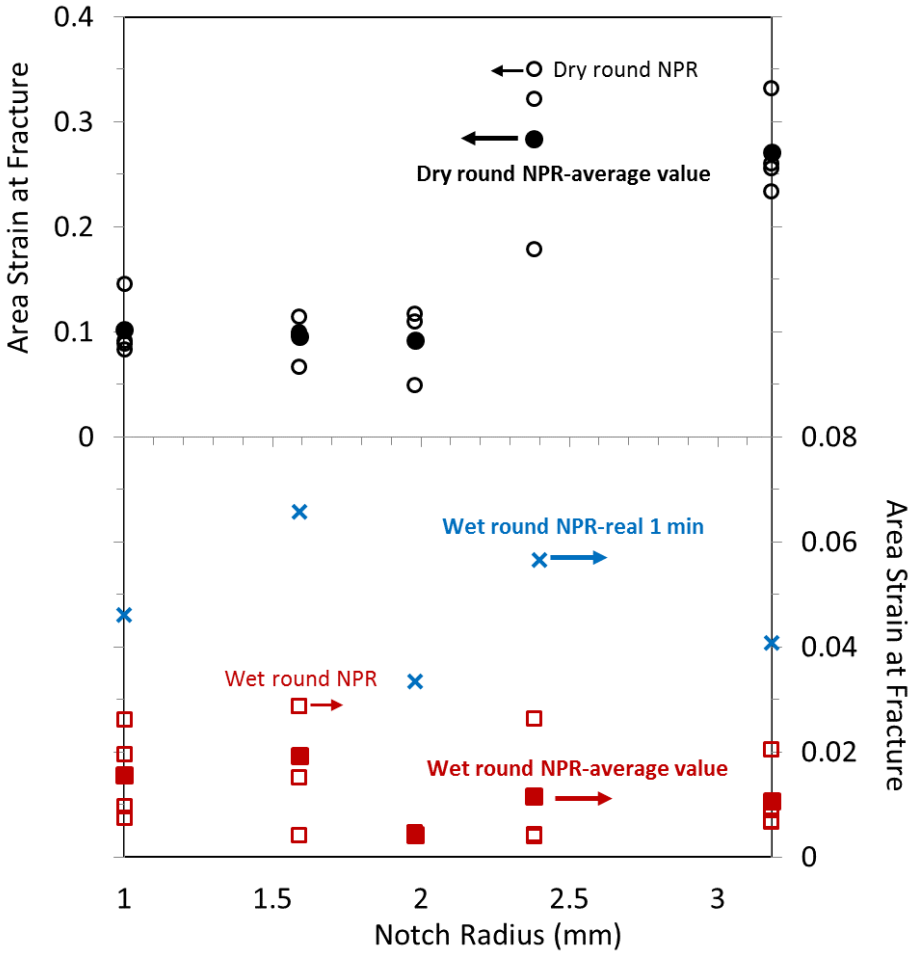

Fig. 2.5 Comparison of area strain at fracture between dry (black) and wet (red and blue) round NPR specimens

The results in Fig. 2.5 indicate that all wet round NPR specimens fractured at a much smaller area strain than their dry counterparts. Without any exposure to primer, area strains

at fracture for round NPR specimens R1.00, R1.59 and R1.98 are similar, but the area strains at fracture for R2.38 and R3.18 are distinctively larger. Furthermore, specimens with the latter two notch radii exhibited necking before fracture, but the former three did not. On the other hand, the area strains at fracture for all wet specimens do not show much difference or dependency on the notch radius. Overall, Fig. 2.5 suggests that the immersion in primer has caused a decrease in area strain at fracture for all specimens, but the decrease is much more significant for R2.38 and R3.18 specimens, resulting in a similar range of area strains at fracture as those for the other round NPR specimens.

For flat NPR and ring specimens, as shown in Fig. 2.6, the immersion in primer has a less significant effect on the engineering stress-stroke curve than that for the round NPR specimens.

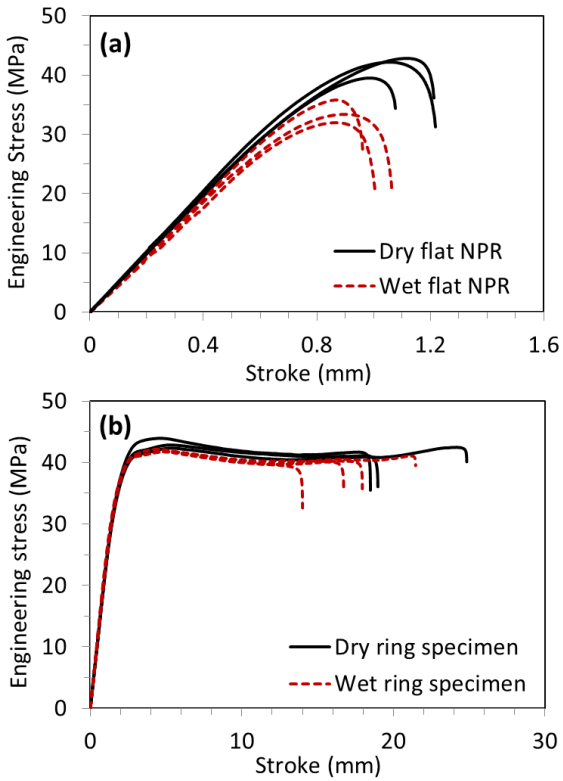

Fig. 2.6 Engineering stress-stroke curves for (a) flat NPR and (b) ring specimens, with (dashed red) and without (solid black) the immersion in primer for 1 minute

Results presented in this chapter suggest clearly that ductility for all wet specimens is smaller than their dry counterparts. However, the extent of the decrease varies with the type of specimens used for the testing. For round NPR specimens, especially for those with notch radius of 2.38 mm and 3.18 mm, ductility decreased significantly by the immersion in primer for 1 minute, as shown in Fig. 2.4. Figure 2.4 also suggests that the initial slope of the curves was decreased by the immersion in primer. For flat NPR specimens, as shown in Fig. 2.6(a), the slope drop by the immersion in primer is less noticeable but still exists. For the ring specimens, as shown in Fig. 2.6(b), the immersion in primer had little influence on the mechanical properties, including ductility, the initial slope of the curve and the peak engineering stress. In fact, appreciable necking still occurred in ring specimens after the immersion in primer for 1 minute.

Overall, the effect of primer on the mechanical properties seems to depend on the type of specimens used for the testing. The reason for the dependency is not clear at the moment when the work was prepared, but it should be pointed out that the current study does not consider residual stress which is known to exist in extruded pipes. The exposure to primer must have affected the level and distribution of residual stress in the pipe, which may in turn affect the measured mechanical properties for the wet specimens. Further study taking into account the influence of residual stress on the measured mechanical properties is needed to understand the discrepancy of the influence of the immersion in primer on the measured mechanical properties based on those types of specimens. Furthermore, it should be noted that tests on wet specimens were conducted only after a half-day drying process. It is not known whether further drying may affect the trend of change in mechanical properties for the three types of specimens, which requires further investigation to clarify.

2.4 Conclusions

Tensile tests were conducted on three types of coupon specimens of CPVC pipe, i.e., round NPR, flat NPR and ring specimens, to investigate the influence of immersion in primer on the mechanical properties. The results show that the immersion in primer for 1 minute does have an influence on the mechanical properties, but the extent of influence varies among the three types of specimens. Overall, the results indicate that the main influence is a decrease in ductility, but the extent of the decrease is, in a decreasing order of round NPR, flat NPR and ring specimens. For the round NPR specimens, the extent of decrease in ductility further depends on the notch radius.

The study concludes that exposure to primer during the pipe joining process affects the mechanical properties of CPVC pipe. However, further study is needed to transfer the knowledge obtained from the coupon testing to the evaluation of CPVC pipe in service. A future study should consider the influence of exposure to primer on the level and distribution of residual stress in the pipe. The work is being conducted and the results will be presented at the conference.

Chapter 3: Ductility loss of CPVC pipe due to exposure to primer

This chapter investigates the influence of primer on mechanical properties and fracture behavior for ring specimens, prepared from commercial chlorinated polyvinyl chloride (CPVC) pipe. After immersing the specimens in primer for 30 minutes, the specimens were dried for eight different periods, ranging from half day to 113 days, and then fractured in tension along the hoop direction. Results suggest that the longer the drying time, the higher the recovered strength, with the specimens after the longest drying time showing up to 63% of the strength for the virgin pipe. However, such a level of recovery cannot be achieved for ductility. Examination of specimens indicated that the exposure to primer created a core-shell structure on the cross section, of which the area ratio was independent of the drying time. It is believed that exposure to primer caused swelling and formed the shell region. Presence of the shell region has two roles in the ductility reduction. One is to provide multiple sites along the border between the shell and the core regions for crack initiation, and the other to enhance stress concentration at the crack tip. The chapter concludes that exposure to primer in the solvent welding process may reduce ductility of CPVC pipe, thus affecting its resistance to slow crack growth in long-term applications.

3.1 Introduction

Chlorinated polyvinyl chloride (CPVC) pipe is one of the most popular plastic pipes for hot water distribution [4, 25]. Joining CPVC pipes is usually through solvent welding [2, 42, 102]. The process uses primer [40] to soften the pipe surface and then applies cement to fill the gap between the matching surfaces [41] of the pipe joint in order to ensure consistency of the joint strength. Work in literature indicates that after primer is fully evaporated, strength in the welded region can reach up to 70% of the strength for the

parent material [1]. However, Titow et al. [46, 47] reported that for a joining process conducted at room temperature, primer is usually present in the bonding zone, not fully evaporated.

Primer is a blend of solvents, usually including methyl ethyl ketone (MEK), acetone, cyclohexanone and tetrahydrofuran (THF), and is applied to plastic pipes and fittings prior to the use of a solvent cement to enhance the adhesion [103]. According to ASTM F656 [40], a suitable primer should have the ability to dissolve at least 10 wt% of PVC or CPVC resin at room temperature within one hour. On the other hand, cement used in the solvent welding of CPVC pips contains a minimum content of 10 wt% of CPVC resin, and the solvent should be able to dissolve an additional 3 wt% of CPVC compound or the equivalent CPVC resin at room temperature [41]. Note that a commercial cement generally contains solvents similar to those in primer, such as THF and cyclohexanone, in order to meet the specific requirements [41, 45].

It is well known that absorption of solvents or plasticizers can weaken plastics, thus causing failure at a stress level much lower than their yield strength [29, 104]. Amorphous polymers are more likely to be attacked by solvents than semi-crystalline polymers, because the former are lack of the long-range order in microstructure and thus, have relatively large free volume [9]. Knight [29] indicated that in general, good and moderate solvents have the ability to penetrate the plastics, thus separating polymer molecules or weakening intermolecular interaction, to form solution or cause swelling, respectively. However, for PVC and CPVC which are amorphous polymers, even a weak solvent or non-solvent may be able to weaken the polymer by facilitating the crack propagation. Although application of primer and solvent cement is widely accepted for joining CPVC

pipes, premature failure that leads to leakage has been reported at the solvent-welded joints. Solvents used in the joining process have been suspected to be responsible for the leakage [11]. Furthermore, experience has shown that primer and solvent cement used during the pipe installation, which contain solvents for CPVC, may lead to the environmental stress cracking of the polymer, especially at sub-zero temperatures [12], but the associated mechanism is yet to be clearly understood.

In addition to the above issues, it is always important to evaluate quality of solvent-welded joints before they are put in service. Currently, the standard specifications for PVC or CPVC pipe joints mainly focus on the strength-related properties, such as burst pressure [56], sustained pressure [57, 59] and joint tightness [105]. Existing studies on solvent welding of PVC or CPVC pipes are also centered on the strength-based evaluation. Although shear strain at the solvent-welded lap joint has been considered [106, 107], not much attention has been paid to normal strain or ductility change of the pipe material at the joint.

In order to understand the effects of solvents used in the solvent welding process on the mechanical behavior of CPVC pipe, work has been conducted to examine the induced change in mechanical properties, cross sectional morphology and fracture behavior of CPVC pipe. Since the primer for CPVC pipe contains almost all solvents involved in the solvent welding process, rather than considering each of the solvents, primer is used in the current study. A previous study using notched pipe ring specimens [108] has shown that even one-minute exposure to primer yields significant changes in strength and ductility of CPVC pipe. The current study examines such changes using ring specimens of constant cross section, in order to simplify stress and strain states introduced in the mechanical

testing. In the current study, drying time is used as the main variable to change primer content in the specimens, after the specimens have been immersed in the primer for 30 minutes. Drying time used to change the primer content in the specimens is up to 113 days.

3.2 Experimental details

3.2.1 Specimen preparation

Ring specimens were prepared from commercial CPVC 4120 SCH80 2-inch (50-mm) pipes. The nominal outer diameter and minimum wall thickness of the CPVC pipes are 60.33 mm and 5.54 mm, respectively. Figure 3.1 gives a schematic diagram of the ring specimens, in which the nominal width (w_o) was chosen to be same as the average wall thickness (t_o) in order to have an aspect ratio of unity for the cross section.

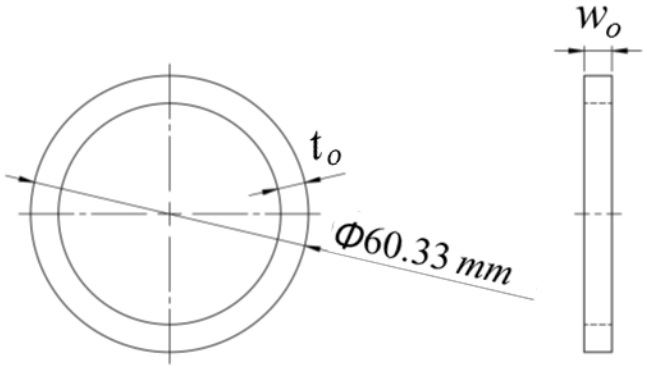

Fig. 3.1 Dimensions of ring specimens used in the testing. Value for w_o is set to be equal to t_o of the particular pipe.

Primer treatment was given by immersing the ring specimens in a primer for 30 minutes. The primer used is a commercial product for CPVC pipe, in which the main ingredients are acetone, cyclohexanone, THF and MEK. In this chapter, ring specimens without any primer treatment are referred to as dry specimens. On the other hand, the primer-treated specimens are referred to as 'wet' specimens, denoted as 'W', with the number following

‘W’ representing the number of days used to dry the specimens, which is in the range from 0.5 to 113 days. The drying process was to place specimens in a fume hood at the ambient temperature of around 23ºC for the first 3.5 days, after which the specimens were placed in an oven at 30ºC till the day for the testing. As a result of this drying process, specimens of W0.5 and W3.5 were only dried in the fume hood at the ambient temperature. This is because after immersion in the primer for 30 minutes, these specimens have relatively tacky surfaces and thus drying these specimens at ambient temperature should provide a sufficient evaporation rate of the primer from the specimens. After 3.5 days, the drying temperature was raised to 30ºC which is to facilitate the drying process but not to soften the material.

3.2.2 Tensile tests

All tensile tests were conducted using a Qualitest Quasar 100 universal testing machine at a cross-head speed of 1 mm/min. Figure 3.2 provides a schematic diagram for the standard D-split test set-up [64] used in this study. Changes of load (F) and stroke (S) were recorded during the test as functions of time. In addition to the standard test set-up, two home-made, strain-gauge-based extensometers were mounted on the ring specimens during the test, to record contraction of width and thickness during the test. At least three tests were carried out for each primer-treating condition to verify repeatability of the data.

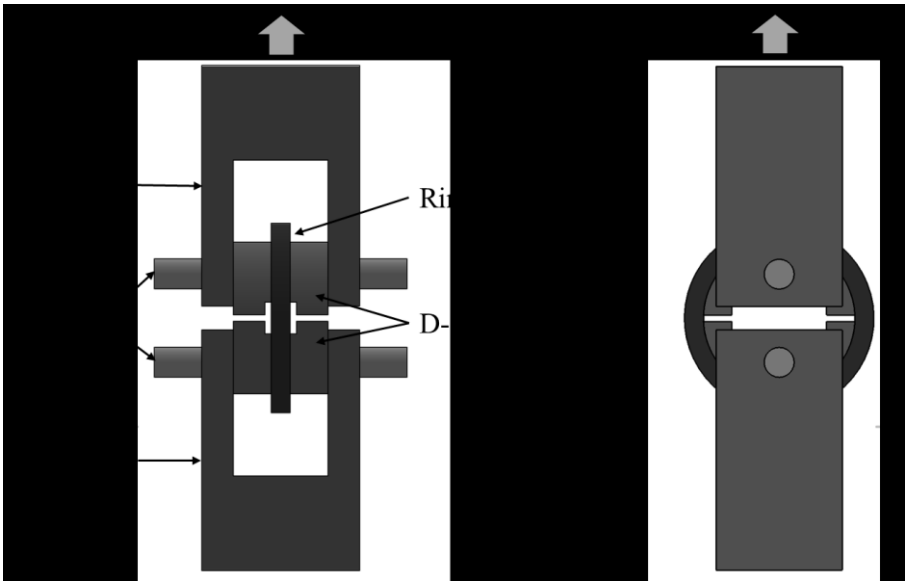

Fig. 3.2 Schematic diagram of the D-split tensile test set-up (without showing the extensometers): (a) front view, and (b) side view

Results from the D-split tests were used to calculate engineering stress (σ_{eng}), true stress (σ_{true}) and area strain (ε_{area}) based on the following equations.

$$\sigma_{eng} = \frac{F}{2 \cdot w_o \cdot t_o} \tag{3.1}$$

$$\sigma_{true} = \frac{F}{2 \cdot w \cdot t} \tag{3.2}$$

$$\varepsilon_{area} = \ln\left(\frac{w_o \cdot t_o}{w \cdot t}\right) \tag{3.3a}$$

where w and t represent width and wall thickness, respectively, of the specimen with subscript 'o' denoting their values before the test. The maximum measured area strain (ε_m) was calculated using Eq. (3.3b):

$$\varepsilon_m = \ln\left(\frac{w_o \cdot t_o}{w_f \cdot t_f}\right) \tag{3.3b}$$

where w_f and t_f represent the last measurement of specimen width and wall thickness by

extensometers before the drastic load drop due to the initiation of fracture.

3.2.3 Specimen examination and fracture surface analysis

Cross-sectional dimensions of ring specimens after the exposure to primer in different periods of drying time were recorded, to investigate the influence of primer on the specimens. In addition, fracture surfaces generated in the D-split tests were examined using a Zeiss Sigma field emission scanning electron microscope (SEM), operated in a variable pressure mode using a backscattering detector to collect the signals. These samples did not have any coating. Therefore, the SEM chamber was back-filled with N_2 gas to minimize charging on the sample surface.

3.3 Results and discussion

3.3.1 D-split tensile tests

Typical engineering stress-stroke curves are presented in Fig. 3.3, including both dry and wet specimens. Note that since the test results are highly repeatable (based on results for W113, as given in the insert of Fig. 3.3), only one curve for each drying period is presented here.

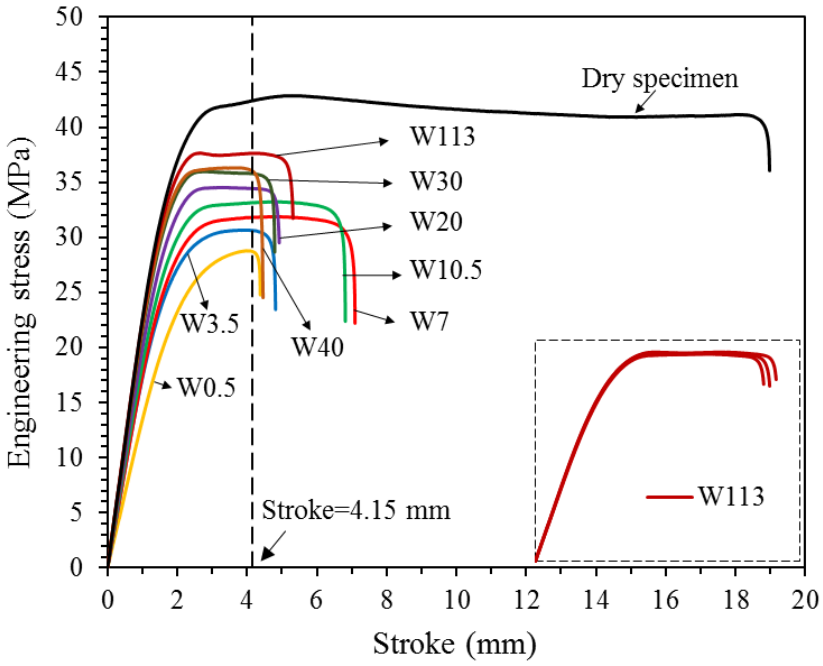

Fig. 3.3 Engineering stress-stroke curves for wet (W) and dry specimens (numbers following 'W' represent the number of days to dry the specimen before the test)

Figure 3.3 suggests that all wet specimens fractured at strokes of less than 8 mm, which are much smaller than that for dry specimens of over 18 mm. In addition, specimens with short drying time, especially W0.5, showed a much smaller initial slope for the engineering stress-stroke curve than that for the dry specimens. With the increase of drying time, the curves in Fig. 3.3 approach the slope for dry specimens. Furthermore, the curve profile for W113 has some similarity to that for the dry specimen, i.e., with twin peaks, which indicates that W113 contains possibly only a very limited amount of primer.

Figure 3.4 summarizes the initial slope of engineering stress-stroke curves, to reflect the change of elastic modulus with the drying time. Error bars in the figure indicate the range of experimental measurements, and horizontal dash line across the figure represents the average value of the initial slope for the dry specimens. The figure suggests clearly that the drying time of 113 days is sufficient to recover the initial slope of engineering

stress-stroke curve, to the same level as that for the dry specimens.

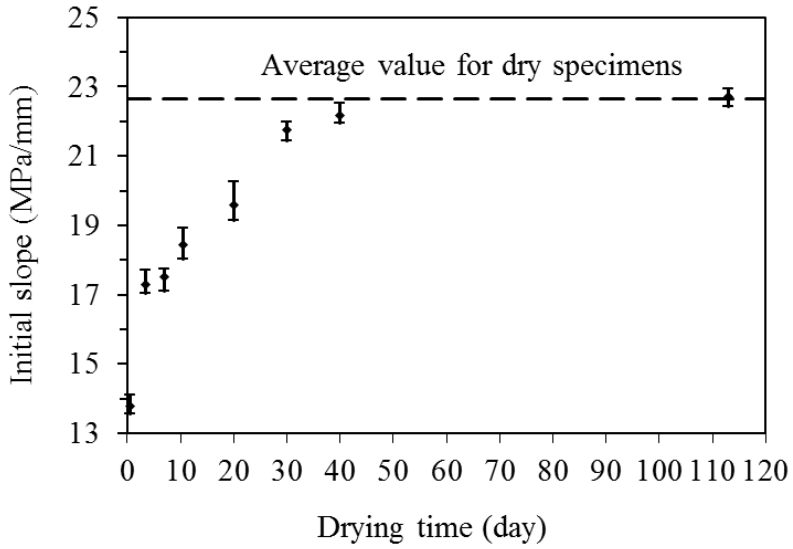

Fig. 3.4 Initial slope of engineering stress-stroke curves as a function of drying time

Figure 3.5 summarizes yield stress as a function of drying time, in which error bars indicate the range of experimental data, and the yield stress is represented by the engineering stress at the stroke of 4.15 mm at which engineering stress for W0.5 specimens reaches the peak value, as indicated in Fig. 3.3. The horizontal dashed line in Fig. 3.5 represents the average yield stress (also at the stroke of 4.15 mm) for dry specimens. Figure 3.5 suggests that yield stress for wet specimen increases with the increase of drying time, and that yield stress for W113 specimen has reached 86% of that for the dry specimens.

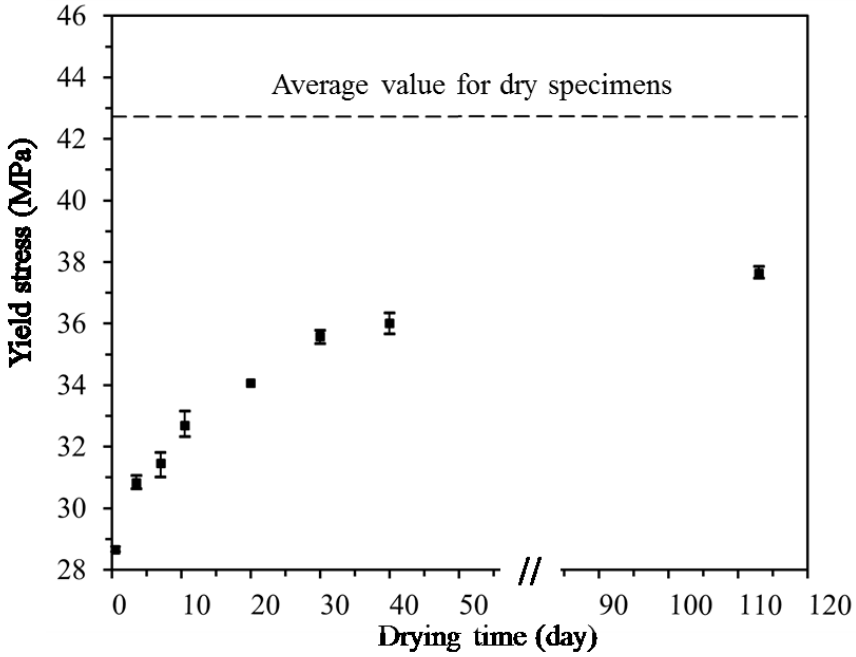

Fig. 3.5 Summary of yield stress as a function of drying time

Figure 3.6 summarizes values for maximum measured area strain as a function of drying time. The figure suggests that all wet specimens have maximum measured area strains that are less than 50% of that for dry specimens. The figure further suggests that for wet specimens, the value of maximum measured area strain increases first with the increase of drying time, up to 10.5 days, and then decreases till a drying time of 30 days, after which the maximum measured area strain remains at a relatively constant level. The trend of change shown in Fig. 3.6 suggests that the maximum measured area strain is unlikely to recover to a level close to that for the dry specimens.

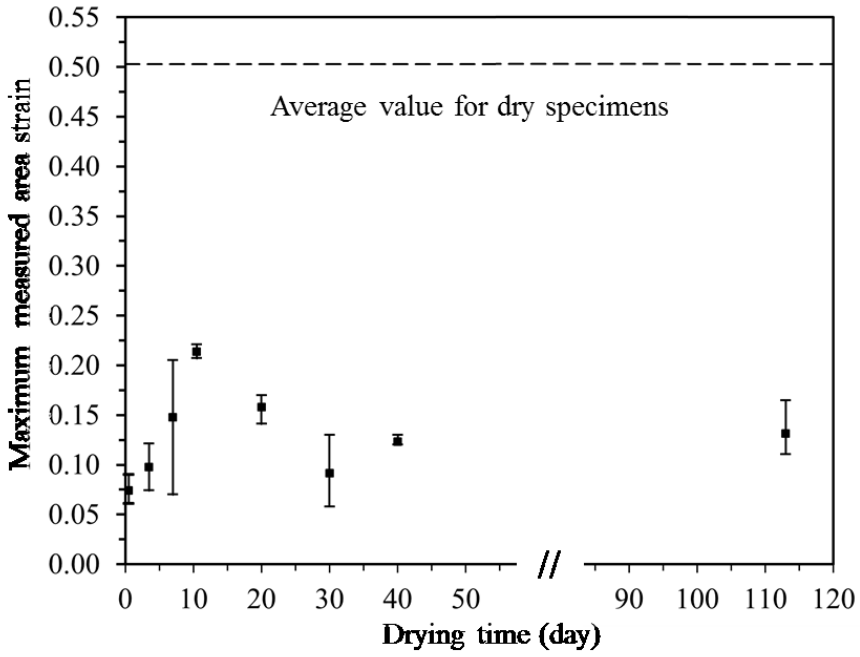

Fig. 3.6 Maximum measured area strain as a function of drying time

In addition to the mechanical testing, cross sections of dry and wet specimens were also examined. Figure 3.7(a) presents a typical view of cross sections for specimens of different drying times. These cross sections were prepared by cutting through the untested specimens using a fresh razor blade. The cutting direction is indicated by an arrow in the top, left photograph (for a dry specimen). Each photograph contains a vertical, whitening strip on the right side, which resulted from unstable crack growth in front of the razor blade before the end of the cutting. In addition, cross sections for all wet specimens show a core-shell, two-phased structure, as indicated in the photograph for W3.5, i.e., the middle photograph on the top row in Fig. 3.7(a).

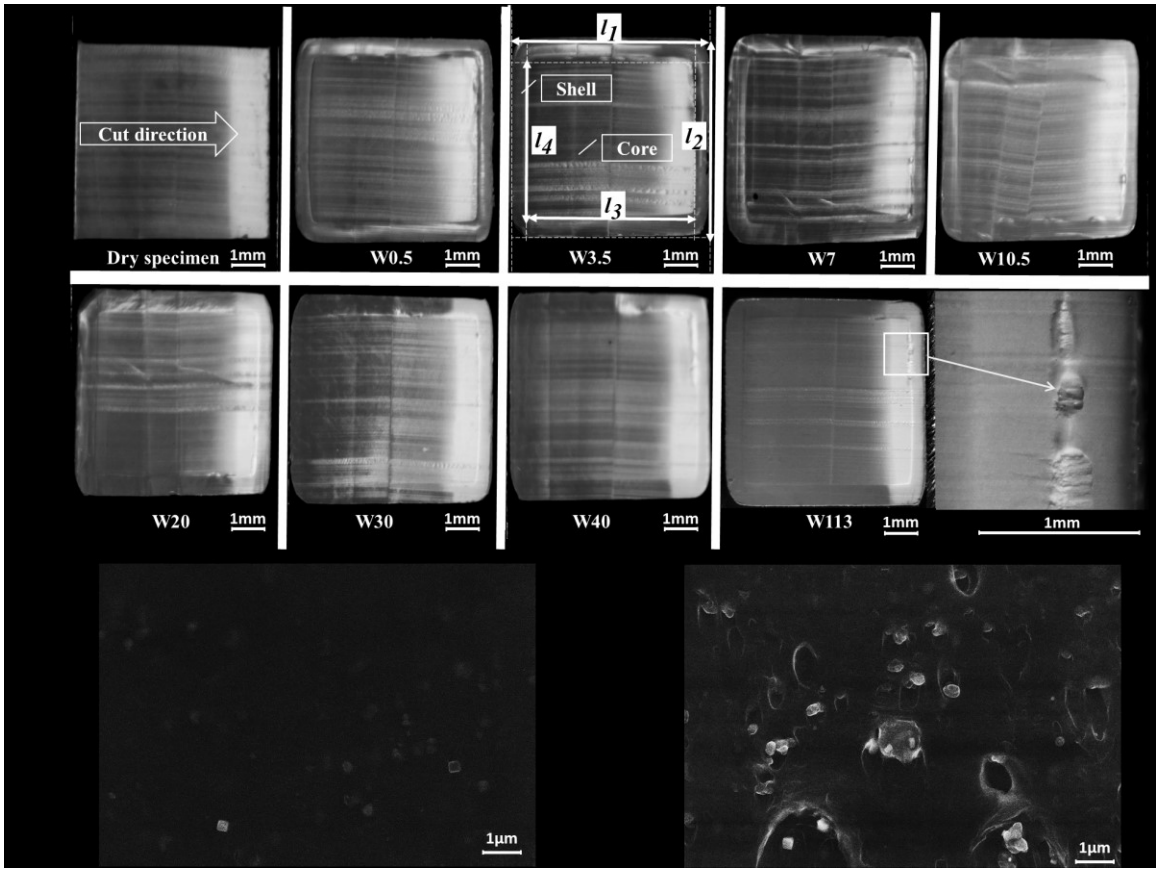

Fig. 3.7 Photographs of cross sections from dry and wet specimens, prepared using a razor blade: (a) the overall view of cross sections, and (b) high magnification for a non-whitening region (left) and a whitening region (right) on the cross section for W113

Figure 3.7(b) presents an example of the surface topography between the non-whitening zone (left) and the whitening zone (right), taken from the cross section of a W113 specimen. These micrographs indicate that cavitation occurred around particles that are titanium-based material, according to energy dispersive spectroscopic (EDS) signals collected during the SEM examination. These cavities must be the source for the whitening [109, 110].

As highlighted in the photograph for W3.5 in Fig. 3.7(a), cross sections for all wet specimens appear to consist of a shell outer layer and an enclosed rectangular core region.

A border between the core and shell regions is visible on the cross sections of all wet specimens, which is clearer in specimens with drying time shorter than 20 days. Defects are also detected along the border between the core and the shell regions, for which the visibility increases with the increase of drying time. An enlarged view of defects along the core-shell border is given in the bottom right photograph of Fig. 3.7(a), taken from a W113 specimen.

Table 3.1 summarizes dimensions of core and shell regions measured from each specimen, in which l_1, l_2, l_3 and l_4 are defined using the photograph for W3.5 in Fig. 3.7(a) (in the middle of top row). The table also includes l_1 and l_2 for a dry specimen which are in general smaller than l_1 and l_2 for wet specimens, suggesting that immersion of the specimens in primer caused swelling of the cross section. Based on values in Table 3.1, ratio of the area for the shell region (A_{shell}) to the overall cross sectional area (A_{total}) was determined using Eq. (3.4) below, and presented in Fig. 3.8 in terms of drying time. The figure suggests that even though values for individual dimensions in Table 3.1 may show some variation, values for the area ratio are fairly consistent, of around 32%, and are independent of the drying time used to remove primer from the specimens. Note that repeatability of the dimensional measurement has been confirmed by two additional W113 specimens.

Table 3.1 Cross sectional dimensions of dry and wet specimens (Lengths for l_1, l_2, l_3 and l_4 are defined in the photograph for W3.5 in Fig. 3.7(a))

Specimens	l_1 **(mm)**	l_2 **(mm)**	l_3 **(mm)**	l_4 **(mm)**
Dry specimen	6.10	6.12	--	--
W0.5	6.21	6.40	5.28	5.18
W3.5	6.29	6.23	5.31	5.00
W7	6.24	6.52	5.36	5.21
W10.5	6.18	6.32	5.28	5.17
W20	6.06	6.38	5.01	5.12
W30	6.36	6.44	5.24	5.25
W40	6.31	6.50	5.36	5.17
W113-1	6.20	6.22	5.37	5.01
W113-2	6.17	6.37	5.29	5.13
W113-3	6.22	6.48	5.36	5.14

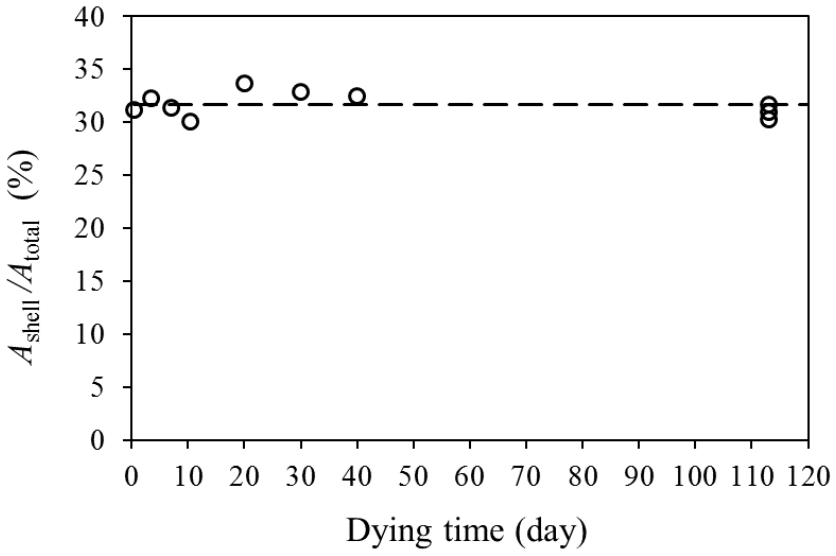

Fig. 3.8 Area ratio of shell region to the total cross section as a function of drying time

$$\frac{A_{\text{shell}}}{A_{\text{total}}} = \frac{l_1 \times l_2 - l_3 \times l_4}{l_1 \times l_2} \times 100\% \tag{3.4}$$

3.3.2 Fracture surface analysis

Fractographic analysis was conducted to examine any change in fracture behavior of wet specimens and possible relationship of fracture behavior with the primer treatment. Figure 3.9 summarizes typical fracture surfaces generated from the mechanical testing, using white arrows to indicate the location for crack initiation. As shown in Fig. 3.9(a), crack initiation in all dry specimens was from one site, but the remaining photographs in Fig. 3.9 suggest that crack initiation in the wet specimens were from multiple sites on the fracture surface. For clarity, each of Fig. 3.9(a), (b), and (e) includes an enlarged view of a selected region that contains the transition from slow to fast crack growth in 9(a) and the crack initiation site in 9(b) and 9(e). Note that four wet specimens chosen for Fig. 3.9 were because of their drying time, i.e., W0.5 for the shortest, W10.5 and W40 for the medium, and W113 for the longest drying time. Photographs in Fig. 3.9 also suggest that the fracture surface area for the dry specimen is significantly smaller than that for the wet specimens, which is mainly because the dry specimen fractured at a much larger area strain and was thus subjected to a bigger transverse contraction.

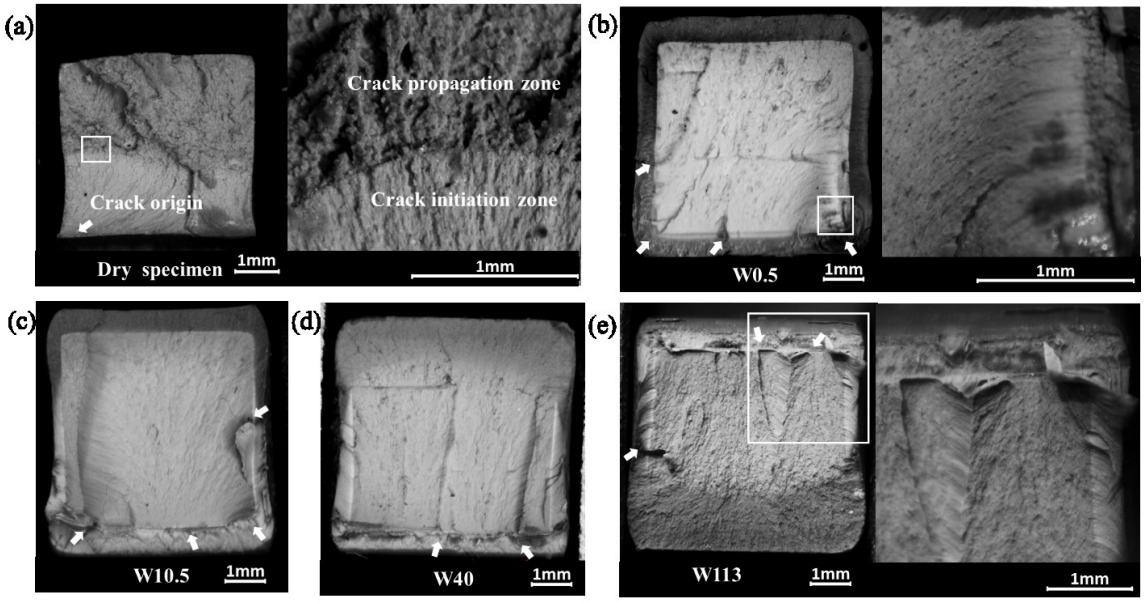

Fig. 3.9 Photographs of fracture surfaces from (a) dry specimen, (b) W0.5, (c) W10.5, (d) W40, and (e) W113

As shown in Fig. 3.9(a), fracture surface of the dry specimen is relatively flat and is believed to be developed on one cross section. For wet specimens, on the other hand, each fracture surface contains ridges that resulted from the coalescence of cracks from different cross sections [111, 112]. Interestingly, core and shell regions depicted in Fig. 3.7 are also visible on the fracture surfaces of wet specimens, and crack initiation in wet specimens are always along the border between the core and shell regions. Furthermore, photographs in Fig. 3.9 suggest that cracks along the border between the core and shell regions always grew towards the core region. Therefore, the shell region should not have played any significant role on carrying the load during the test.

Overall, the micrographs suggest that the core-shell structure on the cross section of wet specimens is an indication of material inhomogeneity introduced by the immersion of the specimens in primer. The shell region appears to be a relatively brittle layer that has a lower load-carrying capability than the core region, and thus the former is prone to crack

formation at an earlier stage of the mechanical testing than the latter. The earlier formation of cracks in the shell region enhances stress concentration in front of the cracks, thus further reducing ductility and load-carrying capability of the wet specimens.

3.4 Discussion

Based on results presented above, further analysis was conducted, first to examine the core-shell structure shown in Fig. 3.7(a) and the corresponding mechanical properties, and then to explore possible explanations for the different extent of influence of primer on the strength and ductility, as depicted in Fig. 3.5 and Fig. 3.6.

Formation of the core-shell structure is based on the assumption that diffusion of primer into the ring specimen is incomplete in 30 minutes used in the study, and the shell region indicates the depth of diffusion of the primer in 30 minutes. With this assumption and the assumption that mechanical strength for the core region is same as that for the dry specimen, the following analysis was conducted to evaluate effects of the drying time on mechanical strength for the shell region. As a first attempt of the analysis, primer concentration in the shell region is treated as uniform, with negligible difference from the specimen surface to the border between the shell and the core regions.

Based on the above assumptions, stress generated in the shell region (σ_{shell}) during the D-split test was determined using Eq. (3.5) below, with the stress applied to the core region (σ_{core}) being equivalent to that for the dry specimens at the same stroke. In this study, stroke of 4.15 mm is used to determine the stress for the analysis, which is the peak stress for W0.5 as shown in Fig. 3.3.

$$\sigma_{\text{shell}} = \frac{F_{\text{t}} - \sigma_{\text{core}} \cdot A_{\text{core}}}{A_{\text{shell}}} \tag{3.5}$$

where F_t is the total force applied to the wet specimen at the stroke of 4.15 mm, σ_{core} the engineering stress of dry specimen at the same stroke, and A_{core} and A_{shell} areas of core and shell regions, respectively, based on values listed in Table 3.1, with the assumption of a rectangular shape for both regions. The σ_{shell} values so-calculated are summarized in Fig. 3.10 as a function of drying time. Error bars in the figure are believed to be from scattering in the experimental measurements and difference between the idealized rectangular shape of the cross section and the true cross-sectional geometry.

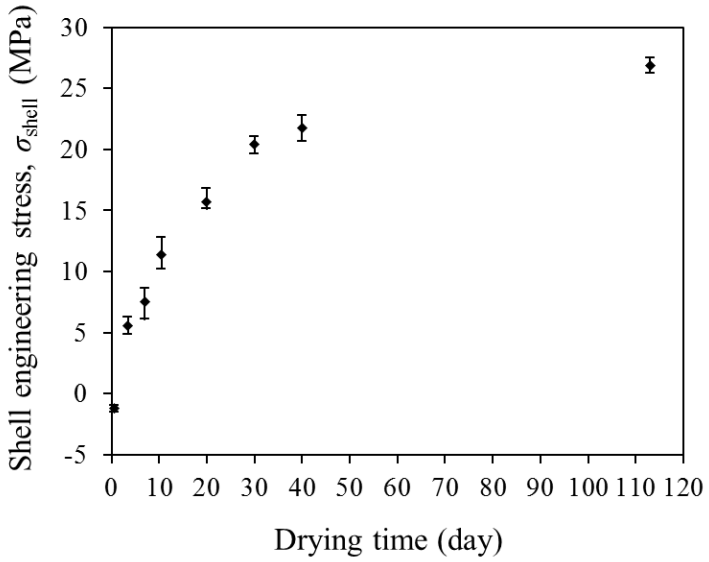

Fig. 3.10 Variation of engineering stress for the shell region, at the stroke of 4.15 mm, as a function of drying time

As shown in Fig. 3.10, the nearly zero value of σ_{shell} for W0.5 supports our assumption that the shell region was formed by diffusion of primer into the specimen, and that the diffusion caused the loss of load-carrying capability for the shell region. With the increase of drying time, content of primer in the shell region is expected to decrease, and thus its strength recovers. However, our results suggest that the recovered strength in the shell

region is only up to 27 MPa, about 63% of 43 MPa for the dry specimen.

In contrast to the strength recovery with the increase of drying time, maximum measured area strain suffers a permanent loss from the exposure to primer, as depicted in Fig. 3.6. The figure shows that the maximum measured area strain increases initially with the increase of drying time to around 10.5 days, but then decreases till the drying time of around 30 days. Further increase of the drying time causes little change in the maximum measured area strain which remains around 30% of the value for the dry specimen. Such a significant loss in ductility is believed to be due to two major changes in the fracture behavior. One is the multiple sites for crack initiation along the border between the core and the shell regions, and the other the earlier formation of cracks in the shell region than in the core. Results presented here suggest that the major effect of exposure to primer on the mechanical behavior of CPVC pipe should be the reduction of its ductility, which according to the work in the literature, has not attracted much attention in the research community.

It should be noted that in the solvent welding process, primer is used to soften pipe surfaces. Even though solvent cement is applied soon after the surface is exposed to the primer, there is always area that is not covered by the solvent cement. Our results suggest that the exposure to primer generates a thin shell region with low ductility, which can lead to premature crack formation, thus affecting reliability of the pipe in a long-term service. This issue can be significant in view that service life of CPVC pipe is expected to be more than 50 years. Therefore, in addition to the strength-based criteria, ductility should also be considered for evaluation of CPVC joints that are created from the solvent welding.

The above discussion is also based on the assumption that perfect adhesion exists

between the core and the shell regions. In order to fully understand the influence of primer on the change in mechanical properties for CPVP pipe, we think further study is needed in the following two areas. One is to examine any strength variation at the core-shell interface with the increase of drying time, and the other to understand mechanisms involved for crack initiation and growth that results in fracture of the wet specimen in the D-split test. With the information, it is then possible to evaluate influence of exposure to primer on the long-term performance of CPVC pipe.

3.5 Conclusions

The effect of drying time on CPVC pipe, after immersion in primer for 30 minutes, has been studied by examining the changes in mechanical properties, cross sectional surface morphology and fracture behavior, using ring specimens prepared from the pipe. Results show that the exposure to primer caused swelling of the cross section and generated a core-shell structure for which the area ratio is independent of the drying time. The results also show that both material strength and ductility decreased after the exposure to primer. Although strength can be partially recovered in the drying process, up to 63% of the virgin material, ductility loss of at least 57% of that for the virgin material is permanent. Therefore, the exposure to primer causes much more significant loss in ductility than in strength.

The study concludes that the main effect of primer on the mechanical properties for CPVC pipe is the loss of ductility. This can increase vulnerability of the pipe to the presence of defects, especially for the long-term, load-carrying applications. As a result, it is suggested that strain-based criteria should be included in the specification for the quality control of the solvent-welded joints. Moreover, primer should be carefully applied to CPVC pipe surface, to avoid unnecessary contact of primer with pipe surface that will not

be covered by solvent cement in the joining process. It is also interesting to conduct study to ascertain whether the application of cement is effective in compensating for the loss in ductility of the substrate due to the exposure to primer, which to the authors' knowledge, remains unknown at this stage.

Chapter 4: A refined one-slit-ring method to quantify residual hoop stress in CPVC pipe – application to specimens after immersion in primer

A refined one-slit-ring method is herein presented to use single ring specimen of inhomogeneous cross section, such as that generated by partial diffusion of an aggressive agent into the specimen, to characterize the residual hoop stress distribution (σ_{res}). The refined one-slit-ring method is applied to chlorinated polyvinyl chloride (CPVC) pipe, using primer as the aggressive agent. This study described in this chapter first confirms the applicability of the original one-slit-ring method to virgin CPVC pipe, i.e., without the exposure to primer. Derivation of the analytical expression for σ_{res} is then presented for a ring specimen of CPVC pipe with a cross section of core-shell structure, due to immersion in primer for 30 minutes. A finite element (FE) model is used to verify the σ_{res} function, using a temperature field to generate σ_{res} so that the same diametrical change is generated by the FE model as that measured experimentally. The analytical expression of σ_{res} is then used to characterize the change of σ_{res} in CPVC pipe ring specimens after different periods of drying in air. The results show that the immersion in primer significantly reduced σ_{res} in the shell region, and also caused a reduction of σ_{res} in the core region but to a lesser extent. With the increase of drying time, σ_{res} in the shell region increases in the first 40 days and σ_{res} in the core region decreases accordingly. Difference of σ_{res} at the interface becomes negligible after the drying time reaches 30 days. The study demonstrates the easiness of using the refined one-slit-ring method to evaluate the influence of an aggressive agent on the change of σ_{res} in plastic pipes, which has a good potential to be extended to the evaluation of environmental stress cracking resistance of plastic pipes.

4.1 Introduction

It is well known that the cooling process used in the extrusion process for manufacturing plastic pipes, introduces residual stress [66–69]. In general, the residual stress is tensile on the inner surface, and compressive on the outer surface [16, 19, 69, 70]. Although the presence of compressive residual stress on the outer surface can benefit the pipes in their scratch-resistance, the tensile residual stress on the inner surface may lead to premature pipe failure [15–18]. As a result, it is important to control the residual stress level so that benefits for the pipes are maximized without any trade-off in terms of the long-term performance.

Various methods have been developed to measure the residual stress, among which mechanical methods are popular for plastic materials. The mechanical methods are based on the principle that material removal in a load-free state generates deformation [65, 71]. Popular mechanical methods include hole drilling [72], layer removal [73] and slitting methods [74]. The traditional hole drilling method is simple and quick, by measuring strain introduced from drilling near the surface. Because the hole drilling only affects a local area, this method is often classified as a semi-destructive method [75]. Its major limitation is on the measurement accuracy, which is easily affected by local temperature fluctuation from either the drilling process itself or the wire soldering process that is performed to connect strain gauges to the signal amplifier [77]. The layer removal and slitting methods, on the other hand, are destructive in nature, but popular for establishing the residual stress distribution across the pipe wall thickness. The former involves successive removal of material layers to monitor the strain change in the surrounding area. This method is straight forward to use, but it is time-consuming and may have measurement errors accumulated

through the consecutive material removal process [79–81]. The slitting method introduces a cut of progressively increasing depth, and uses the recorded deformation change to quantify the residual stress. This method is much faster to carry out than the layer removal method, and can be applied to both near surface and through-thickness measurements [65, 71]. The slitting method has been applied to analysis of residual stress in different configurations, such as cylinders and semi-infinite solid [113]. When dealing with pipes, ring specimens are usually used and therefore, it is also referred to as ring slitting method [66].

The focus of this chapter is on the ring slitting method, of which the principle was first introduced by Vaidyanathan and Finnie [82] and practical application proposed by Cheng et al. [79, 80, 83, 84]. The original ring slitting method requires generation of a slot and accurate measurement of the corresponding strain changes [85, 114] to obtain reliable residual stress distribution. The first generation of its modification was proposed by William et al. [66, 86], in which the use of strain to quantify the residual stress is replaced by the measurement of the gap displacement, introduced through slitting of rings after some layers were removed. Based on the same principle, but without the assumption of linear or symmetrical distribution of residual hoop stress, Poduška et al. [70, 87] gave a practical demonstration that determined residual hoop stress distribution by measuring the deflection of axially slit ring specimens of thirteen different wall thicknesses, thus referred to here as 13-slit-ring method. The measured residual stress is expressed using an exponential function of position in the wall thickness direction which satisfies the force balance condition on the cross section.

Although the 13-slit-ring method provides good results for extruded polypropylene (PP)

and polyethylene (PE) pipes [19, 70], it has a main drawback of requiring a time-consuming process for specimen preparation. Therefore, a method [19, 88] was developed to further simplify the test procedure, by removing the time-consuming specimen preparation procedure and enabling the use of only one ring specimen to determine the residual hoop stress distribution. This method is referred to as one-slit-ring method here, which is based on the assumption that the following exponential function can describe the residual hoop stress distribution.

$$\sigma_{\text{res}} = C_1 + C_2 e^{kx} \tag{4.1}$$

where σ_{res} is the residual hoop stress, x the normalized position along the wall thickness direction, with 0 being the inner surface and 1 the outer surface, and C_1, C_2 and k constants. Since residual stress in pipes is generated from an inhomogeneous cooling process where the temperature gradient also follows an exponential function [70], it is reasonable to use the expression given in Eq. (4.1) to describe the residual stress variation across the pipe wall thickness.

As suggested in ref. [19], k in Eq. (4.1) is assumed to be a material-dependent constant, thus fixed for a given material. Previous work by Poduška et al. [19, 70] showed that k value can be regarded as 3.2 for both PP and PE pipes. Following their work, based on the conditions that the total normal force on a given cross section of a slit ring specimen is zero and that the diametrical change from slitting a ring specimen is equivalent to that caused by a pure bending moment generated from the residual stress on the cross section. The work shown in ref. [19] gives the following expressions for C_1 and C_2 in Eq. (4.1).

$$C_1 = -\frac{C_2}{3.2}(e^{3.2} - 1) = -7.35C_2 \tag{4.2a}$$

$$C_2 = \frac{[(D_o - h)/2 - R](\Delta D / 2)E}{[R - (\Delta D / 2)][-0.004R + 0.004(D_o / 2 - h) - 1.68h]} \tag{4.2b}$$

where D_o is the outer diameter of the pipe, h the wall thickness, E Young's modulus, ΔD the measured diametrical change by slitting the ring, and R radius of the neutral plane.

The one-slit-ring method provides a expedient way to estimate residual hoop stress distribution in an extruded pipe as only one ring specimen is needed to establish the residual hoop stress distribution across the pipe wall thickness. However, the method is only suitable for specimens of homogeneous material properties. For ring specimens with inhomogeneous material properties, such as a core-shell structure on the cross section due to partial diffusion of primer from the specimen surface [115], the original one-slit-ring method is not applicable. Work presented in this chapter is to address this issue, by refining the approach used to derive the expressions for C_1 and C_2 so that the one-slit-ring method can be applied to pipes with non-uniform material properties.

Validity of the refined one-slit-ring method was examined using ring specimens from chlorinated polyvinyl chloride (CPVC) pipe, with a core-shell structure on the cross section generated from immersion of the ring specimens in primer for 30 minutes. The first part of the study is to verify applicability of the one-slit-ring method to CPVC pipes by comparing the residual hoop stress distribution determined from this method with that from the 13-slit-ring method. The second part of the study presents the approach we used to refine the one-slit-ring method so that it can be used to determine residual hoop stress distribution

in ring specimens that have a cross section with a core-shell structure. Using this refined one-slit-ring method, the influence of drying time after the ring specimens were immersed in primer for 30 minutes is presented. Results from finite element (FE) simulation are also presented to validate the refined one-slit-ring method.

4.2 Specimen preparation and test procedure

4.2.1 Material and specimens

Ring specimens used for the experimental testing were prepared from commercial CPVC 4120 SCH80 2-inch pipes. Nominal outer diameter and minimum wall thickness are 60.33 mm and 5.54 mm, respectively. A schematic drawing of the ring specimens is shown in Fig. 4.1, in which D_o is the original outer diameter of the ring specimen. The specimen width (w) was designed to be close to the average pipe wall thickness (h), i.e. $w/h \approx 1$, so that as indicated in ref. [87], any possible residual stress in the longitudinal direction should have a negligible effect on the measured residual stress in the hoop direction.

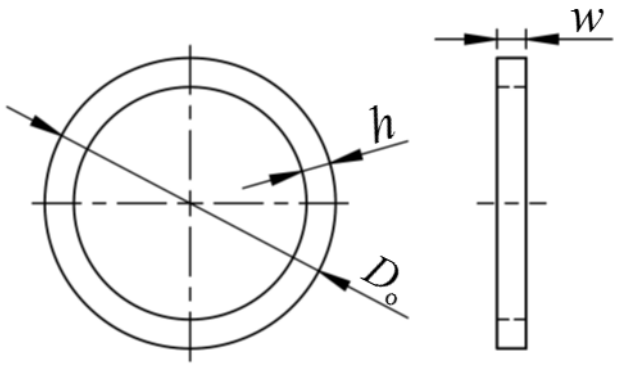

Fig. 4.1 Schematic drawing of ring specimen

The first series of tests was to use the 13-slit-ring method to establish a residual hoop stress distribution across wall thickness of CPVC pipe. The results were then used to justify suitability of the one-slit-ring method for determining the residual hoop stress distribution

in CPVC pipe. A CPVC pipe section of 2 inches in diameter was used to prepare ring specimens of different diameters that were needed for the 13-slit-ring method. Four duplicates were used for each specimen dimension, to verify repeatability of the test results. The specimen preparation procedure followed that described in ref. [70], that is, by removing either i ($i \le 6$) layers of material from the inner surface or o ($o \le 6$) layers from the outer surface, and with each layer being one-tenth of the average pipe wall thickness (h). Therefore, a ring specimen with i inner layers or o outer layers removed, denoted as specimen-io, has the wall thickness of $h-(i+o)h/10$. Note that ring specimens used in the current study have a width (w) that is the same as the average wall thickness of the CPVC pipe section, which is different from those used in ref. [70] which used a constant w value of 8 mm.

In addition to the above specimens io which have i and o layers removal from the inner and outer surfaces, respectively, another set of ring specimens with wall thickness that is the same as that of the original pipe section, was prepared. Some of these ring specimens were immersed in primer for 30 minutes, and dried in air for different periods of time, i.e., 0.5, 3.5, 7, 10.5, 20, 30, 40 and 113 days, to be referred to as wet specimens and denoted as W0.5, W3.5, W7, W10.5, W20, W30, W40 and W113, respectively. The drying procedure for the first 3.5 days was to place the wet specimens in a fume hood at room temperature, and for the remaining drying time the specimens were placed in an oven set at 30°C. The ring specimens without any primer treatment are denoted as dry specimens.

4.2.2 Test procedure

An accurate ring-cutting process and measurement of the outer diameter change are essential for the one-slit-ring method to determine the correct residual hoop stress

distribution across the pipe wall thickness. In this study, an in-house-designed mold, manufactured using 3D printing of poly(acrylonitrile-butadiene-styrene) (ABS), was used to ensure consistency in the ring-cutting process. The 3D-printed mold, as shown in Fig. 4.2(a), has a shape of equilateral triangle, for accurate cutting of a 120-degree arc segment from the ring specimens. Slots were introduced to the mold frame so that a razor blade can be accurately placed in the cutting position. The diametrical change of the specimen from the cutting was measured using a non-contact Optical Comparator (MITUTOYO PH-3500) which has a measurement resolution of 1 μm. Since the measurement was not through any contact, possible errors due to contact were eliminated. Figure 4.2(b) shows the set-up of the Optical Comparator for the diametrical measurement.

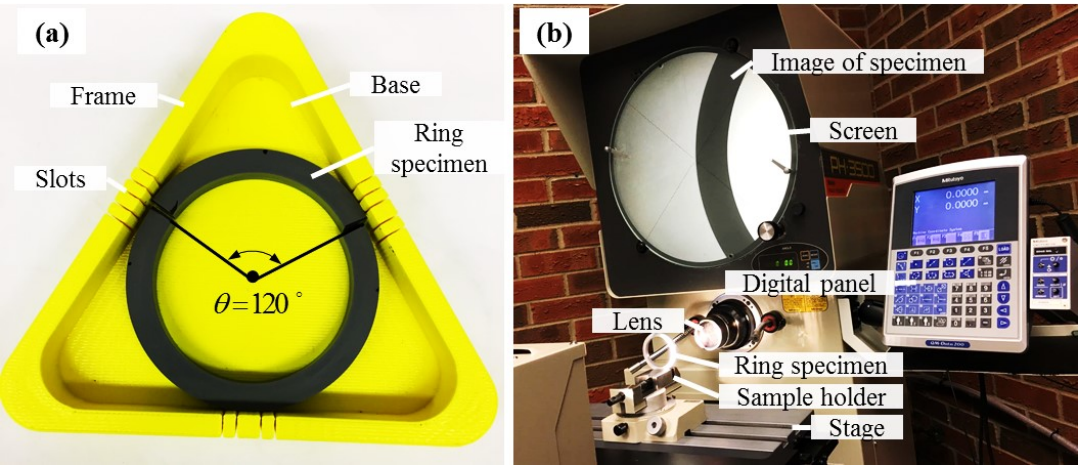

Fig. 4.2 (a) 3D-printed mold and (b) set-up of the Optical Comparator for measurement of outer diameter change

4.3 Measurement of residual hoop stress using 13-slit-ring and one-slit-ring methods

Figure 4.3 summarizes the measured outer diameter changes of 13 ring specimens with different *io* values, after cutting off an arc section of 120°. Bars in the figure indicate the maximum and minimum values of the outer diameter changes.

Due to viscous nature of plastic materials, the diameter of the ring specimens after the cutting is expected to vary with time [66, 86], and thus, the diameter change for all specimens was measured immediately after cutting, to ensure consistency of the measurement. The elastic modulus used in the residual stress calculation, determined using FE analysis as to be detailed later, was set to be 2,100 MPa. Following the procedure detailed in ref. [70], the residual stress values are summarized in Fig. 4.4 using open squares (□), plotted as a function of relative position along the pipe wall thickness direction, x.

Figure 4.4 also includes two fitting curves. The curve represented by the dashed line is based on the best fit using a MATLAB program that allows variation for all three parameters (C_1, C_2, and k). The other curve, represented by the solid line, is based on the best fit by varying C_1 and C_2 values, with k fixed at 3.2. Figure 4.4 shows clearly that the two curves almost overlap with each other, suggesting that it is possible to express the variation of residual hoop stress using an expression with a k value fixed at 3.2, thus allowing variation of C_1 and C_2 only. In view of this possibility, the one-slit-ring method, with a k value set at 3.2, was used in the rest of the study to analyze the residual hoop stress distribution in CPVC pipe ring specimens.

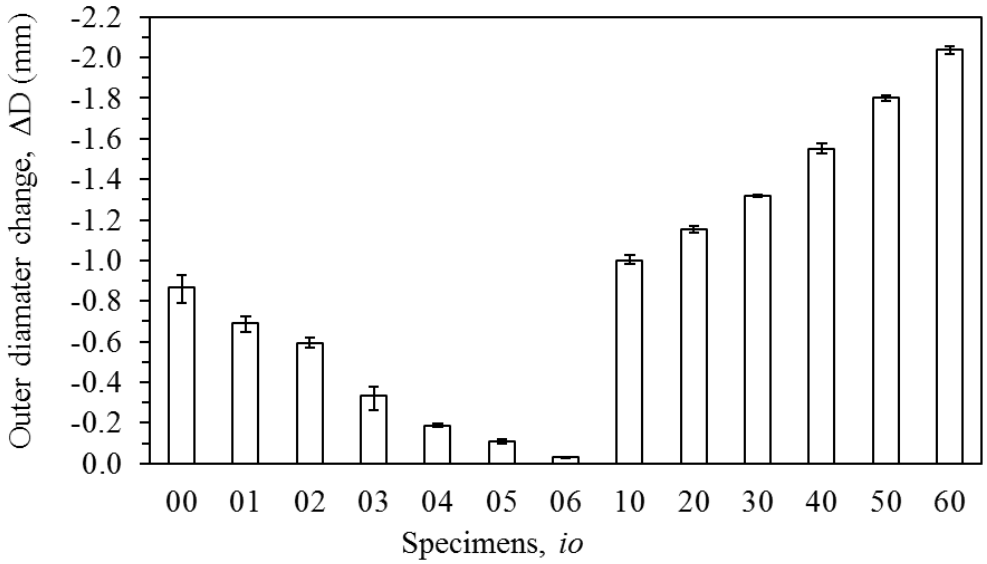

Fig. 4.3 Summary of outer diameter changes of thirteen slit ring specimens

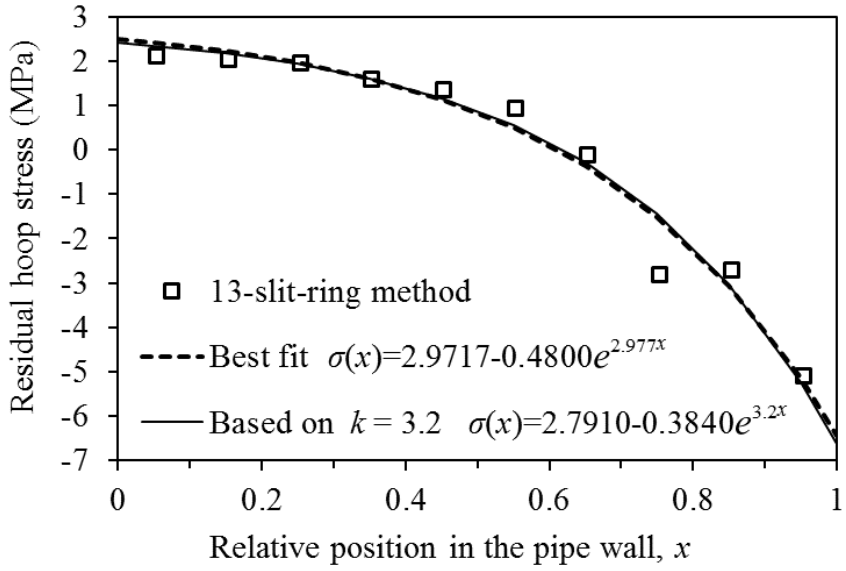

Fig. 4.4 The measured residual hoop stress distribution using the 13-slit-ring method (□) and two curves that are used to fit the measured values

4.4 Refinement of the one-slit-ring method

As mentioned earlier, the original one-slit-ring method [19] is only applicable to ring specimens of uniform mechanical properties. After the immersion in primer for 30 minutes, however, the ring specimens develop a core-shell structure on the cross section with

different mechanical properties. Therefore, the original one-slit-ring method is no longer applicable. In view of this limitation, the one-slit-ring method has been refined to extend its applicability to specimens with cross section of a core-shell structure. This section details derivation of expressions for the original and the refined one-slit-ring method. It should be noted that derivation of the expression for C_2 below considers the possible change of the neutral plane on the cross section during bending of the curved beam, while in the original expression in ref. [19], as given in Eq. (4.2b), the derivation was based on the assumption that the neutral plane position on the cross section is fixed, not changing with deformation. Nevertheless, in the scenario of small deformation considered in this study, the difference of the C_2 value from the two derivation approaches is very small.

4.4.1 The original one-slit-ring method

As suggested in ref. [70], the key concept for the slit-ring method is based on the following two assumptions. One is that the resultant normal force from the residual stress on the cross section is zero, and the other that the diameter change from the slitting is equivalent to the diameter change caused by a bending moment generated from the residual hoop stress on the cross section.

Based on the curved beam theory [116], under pure bending and for small deformation, hoop stress $\sigma(r)$ (representing residual hoop stress in this study) can be expressed in terms of the change in central angle of the curved beam as a function of radius r, as expressed below.

$$\sigma(r) = -\frac{E\Delta\theta}{\theta}\frac{R-r}{r} \tag{4.3}$$

where E is the elastic modulus in the hoop direction, θ and R central angle and radius

of the neutral plane, respectively, of the curved beam before $\sigma(r)$ is applied, and $\Delta\theta$ the change of θ due to the application of $\sigma(r)$.

Since total arc length along the neutral plane remains constant during the deformation, we have

$$R \cdot \theta = R_{\mathrm{d}} \cdot (\theta + \Delta\theta) \tag{4.4}$$

where R_{d} is the radius of the neutral plane for the deformed beam after the central angle is changed to $\theta + \Delta\theta$.

With Eq. (4.3) for the expression of $\sigma(r)$, equilibrium of normal force on the cross section can be expressed as

$$F = \int_{D_{\mathrm{o}}/2-h}^{D_{\mathrm{o}}/2} (-\frac{E\Delta\theta}{\theta}\frac{R-r}{r}) w dr = 0 \tag{4.5}$$

and bending moment (M) generated by $\sigma(r)$ as

$$M = \int_{D_{\mathrm{o}}/2-h}^{D_{\mathrm{o}}/2} -(R-r)(-\frac{E\Delta\theta}{\theta}\frac{R-r}{r}) w dr \tag{4.6}$$

where reference for the bending moment is based on ring specimen before the slitting, w the ring specimen width, h pipe wall thickness, and D_{o} the outer diameter of the ring specimen before the slitting.

From Eq. (4.5), with fixed values for E, w and $\Delta\theta/\theta$, we have

$$R = \frac{h}{\ln\dfrac{D_{\mathrm{o}}}{D_{\mathrm{o}} - 2h}} \tag{4.7a}$$

Similarly, the radius of the neutral plane in the deformed beam is

$$R_{\mathrm{d}} = \frac{h}{\ln \dfrac{D_{\mathrm{o}} + \Delta D}{D_{\mathrm{o}} + \Delta D - 2h}} \tag{4.7b}$$

By replacing $\Delta\theta/\theta$ in Eq. (4.6) by $R/R_{\mathrm{d}} - 1$ from expression (4.4), through integration, Eq. (4.6) gives

$$M = \frac{(R - R_{\mathrm{d}})(D_{\mathrm{o}} - h - 2R)Ehw}{2R_{\mathrm{d}}} \tag{4.8}$$

Alternatively, rather than expressing $\sigma(r)$ using Eq. (4.3), since $\sigma(r)$ is residual hoop stress generated from the pipe cooling process, it can be expressed using Eq. (4.1) with $k = 3.2$. Then, the expressions for force equilibrium and bending moment (M_{r}) on the cross section are:

$$\int_0^1 (C_1 + C_2 e^{3.2x}) whdx = 0 \tag{4.9}$$

$$M_{\mathrm{r}} = \int_0^1 (C_1 + C_2 e^{3.2x})(x_{\mathrm{n}} - x) wh^2 dx \tag{4.10}$$

where x_{n} is the normalized position of neutral plane on the cross section. That is,

$$C_1 + C_2 e^{3.2x_{\mathrm{n}}} = 0 \tag{4.11}$$

With the consideration of small deformation and thus conservation of the cross-sectional area (wh) during the deformation, Eq. (4.9) gives the following relationship between C_1 and C_2.

$$C_1 = \frac{1 - e^{3.2}}{3.2} C_2 \approx -7.354 C_2 \tag{4.12}$$

From Eq. (4.11) :

$$x_{\mathrm{n}} = \frac{\ln((e^{3.2} - 1)/3.2)}{3.2} \approx 0.6235 \tag{4.13}$$

By substituting C_1 and x_{n} from Eqs. (4.12) and (4.13) into Eq. (4.10), and through integration, we have

$$M_{\mathrm{r}} = -1.691 w h^2 C_2$$

The above expression for M can then be combined with Eq. (4.8), to obtain the following expression for C_2:

$$C_2 = \frac{-(D_{\mathrm{o}} - h - 2R)(R - R_{\mathrm{d}})E}{3.382 h R_{\mathrm{d}}} \tag{4.14}$$

Since values for the geometrical terms on the right hand side of Eq. (4.14) are either measured (D_{o} and h), or calculated (R and R_{d}) using Eqs. (4.7a) and (4.7b) based on the measured value of ΔD, the residual hoop stress distribution based on Eq. (4.1) can be determined from the value of ΔD. Note that the unit for E used in above expressions is MPa and that the value of k in Eq. (4.1) is 3.2.

4.4.2 The refined one-slit-ring method (for cross section with a core-shell structure)

In view that after the immersion in primer for 30 minutes, due to diffusion of primer from the specimen surface, the cross section of ring specimens develops a core-shell structure with different mechanical properties. Therefore, this type of slit ring specimens can be regarded as a composite curved beam, as shown in Fig. 4.5(a), in which the cross section consists of 5 zones, each of which has uniform mechanical properties. In the following derivation, all four zones in the shell region are assumed to have the same mechanical properties. Therefore, the cross section is regarded as two phases with different E values. As reported previously [115], after immersion of the ring specimens in primer

for 30 minutes, the area ratio of the shell region to the whole cross section is around 32% which does not change when increasing the drying time. This allows us to calculate thickness (a) of the shell region using the following expression.

$$1-\frac{(w-2a)(h-2a)}{wh}=32\% \tag{4.15}$$

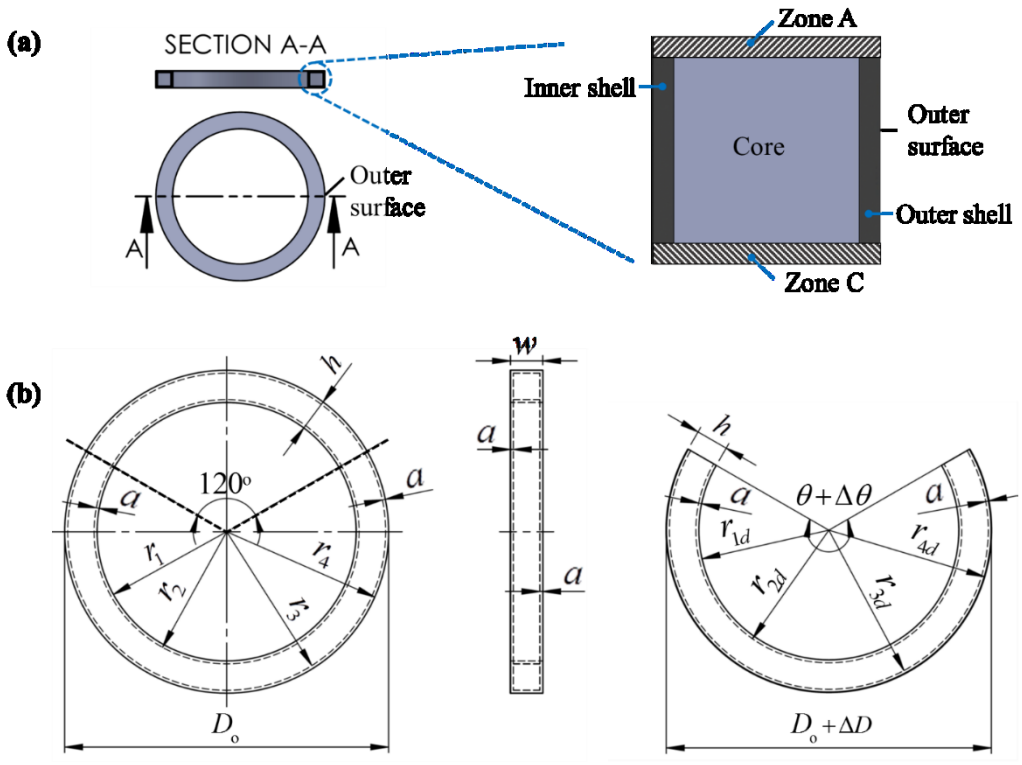

Fig. 4.5 Schematic depiction of (a) core-shell structure with the zone partition in which zone B consists of three regions: inner shell, core and outer shell, and (b) notation of dimensions: full ring(left) and slit-ring (right).

Figure 4.5(a) depicts the core-shell structure of a ring specimen after the immersion in primer. As shown in the right diagram of Fig. 4.5(a), the core-shell structure is divided into zones A, B and C of which zones A and C consist of the shell material only, and thus have uniform elastic modulus. Zone B, on the other hand, consists of inner shell (left), core (middle), and outer shell (right) with different elastic modulus values. These values are

summarized below, based on notation defined in Fig. 4.5(b).

$$\text{In zones A and C:} \quad E(r) = E_s \text{ for } r \in [r_1, r_4]$$

$$\text{In zone B:} \quad E(r) = \begin{cases} E_c & \text{for } r \in [r_2, r_3] \\ E_s & \text{for } r \in [r_1, r_2) \cup (r_3, r_4] \end{cases} \tag{4.16}$$

where E_s is the elastic modulus for the shell region and E_c for the core region. Here, since the core region is not affected by the primer, its value for elastic modulus (E_c) is assumed to be same as that for the dry specimen, i.e. without immersion in primer. The value for E_s is determined from FE simulation, as to be detailed in Section 4.5.1. Note that in the following derivation, r with subscript including "d" stands for radius after the specimen is slit, as shown in the right figure of Fig. 4.5(b). Note that all r_i values in Fig. 4.5(b) (for i from 1 to 4) can be expressed in terms of D_o, a, h and ΔD.

$$r_1 = \frac{D_o}{2} - h,\ r_2 = \frac{D_o}{2} - h + a,\ r_3 = \frac{D_o}{2} - a,\ r_4 = \frac{D_o}{2} \text{ and } r_{id} = r_i + \frac{\Delta D}{2} \quad (i = 1, 2, 3, 4)$$

The derivation of the expression for the residual hoop stress distribution in the ring specimens with a core-shell structure cross section is based on the same approach as that described above, that is, the residual hoop stress distribution follows Eq. (4.1), its resultant total force on the cross section is equal to zero, and the diameter change by slitting the ring is equal to the diameter change from bending moment generated from the residual hoop stress on the cross section. The main difference of the derivation here from that in the previous section is that coefficients C_1 and C_2 in Eq. (4.1) may have different values in difference regions of the cross section, due to the possible difference in elastic modulus. Furthermore, it is assumed here that zones A, B and C in Fig. 4.5(a) share the same neutral plane of which the radius is denoted as R_w. Note that Eq. (4.3) can still be used to describe

the hoop stress distribution on the cross section of the composite beam with a core-shell structure on the cross section, but the value for E may vary with location on the cross section.

The resultant total force from the residual hoop stress on each zone of Fig. 4.5(a), namely F_{A}, F_{B} and F_{C} for zones A, B and C, respectively, can be expressed using the following equations based on Eq. (4.3), with the corresponding value for E given in Eq. (4.16).

In zones A and C:
$$F_{\mathrm{A}} = F_{\mathrm{C}} = \int_{r_1}^{r_4} \frac{-E_{\mathrm{s}}\Delta\theta}{\theta}\left(\frac{R_{\mathrm{w}} - r}{r}\right) a\,dr \tag{4.17a}$$

In zone B:

$$F_{\mathrm{B}} = \int_{r_1}^{r_2} \frac{-E_{\mathrm{s}}\Delta\theta}{\theta}\left(\frac{R_{\mathrm{w}}' - r}{r}\right)(w-2a)\,dr + \int_{r_2}^{r_3} \frac{-E_{\mathrm{c}}\Delta\theta}{\theta}\left(\frac{R_{\mathrm{w}}' - r}{r}\right)(w-2a)\,dr + \int_{r_3}^{r_4} \frac{-E_{\mathrm{s}}\Delta\theta}{\theta}\left(\frac{R_{\mathrm{w}}' - r}{r}\right)(w-2a)\,dr \tag{4.17b}$$

where R_{w} in Eq. (4.17a) represents the radius of neutral plane of zones A and C, while R_{w}' in Eq. (4.17b) is the radius of neutral plane of zone B. As mentioned earlier, the derivation presented here is based on the assumption that the difference between R_{w} and R_{w}' is negligible. This assumption is examined here, as shown below.

From Eq. (4.17a), with a fixed value for $\Delta\theta/\theta$ and $F_{\mathrm{A}} = 0$, we have

$$R_{\mathrm{w}} = \frac{r_4 - r_1}{\ln\frac{r_4}{r_1}} \tag{4.18a}$$

Similarly, from Eq. (4.17b), we have

$$R_{\mathrm{w}}^{'}=\frac{E_{\mathrm{s}}(r_2-r_1)+E_{\mathrm{c}}(r_3-r_2)+E_{\mathrm{s}}(r_4-r_3)}{E_{\mathrm{s}}\ln\frac{r_2}{r_1}+E_{\mathrm{c}}\ln\frac{r_3}{r_2}+E_{\mathrm{s}}\ln\frac{r_4}{r_3}} \tag{4.18b}$$

In the worst case scenario that difference between R_{w} and $R_{\mathrm{w}}^{'}$ is biggest when $E_{\mathrm{s}}=0$, Eq. (4.18b) becomes

$$R_{\mathrm{w}}^{'}=\frac{r_3-r_2}{\ln\frac{r_3}{r_2}} \tag{4.19}$$

With $w=h$, Eq. (4.15) gives $a=0.088h$ which yields the difference between R_{w} and $R_{\mathrm{w}}^{'}$ of only 0.14%. Therefore, the three zones in Fig. 4.5(a) can be assumed to have the same neutral plane.

In view of the closeness of neutral plane positions for zones A, B and C, and simplicity of the expression for the radius of the neutral plane for zone A, i.e. Eq. (4.18a), the radius for the common neutral plane on the cross section of the composite curved beam (Fig. 4.5) hereafter will be expressed in terms Eq. (4.18a), and after slitting, the radius of the neutral plane (R_{wd}) is expressed as:

$$R_{\mathrm{wd}}=\frac{r_{4\mathrm{d}}-r_{1\mathrm{d}}}{\ln\frac{r_{4\mathrm{d}}}{r_{1\mathrm{d}}}} \tag{4.20}$$

Based on the independence of arc length along the neutral plane on the deformation, we have

$$R_{\mathrm{w}}\cdot\theta=R_{\mathrm{wd}}\cdot(\theta+\Delta\theta) \tag{4.21}$$

With Eqs. (4.18a) and (4.20) for positions of the neutral planes before and after slitting, respectively, the bending moment (M_{w}) generated by residual hoop stress on the cross

section of the wet ring specimens can be expressed as:

$$M_{\mathrm{w}} = \left(\int_{r_1}^{r_2} + \int_{r_3}^{r_4}\right) \frac{E_{\mathrm{s}}\Delta\theta(R_{\mathrm{w}} - r)^2}{\theta \cdot r}(w - 2a)dr + \int_{r_2}^{r_3} \frac{E_{\mathrm{c}}\Delta\theta(R_{\mathrm{w}} - r)^2}{\theta \cdot r}(w - 2a)dr + 2\int_{r_1}^{r_4} \frac{E_{\mathrm{s}}\Delta\theta(R_{\mathrm{w}} - r)^2}{\theta \cdot r}adr$$

with $\frac{\Delta\theta}{\theta} = \frac{R_{\mathrm{w}}}{R_{\mathrm{wd}}} - 1$ from Eq. (4.21), the above equation can be rewritten as

$$M_{\mathrm{w}} = \frac{(R_{\mathrm{w}} - R_{\mathrm{wd}})}{R_{\mathrm{wd}}}\left[\left(\int_{r_1}^{r_2} + \int_{r_3}^{r_4}\right) \frac{E_{\mathrm{s}}(R_{\mathrm{w}} - r)^2}{r}(w - 2a)dr + \int_{r_2}^{r_3} \frac{E_{\mathrm{c}}(R_{\mathrm{w}} - r)^2}{r}(w - 2a)dr + 2\int_{r_1}^{r_4} \frac{E_{\mathrm{s}}(R_{\mathrm{w}} - r)^2}{r}adr\right] \tag{4.22}$$

Equation (4.22) allows the use of the R_{wd} value, calculated from Eq. (4.20), to determine M_{w}, provided that values for E_{s} and E_{c} are known. With M_{w} determined, the expression for the distribution of residual hoop stress in the wet ring specimens with a core-shell structure on the cross section can then be derived using the following procedure.

The exponential function given in Eq. (4.1), with $k = 3.2$, was also used to express the residual hoop stress distribution in each region of the wet ring specimens with the same mechanical properties. Since values for coefficients C_1 and C_2 may be different for regions of different mechanical properties, these coefficients are denoted with the corresponding zone included in the subscript. That is, C_{A1} and C_{A2} are coefficients for zone A in Fig. 4.5(a), and C_{C1} and C_{C2} for zone C. For zone B that consists of inner shell, outer shell and core region, C_{i1} and C_{i2} are used for inner shell, C_{o1} and C_{o2} for the outer shell, and C_{co1} and C_{co2} for the core region. Therefore, five equations are used to describe the residual hoop stress distribution on the cross section of wet ring specimens, with totally

ten coefficients for which values need to be determined. That is,

zone A: $\sigma_{\mathrm{A}}(x) = C_{\mathrm{A1}} + C_{\mathrm{A2}} e^{3.2x}$

inner shell of zone B: $\sigma_{\mathrm{is}}(x) = C_{\mathrm{i1}} + C_{\mathrm{i2}} e^{3.2x}$

core region of zone B: $\sigma_{\mathrm{co}}(x) = C_{\mathrm{co1}} + C_{\mathrm{co2}} e^{3.2x}$ (4.23)

outer shell of zone B: $\sigma_{\mathrm{os}}(x) = C_{\mathrm{o1}} + C_{\mathrm{o2}} e^{3.2x}$

zone C: $\sigma_{\mathrm{C}}(x) = C_{\mathrm{C1}} + C_{\mathrm{C2}} e^{3.2x}$

with the condition of strain compatibility at the interface and uniaxial loading, it can be shown that

$$C_{\mathrm{A1}} = C_{\mathrm{i1}} = C_{\mathrm{o1}} = C_{\mathrm{C1}} = \frac{E_{\mathrm{s}}}{E_{\mathrm{c}}} C_{\mathrm{co1}}$$
$$C_{\mathrm{A2}} = C_{\mathrm{i2}} = C_{\mathrm{o2}} = C_{\mathrm{C2}} = \frac{E_{\mathrm{s}}}{E_{\mathrm{c}}} C_{\mathrm{co2}} \quad (4.24)$$

Therefore, for convenience, C_{sh1} is used to represent the value for C_{A1}, C_{i1}, C_{o1} and C_{C1} (i.e., C_1 for the shell region) and C_{sh2} for C_{A2}, C_{i2}, C_{o2} and C_{C2} (i.e., C_2 for the shell region). Equation (4.25) below summarizes the relationships between coefficients for the shell region and those for the core region,

$$C_{\mathrm{sh1}} = \frac{E_{\mathrm{s}}}{E_{\mathrm{c}}} C_{\mathrm{co1}}$$
$$C_{\mathrm{sh2}} = \frac{E_{\mathrm{s}}}{E_{\mathrm{c}}} C_{\mathrm{co2}} \quad (4.25)$$

and Eq. (4.26) to describe the distribution of residual hoop stress on the whole cross section of wet ring specimens:

In the core region: $\sigma_{co}(x) = C_{co1} + C_{co2}e^{3.2x}$

In the shell region: $\sigma_{sh}(x) = C_{sh1} + C_{sh2}e^{3.2x}$ (4.26)

where $\sigma_{co}(x)$ represents the residual hoop stress in the core region, and $\sigma_{sh}(x)$ in the shell region. Note that as before, x represents the position in the radial direction, normalized by h, with 0 being on the inner surface and 1 on the outer surface. The value for x at the interface between the inner shell and the core region is set to be x_1, and between the core region and the outer shell x_2. For the wet specimens with a square cross section,

$$x_1 = \frac{a}{h} \text{ and } x_2 = \frac{h-a}{h}$$

Equation (4.25) indicates that only values for two independent unknowns, such as C_{co1} and C_{co2} need to be determined in order to establish the residual hoop stress distribution in the wet ring specimens. Those two unknowns can be determined using the force equilibrium condition for the residual hoop stresses on the cross section [86, 117] and bending moment from the residual hoop stress to generate the diameter change ΔD, as expressed below.

For force equilibrium on the cross section (F_t):

$$F_t = 2\int_0^1 \sigma_{sh}(x)ahdx + [\int_0^{x_1} \sigma_{sh}(x)dx + \int_{x_1}^{x_2} \sigma_{co}(x)dx + \int_{x_2}^1 \sigma_{sh}(x)dx](w-2a)h = 0 \quad (4.27)$$

For bending moment (M_t) resulted from the residual hoop stress on the cross section:

$$M_t = 2\int_0^1 \sigma_{sh}(x_n - x)ah^2dx + [\int_0^{x_1} \sigma_{sh}(x_n - x)dx + \int_{x_1}^{x_2} \sigma_{co}(x_n - x)dx + \int_{x_2}^1 \sigma_{sh}(x_n - x)dx](w-2a)h^2 \quad (4.28)$$

Since mechanical properties in zones A and C are uniform, their neutral plane position

(x_n) can be determined using Eq. (4.11), as given in Eq. (4.29) below. With the assumption of a common neutral plane for the three zones on the cross section of a composite curved beam and Eq. (4.25), the neutral plane position in zone B (x_n') can be expressed using Eq. (4.30).

$$x_n = \ln(\frac{-C_{sh1}}{C_{sh2}}) / 3.2 \tag{4.29}$$

$$x_n' = \ln(\frac{-C_{co1}}{C_{co2}}) / 3.2 \tag{4.30}$$

By substituting Eq. (4.26) into Eq. (4.27), with Eq. (4.25), we have the first equation for coefficients C_{co1} and C_{co2}.

$$C_{co2} = \frac{\{3.2(w-2a)(x_2-x_1) - \frac{3.2E_s}{E_c}[2a+(w-2a)(1-x_2+x_1)]\}C_{co1}}{(w-2a)(e^{3.2x_2}-e^{3.2x_1}) + \frac{E_s}{E_c}[(w-2a)(e^{3.2}-e^{3.2x_2}+e^{3.2x_1}-1)+2a(e^{3.2}-1)]} \tag{4.31}$$

Similarly, by substituting Eqs. (4.26) and (4.29) into Eq. (4.28), we have

$$\begin{aligned} M_t = (w-2a)h^2(\frac{E_s}{E_c}\int_0^{x_1} + \frac{E_s}{E_c}\int_{x_2}^{1} + \int_{x_1}^{x_2})[(C_{co1}+C_{co2}e^{3.2x})(\ln(\frac{-C_{co1}}{C_{co2}})/3.2 - x)]dx \\ + 2ah^2\frac{E_s}{E_c}\int_0^1[(C_{co1}+C_{co2}e^{3.2x})(\ln(\frac{-C_{co1}}{C_{co2}})/3.2 - x)]dx \end{aligned} \tag{4.32}$$

Since value for M_t can be calculated from Eq. (4.22) using the measured ΔD value, Eq. (4.32) provides the second equation for coefficients C_{co1} and C_{co2}. With known values for E_s and E_c, Eqs. (4.31) and (4.32) can be used to determine the expressions for coefficients C_{co1} and C_{co2}, which can then be used to determine the expressions for C_{sh1} and C_{sh2} using Eq. (4.25). As mentioned earlier, the value for E_c is assumed to be the

same as that for the dry ring specimens, which was used to determine the value for E_s through FE simulation, as detailed in section 4.5.1. The FE simulation was also used to verify the validity of the above analytical expressions for the residual hoop stress distribution on the cross section of wet ring specimens, as detailed in section 4.5.2.

4.5 Finite element simulation

The finite element simulation was conducted using ABAQUS 6.13-4 for the following two tasks: (1) to determine the elastic moduli of the core and shell regions of the wet ring specimens, and (2) to verify the residual hoop stress distribution established using the refined one-slit-ring method.

4.5.1 Elastic moduli

In this study, the elastic moduli of CPVC pipe material after exposure to primer were determined using result from the D-split tensile test [64], with the assistance of FE simulation, where the regeneration of experimental data was achieved. The results of experimental data were reported in previous work [115]. In this section, only the simulation part is demonstrated in detail.

Note that for a wet ring specimen with a core-shell structure on the cross section, a 3D model is needed to provide proper simulation. The FE model consists of one quarter of a ring specimen with a geometry identical to that for the specimen used for the testing, and half of the top D block which is modelled as an analytical rigid body. Note that since immersion of ring specimens in primer caused swelling and the extent of swelling changed with the drying time, nine FE models were built so that each model has dimensions identical to one of the dry, W0.5, W3.5, W7, W10.5, W20, W30, W40 and W113

specimens. Fig. 4.6(a) gives an example of the FE model which is for a W0.5 specimen. Figure. 4.6(b) shows the cross section of the specimen, with the core-shell structure, based on the experimental measurement, shown on the top, and the mesh pattern at the bottom.

In addition to the above consideration, a mesh-dependency analysis was conducted to determine the appropriate mesh size, as shown in Fig. 4.6(c) in which the simulation results, based on the maximum von Mises stress within the model at the applied stroke as 1 mm, are plotted as a function of the total number of elements. The plot suggests that the model with around 100,000 elements, as indicated by an arrow in Fig. 4.6(c), provides reasonable independency of the mesh size of which the mesh pattern is depicted in Fig. 4.6(a) and (b). Note that it was chosen to have an element size along the 90^{o}-arc contour with double bias, from the minimum of 0.3 mm at two ends of the 90^{o}-arc to the maximum of 0.6 mm in the middle, and a uniform element size of 0.2 mm on the cross section, resulting in 98100 C3D8R elements in total.

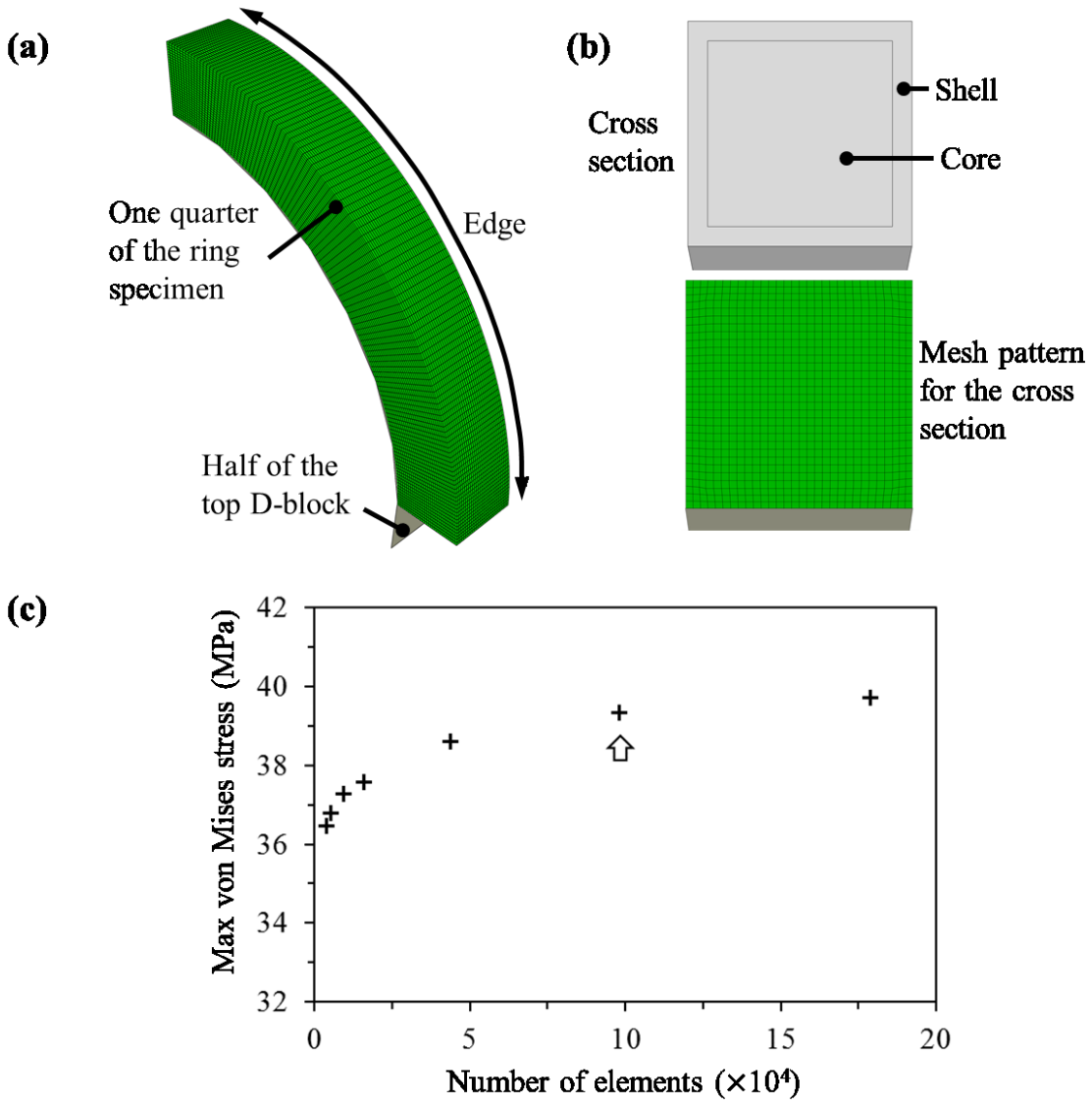

Fig. 4.6 FE model of W0.5 ring specimen: (a) the overall model, (b) cross section, and (c) mesh dependency analysis

In addition to the symmetry boundary conditions, displacement control was applied to the block to record load and displacement in order to generate the engineering stress-stroke curves from the model. The elastic modulus for the core region, E_c, was first determined by adjusting iteratively elastic modulus of the FE model for the dry specimen so that results of engineering stress versus stroke from the FE model fit the corresponding results from

the experimental testing. Then, FE models of wet ring specimens were used in the same iterative process, to determine the elastic modulus of the shell region, E_s, as a function of drying time.

4.5.2 Simulation of residual hoop stress

This part of FE simulation was to apply a temperature field to mimic the residual stress distribution in the ring specimens.

In this part of the FE simulation, nine FE models that were same as those used for determining elastic modulus, as discussed in section 4.5.1, were used to determine the residual hoop stress distribution in both dry and wet ring specimens. The principle for the FE simulation is similar to that presented in refs. [70, 118], but rather than applying inhomogeneous distribution of thermal expansion coefficient across the pipe wall thickness, a temperature field was used to introduce residual stress to the FE models. The function for the temperature field is given below:

$$T(x) = N \cdot e^{3.2x} \tag{4.33}$$

where x is the normalized distance from the inner surface of ring specimens, same as that defined before, and N an adjusting parameter for which the value was determined through an iterative process so that ΔD generated by the FE model of a slit ring has the same value as that measured experimentally. Once the N value is determined, the temperature field is applied to the full-ring model to determine the residual hoop stress. Figure 4.8 shows the flow chart for the FE simulation.

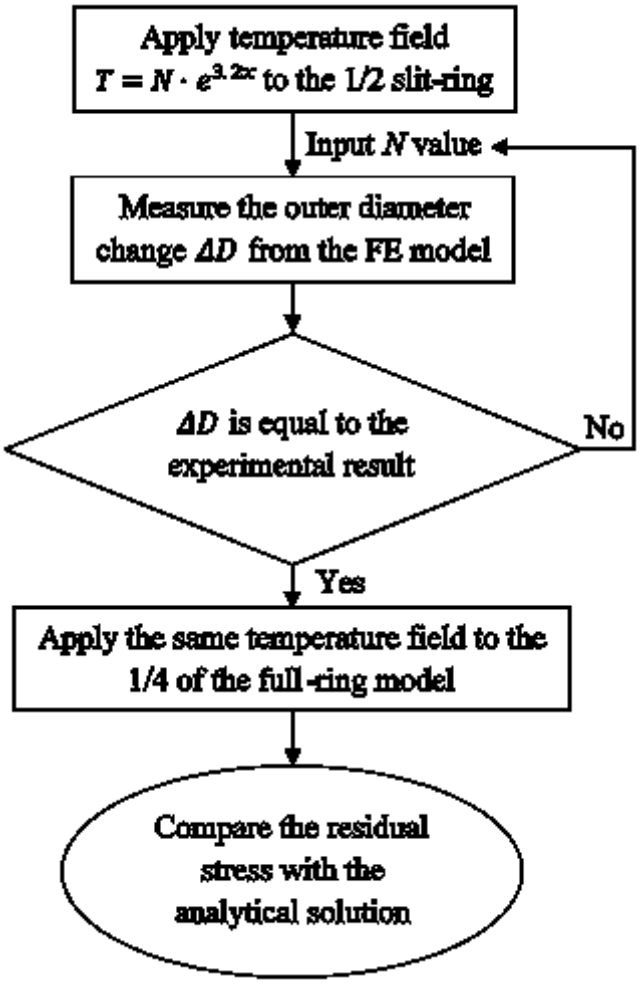

Fig. 4.7 Flow chart for determining residual hoop stress in ring specimens of CPVC pipe using FE simulation

Each of the two FE models for determining the residual hoop stress, namely, slit-ring and full-ring models, consists of three-dimensional, 8-node linear isoparametric elements with full integration (C3D8T), of which the corresponding degrees of freedom are three components of displacement and temperature. Both models are based on linear elastic material properties, with Young's modulus E of 2,100 MPa and Poisson's ratio ν of 0.42. Note that since a temperature field is used to introduce residual stress in the circumferential direction, thermal conductivity for both models is set to be $0.16\ \mathrm{W/(m \cdot K)}$ and three

components of thermal expansion coefficients of 8×10^{-5} K^{-1} in the radial and hoop directions and 0 in the specimen width direction.

4.6 Results and discussion

4.6.1 Elastic moduli and diametrical deformation

The elastic moduli for core and shell regions were adjusted in the FE models in order to generate engineering stress-stroke curves that fit the experimental curves in the linear elastic region. The elastic moduli are summarized in Fig. 4.8(a) as a function of drying time, and examples of curves from simulation and those from experiments, for dry and W0.5 specimens, are presented in Fig. 4.8 (b). Note that elastic modulus for dry specimens, with a value of 2100 MPa, is assigned to be that for the core region (E_c). Figure 4.8(a) suggests that the elastic modulus for the shell region (E_s) increases with the increase of drying time, eventually to have the same value as that for the core region.

Experimentally measured average values for the change of the outer diameter by the slitting and the range of variation (maximum and minimum, as indicated by the scattering bars) are summarized in Fig. 4.9, in terms of drying time after the immersion in primer for 30 minutes. A horizontal dashed line in the figure indicates the average diameter change of dry specimens. Note that values for ΔD in Fig. 4.9 are negative because specimens closed up after the slitting, and that absolute values of ΔD decrease with the increase of drying time.

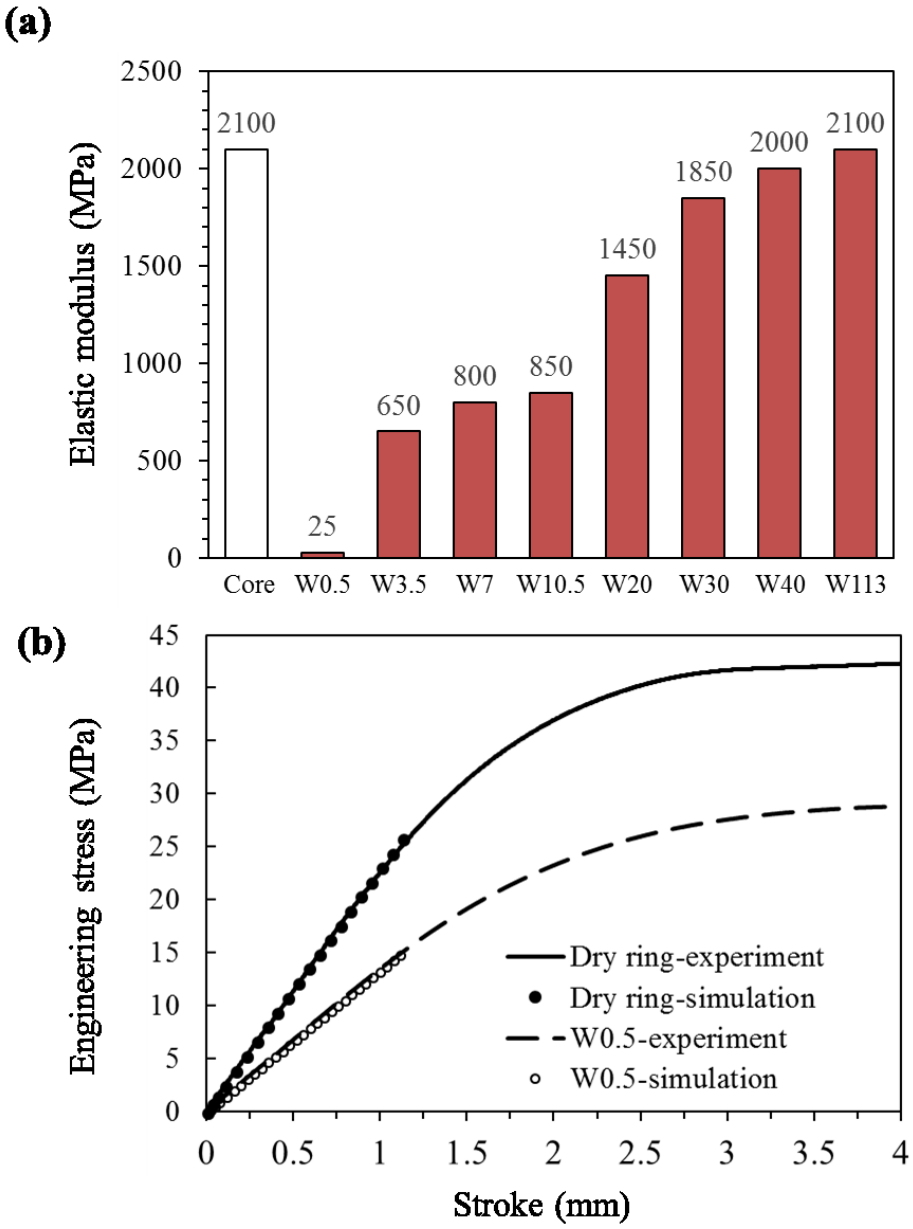

Fig. 4.8 Simulation of elastic modulus: (a) elastic moduli and (b) examples of curve fitting for dry and W0.5 specimens

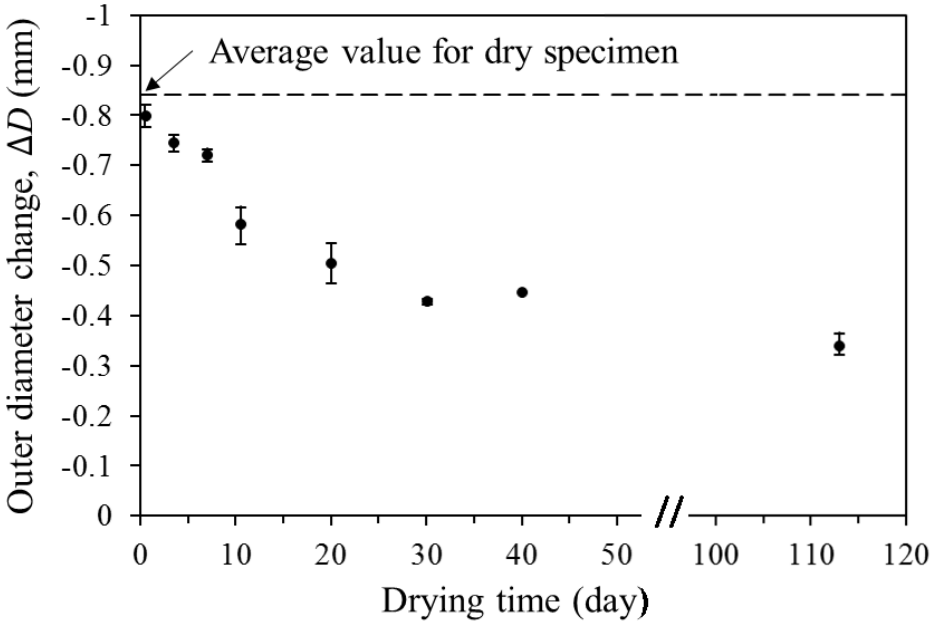

Fig. 4.9 Experimentally measured ΔD values

4.6.2 Determination of residual stress distribution

Based on the outer diameter changes through slitting the ring specimens and the corresponding elastic moduli in the core and shell regions, the variation of residual hoop stress in the dry and wet ring specimens was established using the refined one-slit-ring method proposed here. Table 4.1 summarizes values for four coefficients (C_{co1}, C_{co2}, C_{sh1}, and C_{sh2}) that are needed to use Eq. (4.26) to describe the residual hoop stress distribution in the dry and wet ring specimens after the immersion in primer. Note that for W113, coefficients for the core and shell regions have the same values, since their elastic moduli are the same, as indicated in Fig. 4.8(a).

Table 4.1 Summary of values for coefficients used in Eq. (4.26) to described residual hoop stress distributions in dry and wet specimens

Dry specimen	$C_1 = 2.7353$		$C_2 = -0.3720$	
Wet specimens	C_{co1}	C_{co2}	C_{sh1}	C_{sh2}
W0.5	2.5734	-0.3934	0.0306	-0.0047
W3.5	2.4613	-0.3591	0.7618	-0.1112
W7	2.3814	-0.3463	0.7938	-0.1154
W10.5	1.9475	-0.2806	0.7883	-0.1136
W20	1.5412	-0.2153	1.0624	-0.1486
W30	1.4494	-0.1990	1.2768	-0.1753
W40	1.5301	-0.2088	1.4572	-0.1989
W113	1.1145	-0.1516	1.1145	-0.1516

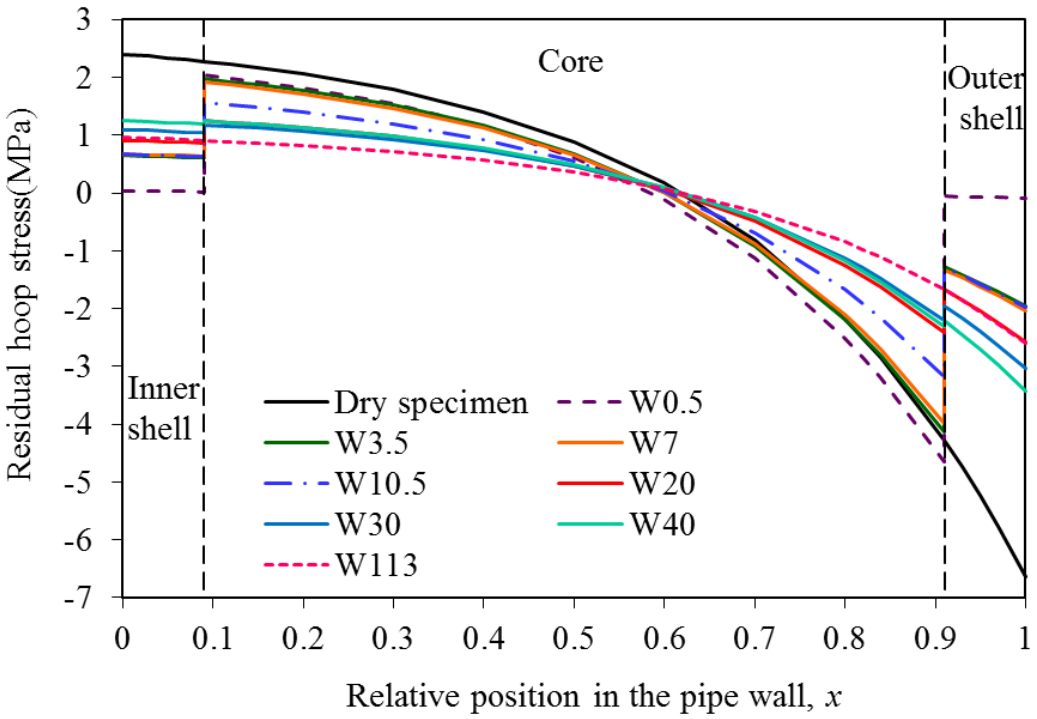

Fig. 4.10 Analytical results of residual hoop stress (Figure with curves in color is available in the electronic version)

Using information in Table 4.1, residual hoop stress distributions along the pipe wall

thickness were obtained and plotted in Fig. 4.10 as a function of relative position in the pipe wall. The figure also includes the residual hoop stress in dry specimens for comparison. The figure used vertical dashed lines to distinguish the three zones on the cross section of wet specimens, i.e., inner shell (left), core (middle) and outer shell (right). The figure shows that wet specimens have the inner shells in tension and the outer shells in compression. The figure also shows that residual hoop tensile stress in dry specimens is higher than that in wet specimens at the same relative position, x.

To further illustrate how the drying time affects residual hoop stress in the CPVC pipe ring specimens, the maximum tensile residual hoop stress in the core region which occurs at the location adjacent to the inner shell are plotted in Fig. 4.11 as a function of drying time. The figure also includes the tensile residual hoop stress in dry specimens at the same relative coordinate as wet specimens, indicated using a horizontal dashed line across the figure. Fig. 4.11 shows clearly that with the increase of drying time, the maximum residual stress in wet specimens decreased significantly in the first 30 days, and then the rate of change becomes much reduced, to a value of around 1 MPa after the drying time of 113 days. It should be noted that if the original one-slit-ring method were used to establish the residual hoop stress distribution in wet specimens, discontinuity of the curves shown in Fig. 4.12 would not be realized and the maximum residual hoop stress level be wrongly estimated.

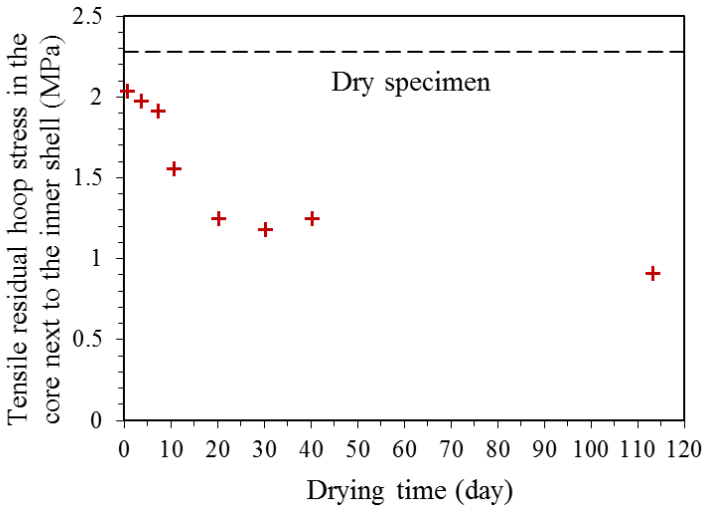

Fig. 4.11 Tensile residual hoop stress in the core region adjacent to the inner shell, plotted as a function of drying time

4.6.3 FE simulation results

The refined one-slit-ring method was verified by comparing results for the residual hoop stress distribution with the prediction from the FE simulation. This is to use the approach described in section 4.5.2 and Fig. 4.7, firstly by applying a temperature gradient field, governed by Eq. (4.33), to a FE model of slit ring so that the FE model can mimic ΔD values measured experimentally. The simulation suggests that with N values equal to 2.21, 2.50, 1.75, 1.33 and 0.95, the ΔD values are equivalent to those for dry, W0.5, W10.5, W40 and W113 specimens, respectively. With those N values, the temperature gradient field is then applied to the FE model of full ring to determine the residual hoop stress distribution.

Figure 4.12 presents an example of the residual hoop stress distribution generated in the full ring model of W0.5 specimen using the temperature gradient field. Figure 4.12(a) gives an overall view of the residual hoop stress distribution, showing the residual stress level in the shell region to be much lower than that in the core region. Figure 4.12(b)

presents the residual stress distribution in the shell region, and Fig. 4.12(c) in the core region. The figure suggests that for W0.5 specimen, residual stress in the shell region is about one hundredth of that in the core region. The difference reduces with the increase of drying time.

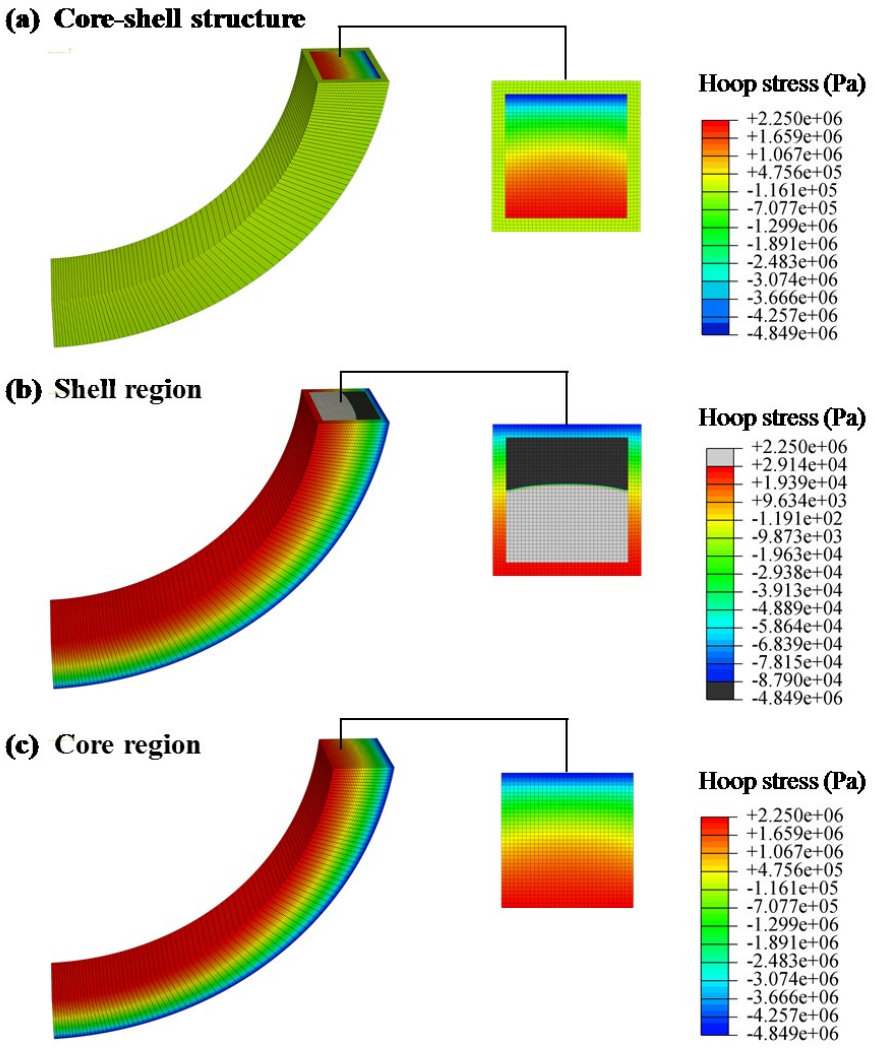

Fig. 4.12 Residual hoop stress distribution in the FE model of W0.5 full-ring specimen, generated by a temperature gradient field: (a) the overview of the whole model, (b) shell region and (c) core region

Figure 4.13 compares residual hoop stress from analytical solution and that from FE simulation, along paths A and B on the cross section as indicated by the insert in each plot.

The comparison shows excellent agreement between the two sets of results, thus supporting validity of the refined one-slit-ring method for predicting the residual hoop stress distribution on ring specimens with core-shell structure on the cross section.

Figure 4.14 presents examples for the residual hoop stress distribution along the center line of the cross section (path B in Fig. 4.13(b)), for dry, W10.5, W40 and W113 specimens, showing good agreement between analytical and simulation results. Therefore, the refined one-slit-ring method can be used to determine the residual hoop stress distribution for the wet ring specimens.

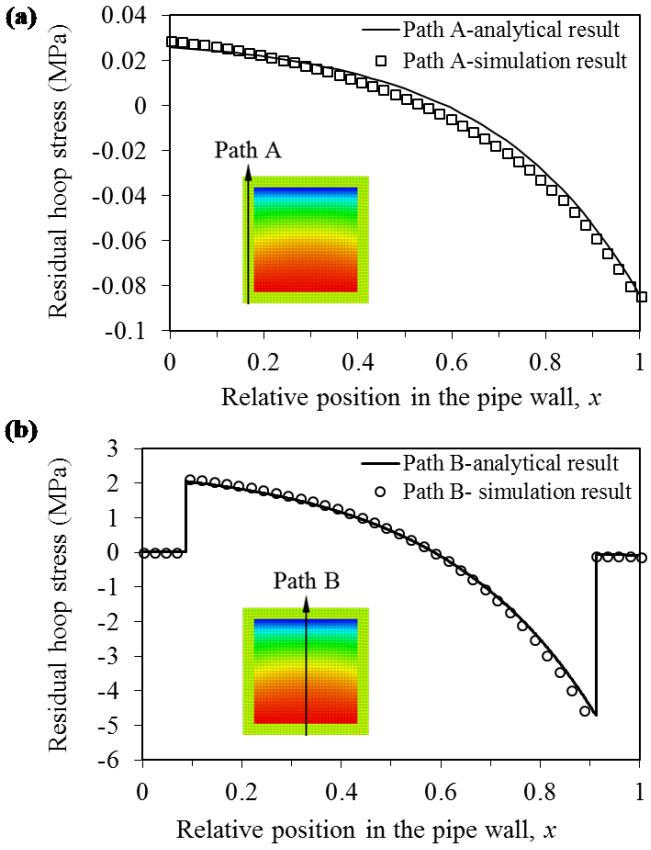

Fig. 4.13 Comparison of residual hoop stress in W0.5 specimen between analytical solution and FE simulation, plotted along (a) path A and (b) path B, as indicated by the insert in each figure (Note that the inserts are same as the cross-sectional view of Fig. 4.12(a))

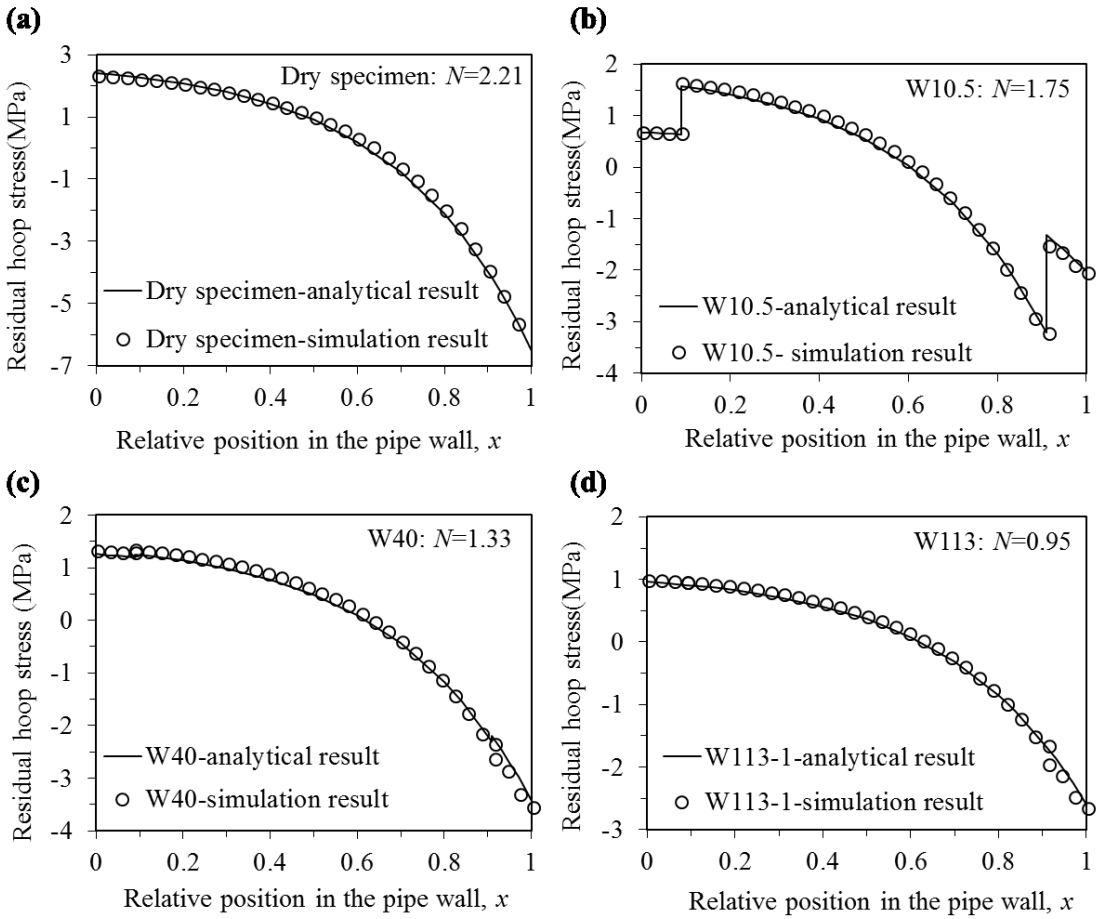

Fig. 4.14 Comparison of simulation results with the analytical results for (a) dry specimen, (b) W10.5, (c) W40 and (d) W133

4.7 Conclusions

A refined one-slit-ring method using single ring specimen is proposed to determine residual hoop stress distribution of CPVC pipe after being exposed to primer to cause the formation of a core-shell structure on the cross section. By measuring the outer diameter changes of ring specimens after the slitting and determining the elastic modulus in the shell region through FE simulation, the variation of the residual hoop stress distribution in the wet ring specimens as a function of drying time was established.

The refined one-slit-ring method provides a simple and expedient approach to

determine the residual hoop stress distribution in CPVC pipe that may have inhomogeneous mechanical properties due to exposure to aggressive agents, such as the core-shell structure on the cross section due to immersion in primer. The refined method made it possible to quickly estimate the distribution of residual stress in pipe ring specimens with a core-shell structure on the cross section, without having to carry out a complex experiment or favor of the less realistic linear distribution. The principle of the approach presented in this chapter may also be applied to the evaluation of the residual stress distribution in pipes that consist of multiple materials, but further study in this area needs to be conducted to confirm such a possibility.

Chapter 5: Characterization of mechanical properties and residual stress of CPVC pipes

This chapter deals with mechanical properties and residual stress of chlorinated polyvinyl chloride (CPVC) pipes of different nominal pipe size (NPS). Commercial CPVC pipes with three NPSs of 1.25-, 2- and 4-inch, and from two different manufacturers were selected for the investigation, Mechanical properties of those pipes were characterized through D-split tensile test on ring specimens, and specially, Young's modulus was determined with the assistance of finite element method by simulating their elastic deformation under tensile loading. Results show that for new CPVC pipes, tensile strength and Young's modulus are independent of NPS and manufacturer, but after long-time use, strength and ductility change in various ways. Residual stress in the hoop direction was characterized using the one-slit-ring method and results show that residual hoop stress is different among pipes of different sizes, with NPS of 2-inch having the lowest level of residual stress. Pipes from the two manufacturers show consistently different residual stress levels for all NPS, which is believed to be caused by different cooling rates used in the manufacturing process. The study concludes that in addition to strength, residual stress and ductility should be considered for evaluation of CPVC pipes, as these values are expected to play an important role in their long-term performance.

5.1 Introduction

Chlorinated polyvinyl chloride (CPVC) is produced by post-chlorination of polyvinyl chloride (PVC), to better its temperature resistance [4, 6, 7]. CPVC pipe is now widely used in commercial and residential buildings due to its good mechanical strength, easy installation and low cost [1, 2, 6, 25]. Since these pipes are designed for a lifetime of more

than 50 years [26], small difference in their short-term test results could have a significant implication for their long-term performance.

It is well known that mechanical properties of extruded pipes are highly dependent on the manufacturing process, during which the polymer compound in powder form is first converted into a viscous plastic mass, and then extruded into the pipe-forming die, followed by a cooling process [48]. Many studies [49–51] indicated that good mechanical properties of pipes can be achieved by facilitating polymer chain entanglements during the melt processing and increasing the degree of gelation or fusion through adjusting parameters such as extrusion temperature and screw speed. Summers [52] suggested that higher processing temperature usually improved the impact strength and stress rupture levels of pipes. Moghri et al. [50] found that the elongation at break [53] of rigid PVC pipes was more sensitive to the level of fusion than its yield strength. In addition to the manufacturing parameters, PVC and CPVC pipes used for water supply are usually subjected to a constant hoop stress, hence the service time may also affect the mechanical properties. Rabinovitch et al. [13] found that elastic modulus and tensile strength increased while elongation at break decreased after physical aging at elevated temperature below the glass transition temperature. Study [54] investigated the change in mechanical performance of pressurized PVC pipe with time, by testing the strip sample prepared by longitudinal cutting of rigid PVC pipes which had been subjected to the burst testing for 10 years, and found that the elastic modulus was unaltered, however, the tensile strength increased compared with that of new pipes, which was demonstrated as a result of preferential orientation of the polymer molecules in the stress field.

Since mechanical properties of extruded pipes are highly dependent on the

manufacturing process and may change with the service time, to ensure the full compliance with the applicable product standard, quality control testing is mandatory [48]. Extruded PVC or CPVC pipes are usually certificated using pressurized pipe tests, to determine the short-term strength [56], as well as the long-term hydrostatic strength through standard tests [57–59], among which the hydrostatic design basis (HDB) refers to the estimated long-term strength in the circumferential direction [48]. Note that above standards mainly focus on the assessment of strength-based properties, though some standards with strain-based criteria have been established for steel pipelines to prevent rupture and buckling [60–62], limited attention has been put on the evaluation of material ductility of extruded PVC or CPVC pipes.

In addition to mechanical properties, it is well-known that residual stress originating from the non-uniform cooling process during manufacturing [19, 86, 119, 120], may also play an important role in the possible length of service life for plastic pipes. Many studies have been conducted to characterize the residual stress in extruded pipes [19] and investigate the effect of the residual stress on their fracture behavior [20–22] as well as lifetime [19]. Davis et al. [23] included through-wall residual hoop stress with the value of 3 MPa acting on the pipe inner surface into the physical probabilistic model to predict the failure rate in PVC pipeline, and Yu [24] showed that an increase of maximum residual stress from 3 MPa to 6 MPa caused a significant increase of failure rate of PVC pipes. Though fracture analyses on PVC or CPVC pipes [10, 35] indicate that residual stress caused by uneven cooling rate can contribute to premature failure, not much study has been conducted to systematically quantify the residual hoop stress distribution in PVC or CPVC pipes.

In view of the need to study the mechanical behavior especially the material ductility of commercial CPVC pipes and to characterize the residual hoop stress in those extruded pipes, this chapter is comprised of two parts: (1) compare the mechanical properties of commercial CPVC pipes with different nominal pipe size (NPS), from two manufacturers in pristine and used conditions; (2) characterize the residual hoop stress distribution of the above pipes using the slit-one-ring method [19, 88], which is validated by our previous work [121], in order to study the relationship between the residual stress in CPVC pipes with NPS.

5.2 Materials and test methods

Materials used in this study are commercial CPVC 4120 Schedule 80 pipes from two different manufacturers, denoted as manufacturers A and B, with three different NPSs: 1.25-inch (32-mm), 2-inch (50-mm) and 4-inch (100-mm). For pipes with NPS of 1.25-inch from manufacturer A, both new and used pipes were examined. The dimensions in Table 5.1 were measured along the circumference to obtain an average value.

Table 5.1 Dimensions of pipes

Manufacturers	NPS (inch)	Outer diameter (mm)	Wall thickness (mm)	Conditions
A	1.25	42.2	5.3	New and used
	2	60.4	6.1	New
	4	114.6	9.1	New
B	1.25	42.3	5.2	New
	2	60.4	5.7	New
	4	114.2	9.0	New

Table 5.1 shows pipes with NPS of 1.25-inch and 4-inch have quite consistent dimensions between the two manufacturers. However, for 2-inch pipes, those from manufacturer A have a thicker wall than those from manufacturer B. Overall, both outer diameter and wall thickness of pipes tested meet the standard specification of CPVC Schedule 80 pipes [122].

Ring specimens were prepared from those pipes, and their denotation includes pipe condition, NPS and manufacturer, such as 'new-1.25-A' stands for the ring specimens from a new pipe with NPS of 1.25-inch, produced by manufacturer A. Note that cross section of the ring specimens has aspect ratio close to unity, i.e., wall thickness (t_o) being close to the specimen width (w_o), as shown in Fig. 5.11(a), to ensure that cross section contraction is similar in width and thickness directions during the necking process [123]. The similar values between w_o and t_o also minimize the possible effect of axial residual stress on the measured hoop residual stress value, as suggested in ref. [87].

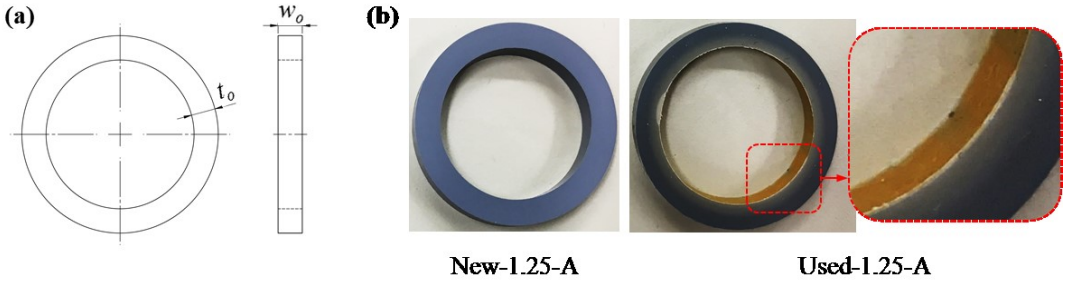

Fig. 5.1 Diagram of the ring specimen design and (b) pictures of new-1.25-A and used-1.25-A

It should also be noted that the exact service time and condition for the used pipes with NPS of 1.25-inch is unknown, but it is believed that the used pipe from manufacturer A as

shown in the right picture of Fig. 5.1(b) has been in service for a long time as it appears to be discolored on the inner surface, compared with that of the pristine counterpart as shown on the left.

D-split tensile tests [64] were conducted using a Qualitest Quasar 100 universal test machine at a crosshead speed of 1mm/min. Figure 5.2(a) shows the test set-up which includes two home-made, strain-gauge-based extensometers to measure thickness and width contraction during the test.

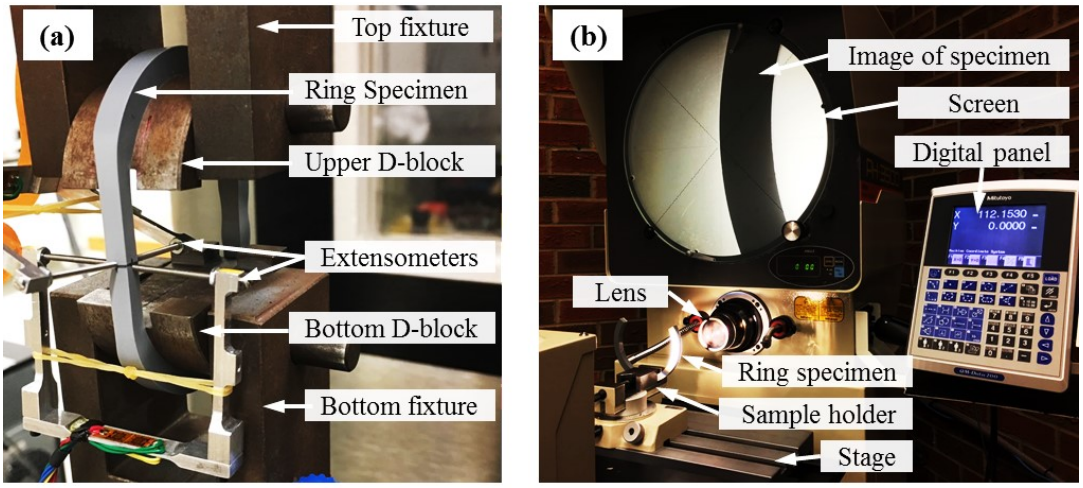

Fig. 5.2 Experimental set-up for (a) the D-split tensile test and (b) Optical Comparator

In addition to the measurement of width (w) and thickness (t), load (F) and stroke (S) were also recorded as functions of time. At least three tests were carried out for each type of specimens to ensure the data repeatability.

Results from the D-split tensile tests were used to calculate engineering stress (σ_{eng}), true stress (σ_{true}) and area strain (ε_{area}) based on Eqs. (5.1) to (5.3) below.

$$\sigma_{\text{eng}} = \frac{F}{2 \cdot w_{\text{o}} \cdot t_{\text{o}}} \tag{5.1}$$

$$\sigma_{\text{true}} = \frac{F}{2 \cdot w \cdot t} \tag{5.2}$$

$$\varepsilon_{\text{area}} = \ln\left(\frac{w_{\text{o}} \cdot t_{\text{o}}}{w \cdot t}\right) \tag{5.3}$$

where w_{o} and t_{o} are the original width and wall thickness, respectively, of the specimen. Maximum measured area strain was calculated using Eq. (5.4):

$$\varepsilon_{\text{m}} = \ln\left(\frac{w_{\text{o}} \cdot t_{\text{o}}}{w_{\text{f}} \cdot t_{\text{f}}}\right) \tag{5.4}$$

where w_{f} and t_{f} represent the last measurement of specimen width and wall thickness by extensometers before the drastic load drop due to the fracture initiation.

The one-slit-ring method proposed by Poduška et al. [19] was used to characterize residual hoop stress distribution in this study, with the applicability of this method to CPVC pipes being verified by our previous work [121]. The method involves the measurement of diametrical change of the ring specimens after the slitting in the longitudinal direction. The diametrical change is due to the release of the residual hoop stress and thus, is used to determine the residual hoop stress in the specimen before slitting. Two of the key parts in the method are the consistent slitting location and an accurate measurement of the resulted diametrical change. In this work, the slitting process was accomplished with the assistance of a specially-designed, 3D-printed device [121] to ensure consistency and accuracy of the slit position. The diametrical change, based on change of the outer diameter, was measured using a MITUYOTO PH-3500 Optical Comparator which provides non-contact measurement with one-micron resolution, as shown in Fig. 5.2(b).

As shown in work [19], the analytical expression of the residual stress distribution was derived based on the curved beam theory, under the assumption that the diametrical change of a ring specimen can be regarded as the result of a bending moment acting on the ring. The residual hoop stress distribution is assumed to follow an exponential function, as shown in Eq. (5.5) below, on the cross section in the wall thickness direction, which also applies to CPVC pipes as verified in our previous work [121].

$$\sigma_{\text{res}} = C_1 + C_2 e^{3.2x} \tag{5.5}$$

where σ_{res} is the residual hoop stress, x the relative position along the wall thickness of the ring specimen, with x quals to 0 and 1 on the inner and outer surfaces, respectively. Two coefficients C_1 and C_2 can be determined by two equilibrium conditions. The first is the self-balance of the residual stress on the cross section [86, 117], as indicated by Eq. (5.6):

$$\int_0^1 (C_1 + C_2 e^{3.2x}) t_{\text{o}} w_{\text{o}} dx = 0 \tag{5.6}$$

Secondly, integrating the residual stress distribution as shown in Eq. (5.5) over the pipe wall thickness gives a bending moment, which is assumed to be equal to the value of pure bending moment M generating the same outer diameter change ΔD as measured [19, 66, 70], and thus can be expressed mathematically as Eq. (5.7):

$$M = \int_0^1 (C_1 + C_2 e^{3.2x})(x_{\text{n}} - x) t_{\text{o}}^2 w_{\text{o}} dx \tag{5.7}$$

where x_{n} is the neutral position of the residual hoop stress in the relative coordinate system and can be derived by:

$$C_1 + C_2 e^{3.2 x_n} = 0 \tag{5.8}$$

For a given diametrical deformation, the bending moment M can be expressed in terms of the radii of neutral surface before (R) and after (R_d) deformation [116]:

$$M = \frac{(R - R_d)(D_o - t_o - 2R) E t_o w_o}{2R_d} \tag{5.9}$$

where D_o is the original outer diameter of the ring specimen before slitting, E the Young's modulus, and R and R_d are dimensions related with the original geometry and the diametrical change ΔD, which are given as below [116]:

$$\begin{aligned} R &= \frac{t_o}{\ln(\frac{D_o}{D_o - 2t_o})} \\ R_d &= \frac{t_o}{\ln(\frac{D_o + \Delta D}{D_o + \Delta D - 2t_o})} \end{aligned} \tag{5.10}$$

From Eqs. (5.6) to (5.9), we have [121]:

$$\begin{aligned} C_1 &= \frac{1 - e^{3.2}}{3.2} C_2 \approx -7.354 C_2 \\ C_2 &= \frac{-(D_o - t_o - 2R)(R - R_d) E}{3.383 t_o R_d} \end{aligned} \tag{5.11}$$

Once R_d is determined by the measured ΔD through Eq. (5.10), the value of C_1 and C_2 can be obtained by Eq. (5.11), and the estimation of the residual hoop stress can be eventually achieved by substituting the two coefficients into Eq. (5.5).

Finite element (FE) simulation was conducted to determine the Young's modulus E along the hoop direction of pipes, by regenerating the initially linear elastic deformation of specimens. The FE simulation was achieved using ABAQUS Standard (version 6.13-4).

Taking advantage of symmetry, as shown in Fig. 5.3, the FE model consists of one-eighth of the ring specimen and one-quarter of the upper D-block which is modelled as an analytical rigid body. The model was composed of over 24,000 C3D8R elements (8-node standard 3D element) with the mesh pattern shown in Fig. 5.3. In addition, as shown in Fig. 5.3, boundary conditions were set on three planes of symmetry, and displacement control was applied to the reference point (RP) of the rigid D-block.

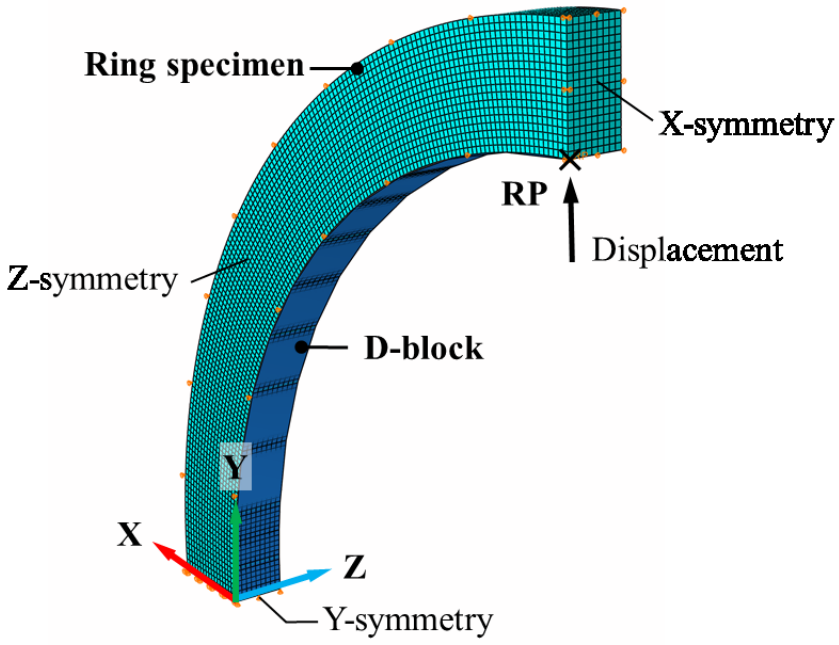

Fig. 5.3 FE model with mesh pattern and boundary conditions

5.3 Results and discussion

5.3.1 Mechanical properties

Engineering stress-stroke curves from the D-split tensile tests, for all CPVC pipes considered in the study, are summarized in Fig. 5.4. The figure shows clearly that all new CPVC pipes have almost the same strength in the hoop direction, of around 44 MPa which is independent of NPS or manufacturer. However, stroke at fracture can be quite different

among specimens of different NPS or manufacturer. Figure 5.4(c) also shows that for specimens of used-1.25-A, the strength is much lower than their pristine counterparts, and the former fractured before reaching the yield point while the latter after.

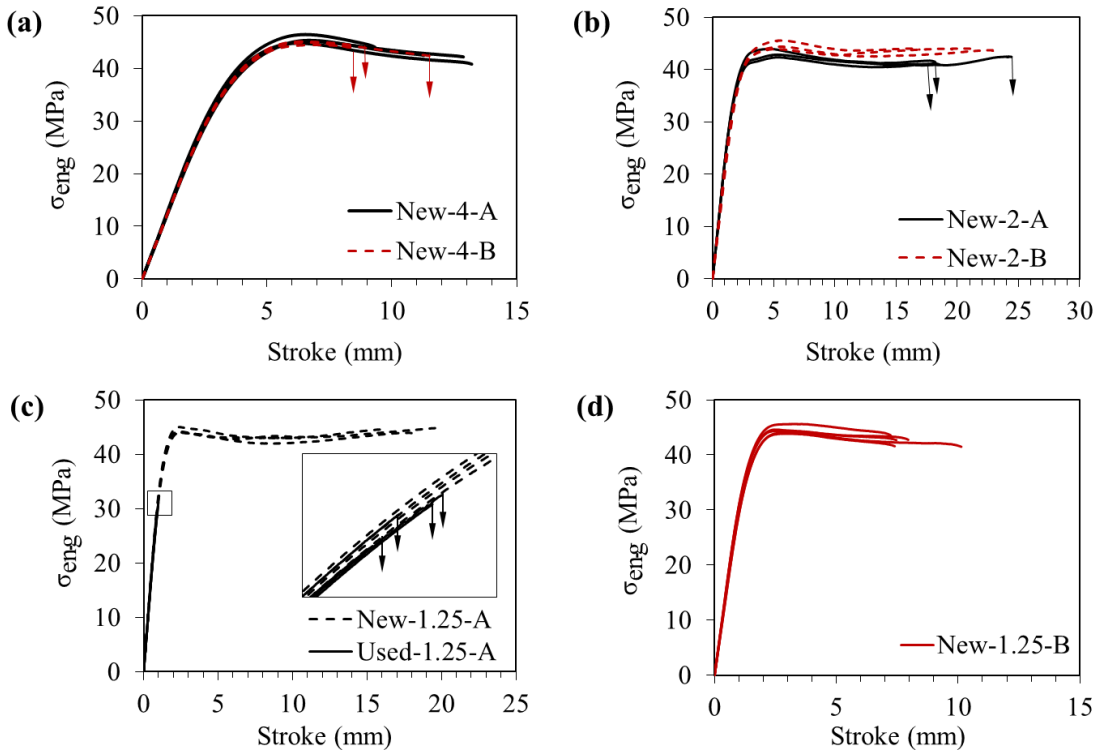

Fig. 5.4 Engineering stress stroke curves for ring specimens from: (a) 4-inch new pipes, (b) 2-inch new pipes, (c) new and used 1.25-inch pipes from manufacturer A and (d) 1.25-inch pipes from manufacturer B

Maximum measured area strain from the study is summarized in Fig. 5.5. The figure shows that the maximum measured area strain varies with NPS and manufacturer, but there is no clear trend of dependence on the NPS or manufacturer. The figure also shows that the maximum measured area strain for the used-1.25-A specimens, with a value smaller than 0.02, is much lower than that for the pristine counterpart, of more than 0.5. Such a difference indicates a degradation of ductility for CPVC pipes during service, which needs further study to provide quantitative information.

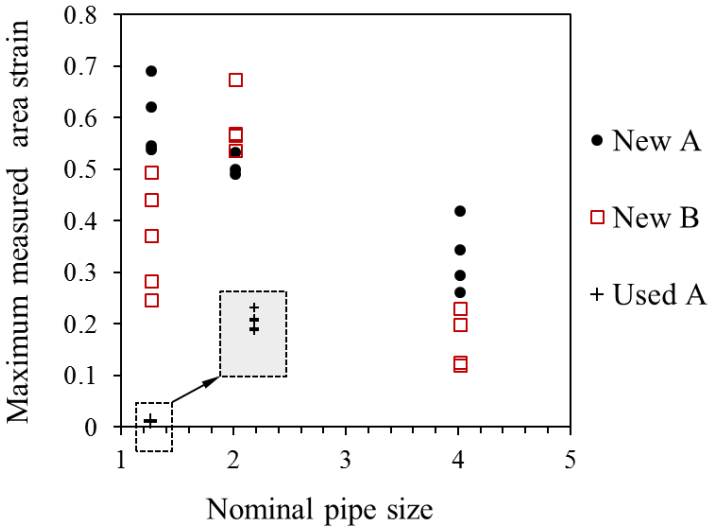

Fig. 5.5 Maximum measured area strain versus NPS

Different from the consistent material strength among various pristine CPVC pipes, the maximum measured area strain, indicating the material ductility, is quite scattering among tested CPVC pipes. One reason of the varying quality among pipes in terms of ductility may be the lack of specific requirement of ductility in the existing standard specifications. Since material ductility plays an important role in the long-term performance of plastic pipes, it is suggested that strain-based evaluation should also be taken into account in the specification.

Figure 5.6 presents the curve of New-4-A from FE simulation compared to the experimentally determined σ_{eng} - stroke curve. The curve from the FE simulation shown in the Fig. 5.6 is based on elastic modulus of 2,100 MPa, and the simulation results show that by using elastic modulus of 2,100 MPa, experiment curves for all types of specimens tested can be well fitted, thus suggesting that the elastic modulus in the hoop direction is independent of manufacturer, NPS or service time.

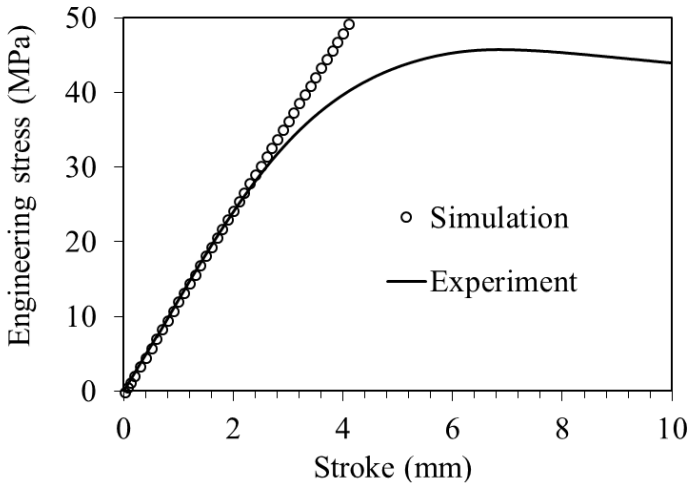

Fig. 5.6 Comparison of experimentally measured data (solid line) and result from FE simulation (circular symbols) of New-4-A

Note that all above results from new-1.25-A and used-1.25-A indicate the hoop strength and material ductility of CPVC pipe can decrease significantly after long-time use while the elastic modulus along the circumferential direction is not changed. Similar trend of longitudinal elastic modulus change but opposite change in tensile strength of PVC pipes in terms of time were presented in study [54]. A possible difference between the longitudinal material properties and their circumferential counterparts may contribute to this discrepancy. Moreover, another reason is believed to be related with the different pipe conditions, which exhibited discoloration in our samples but no change of gloss or color was found in specimens used in ref. [54]. Further study is needed for the verification.

5.3.2 Residual hoop stress distribution

The values of original outer diameter and the diametrical change for all types of specimens after slitting are summarized in Table 5.2, where the two calculated coefficients C_1 and C_2 determined by Eq. (5.11) are also included.

Table 5.2 Outer diameter changes and coefficients

Specimens	Original outer diameter D_o (mm)	Diametrical change ΔD (mm)	Coefficients	
			C_1	C_2
New-4-A-#1	114.5650	-2.3890	3.0431	-0.4138
New-4-A-#2	114.5443	-2.4050	3.0887	-0.4200
New-4-A-#3	114.5977	-2.4333	3.1173	-0.4239
New-2-A-#1	60.3503	-0.8157	2.6437	-0.3595
New-2-A-#2	60.3403	-0.8430	2.7347	-0.3719
New-2-A-#3	60.3743	-0.8727	2.8289	-0.3847
New-1.25-A-#1	42.1897	-0.5240	3.2160	-0.4373
New-1.25-A-#2	42.2140	-0.5123	3.1115	-0.4231
New-1.25-A-#3	42.2273	-0.5110	3.0957	-0.4210
Used-1.25-A-#1	42.3327	-0.2977	1.6489	-0.2242
Used -1.25-A-#2	42.3717	-0.2938	1.6308	-0.2218
Used -1.25-A-#3	42.3073	-0.2523	1.4109	-0.1919
New-4-B-#1	114.1460	-2.3120	2.9356	-0.3992
New-4-B-#2	114.1613	-2.3740	3.0073	-0.4089
New-4-B-#3	114.1530	-2.3080	2.9520	-0.4014
New-2-B-#1	60.5373	-0.6560	1.9545	-0.2658
New-2-B-#2	60.3663	-0.6170	1.8341	-0.2494
New-2-B-#3	60.3170	-0.5847	1.7183	-0.2337
New-1.25-B-#1	42.3797	-0.4727	2.7006	-0.3672
New-1.25-B-#2	42.3603	-0.4550	2.5788	-0.3507
New-1.25-B-#3	42.3253	-0.4463	2.5648	-0.3488

The character of residual hoop stresses in extruded pipes, namely tensile on the pipe inner surface and compressive on the outer surface, forces the ring specimens to close upon release of residual stress by slitting, as indicated by the negative value of ΔD shown in Table 5.2. With similar dimension of diameter and wall thickness, specimens of

used-1.25-A have smaller magnitude of diametrical change compared with new-1.25-A. Besides, the diametrical deformation after cutting of specimens from manufacturer A is always bigger than that from manufacturer B of the same NPS.

On substituting the coefficients C_1 and C_2 listed in Table 5.2 into Eq. (5.5), the estimated residual hoop stresses were plotted along the wall thickness in the relative coordinate system, as shown in Fig. 5.7(a) and (b).

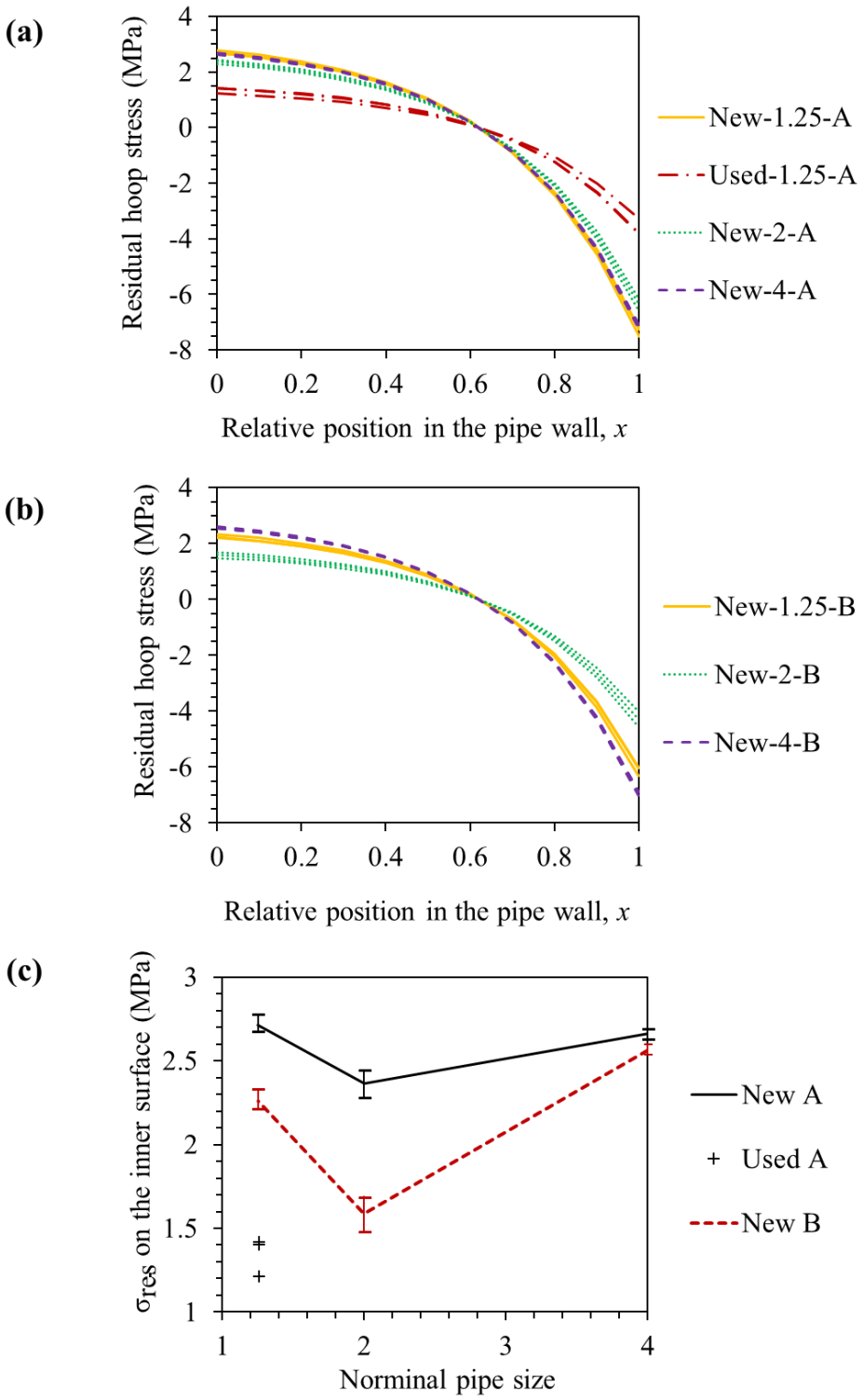

Fig. 5.7 Residual stress distribution: (a) in CPVC pipes from manufacturer A, (b) in CPVC pipes from manufacturer B, and (c) maximum tensile residual stress (on the inner surfaces) as a function of NPS.

Figure 5.7(a) shows that there are two distinguishable groups of residual stress distribution for CPVC pipes from manufacturer A, one for all new pipes with values ranging from 2.5 MPa on the inner surface to -7 MPa on the outer surface, and the other for the used pipes (from 1.4 to -3 MPa). For pipes from manufacturer B, as shown in Fig. 5.7(b), residual stresses in 2-inch pipes are clearly at a lower level than pipes of NPS as 1.25-inch and 4-inch. Although such a difference does exist among pipes from manufacturer A, the difference is smaller. This trend observed from CPVC pipes is different from that of extruded polypropylene (PP) pipes, as presented in [70], which indicates that residual hoop stress distributions in PP pipes with various dimensions (diameter and wall thickness) are very similar, with the experimental evaluated values lying within an interval of about ± 0.2 MPa around the average residual hoop stress. The difference between CPVC pipes and PP pipes suggested that residual stress distribution in CPVC pipes is more complex.

For further study, the tensile residual stresses on the inner surfaces of CPVC pipes are plotted as a function of NPS in Fig. 5.7(c). The value range including all new pipes is from 1.5 MPa to 2.8 MPa, with a V-shaped variation that shows the lowest tensile residual stress in 2-inch pipes. The figure also shows that residual stress in pipes from manufacturer A is always higher than that from manufacturer B of the same NPS, with the biggest difference on 2-inch pipes. Figure 5.7(c) also shows that the tensile residual stress decreases in the used pipes, to a value around 1.3 MPa for the used-1.25-A with the new pipe counterpart about double of the value.

5.4 Conclusions

Mechanical properties and residual hoop stress distributions have been characterized

for CPVC pipes of different sizes (with NPS from 1.25-inch to 4-inch) from two manufacturers. The results show that material strength and elastic modulus in the hoop direction are independent of the pipe size and the manufacturer, with the elastic modulus even unaffected by the service time (based on a used pipe but for an unknown length of service). On the other hand, with different NPS or manufacturer, material ductility can be very different, and it was found that the ductility can be reduced dramatically after a long service period, which indicates the necessity for developing the strain-based specification of the pipe products. The study also found that pipes from different manufacturers have different levels of residual stress, indicating that difference in the residual stress level is dependent on the manufacturing process, possibly the cooling rate. The tensile residual stresses on the inner surface of the pipes show a V-shaped dependence on the NPS, with 2-inch pipe having the lowest residual stress level. This chapter concludes that mechanical properties, especially ductility and residual stress, can vary significantly among pipes of different NPS or manufacturer. Since these properties are important for long-term performance of CPVC pipes, it is recommended to evaluate these properties carefully, not just for new pipes, but also their changes during the service.

Chapter 6: Summary and future work

This chapter summarizes the main contributions of this research work and suggests possible work for future investigation.

6.1 Summary of contributions

CPVC pipe is widely used for hot water transportation due to its good mechanical properties and easy installation. As the most popular joining method for CPVC pipes, the solvent welding process involves application of primer and solvent cement to enhance strength of the pipe joints. The application of primer is to soften the pipe surfaces for the pipe joining but has also been suspected to be responsible for the premature failure of CPVC pipes. However, the relevant mechanism is yet to be fully understood. The occasional occurrence of premature failure in CPVC pipes also indicates that there may be some blind spots when evaluating the long-term performance of CPVC pipes. Though many standard tests have been suggested for CPVC pipes, most of them are based on material strength and limited attention has been put on the material ductility and residual stresses. Therefore, this thesis focuses on the characterization of mechanical properties, especially the material ductility and residual stresses in commercial CPVC pipes, with the consideration of exposure to solvents used in the solvent welding process. The main contributions of this thesis are summarized below.

(1) Effect of primer on mechanical behavior of CPVC pipes

The change in mechanical properties of CPVC pipes due to 1-min exposure to primer was firstly evaluated by coupon specimens of different geometries, including round NPR with different notch radii, flat NPR specimens and ring specimens. The results suggest that

immersion in primer for 1 min does have an influence on the mechanical properties, with the extent of influence varying among those three types of specimens. In addition, the results indicate that the main influence is the decrease in ductility, and the extent of decrease is in a decreasing order of round NPR, flat NPR and ring specimens. For the round NPR specimens, the extent of decrease in ductility further depends on the notch radius.

Ring specimens were selected to further investigate the effect of drying time on the change in mechanical properties after the exposure to primer. Time for the primer treatment was prolonged to 30 min, and eight periods of drying time were selected. Changes in mechanical properties, cross sectional surface morphology and fracture behavior were examined, and results show that exposure to primer caused swelling of the cross section and generated a core-shell structure. Both material strength and ductility decreased after exposure to primer. Although strength can be partially recovered in the drying process, up to 63% of the virgin material, the ductility loss of at least 57% of that of the virgin material is permanent. And the fractography indicates that the significant loss in ductility may be due to the multiple sites for crack initiation along the border between the core and the shell regions.

Overall, the results suggest that the exposure to primer generates a thin shell region with low ductility, which can increase the vulnerability of the pipe to the presence of defects, especially for the long-term and load-carrying application. Therefore, it is suggested that primer should be applied carefully to CPVC pipes, to avoid unnecessary contact of primer with pipe surfaces that will not be covered by solvent cement. Besides, ductility of the pipe joints by solvent-welding is suggested to be added to the standard specifications that currently mainly concern results from strength-based tests.

(2) Proposal of a refined one-slit-ring method for residual stress evaluation

The original one-slit-ring method was first applied to measurement of residual hoop stress in extruded 2-inch CPVC pipes, from which results suggest that noticeable residual stresses exist in CPVC pipes, with tensile residual stress over 2 MPa on the pipe inner surface and compressive residual stress of 6 MPa on the pipe outer surface. Since the immersion in primer of ring specimens formed a core-shell structure with different material properties on the cross section, it is problematic to apply the original method to characterization of the residual stress. Hence, a refined one-slit-ring method has been proposed, which extends the applicability of the original one-slit-ring method to quantification of the residual hoop stress distribution in pipes with core-shell structure on the cross section.

The refined method was applied to study the effect of primer on the residual stress in CPVC pipes. After 30-min exposure to primer, ring specimens were dried for eight different lengths of time before the testing. The diametrical changes of different ring specimens after the release of residual stress were measured, and the residual hoop stress distribution was estimated based on the refined method, followed by verification using finite element (FE) modelling. The results indicate that immersion in primer relieved about half of the residual stress in CPVC pipes, with the decrease of residual hoop stress mainly occurring during the first 30 days of drying. Good agreement was observed between the analytical results and those from FE simulation, supporting validity of using the refined one-slit-ring method to evaluate the residual hoop stress in pipes with core-shell structure.

(3) Characterization of mechanical properties and residual stress in commercial CPVC pipes

Mechanical properties in extruded pipes are highly dependent on the manufacturing process and may change during the service. The thesis characterized and compared the mechanical properties and residual stress levels in different commercial CPVC pipes, including pipes from two different manufacturers. The investigation was conducted on pipes with three nominal pipe sizes (NPSs), including 1.25-, 2- and 4-inch. In particular, for 1.25-inch pipes, conditions in both pristine and used were considered. Results show that tensile strength and Young's modulus in the hoop direction are independent of NPS and manufacturer, with Young's modulus even unaffected by the service time. On the contrary, with different NPS and manufacturer, material ductility can be very different, and can be reduced dramatically after a long service period. This indicates the necessity of developing a strain-based specification of the pipe products. Results show that pipes from two manufacturers have consistently different levels of residual stress for all NPSs, which is believed to be caused by different cooling rates used in the manufacturing process. In addition, tensile residual stresses on the inner surface of the pipes show a V-shaped dependence on NPS, with 2-inch pipe having the lowest residual stress level. It concludes that in addition to the measured strength, residual stress and ductility should be considered for evaluation of CPVC pipes, as these values are expected to play an important role in their long-term performance.

6.2 Future work

Research work presented in this thesis shows that primer used in the solvent welding process affects the mechanical properties of CPVC pipes and the main effect is on ductility. Further research is needed to clarify the effect of the solvent welding process on the long-term performance of CPVC pipes, such as considering the application of solvent

cement after primer, which may or may not compensate the ductility loss caused by the application of primer. In addition, further studies can be conducted to understand reasons for the different levels of ductility loss in CPVC pipe with different specimen geometries.

When evaluating the mechanical properties in the shell region that is caused by diffusion of primer, the mechanical properties in the shell region is assumed to be uniform. A detailed analysis should be conducted to verify this assumption and examine possible improvement in the prediction by considering the gradual change of material properties in the shell region, in order to obtain better quantitative results. Further study may also consider the defects that exhibit along the border between the core and shell regions.

Although results in this thesis indicate that material ductility can decrease significantly after the long-term use, more study is needed to quantify the change in mechanical properties during the service. Different material ductility and residual stress level were found in CPVC pipes from different manufacturers in this thesis, and further study can be conducted to provide better correlation between manufacturing parameters and mechanical behaviors of CPVC pipes.

A study to establish a comprehensive analytical model is suggested, to estimate the mechanical behavior of CPVC pipe specimens through correlating the mechanical property change and residual stress decrease after the exposure to primer. Further study is also needed to transfer the knowledge obtained from the coupon testing to evaluation of the long-term performance of CPVC pipes in service.

Bibliography

[1] R. Jordan, "Joining of Plastics: handbook for designers and engineers," 3rd Edition, Munich: Hanser Publishers, pp. 111–112, 2010.

[2] P. A. Schweitzer, *Mechanical and corrosion-resistant properties of plastics and elastomers*. CRC Press, 2000.

[3] G. T. Dalal, "Chlorinated poly(viny1 chloride)(CPVC) engineehng thermoplastic now a viable alternative," *J. Vinyl Technol.*, vol. 7, no. 1, pp. 36–41, 1985.

[4] M. W. Allsopp and G. Vianello, "Poly(vinyl chloride)," Weinheim, Germany: Ullmann's encyclopedia of industrial chemistry, 2000.

[5] N. Merah, T. Al-Qahtani, and Z. Khan, "Effects of strain rate and temperature on tensile properties of CPVC pipe material," *Plast. Rubber Compos.*, vol. 37, no. 8, pp. 353–358, 2008.

[6] J. Mora-Rodríguez, X. Delgado-Galván, H. M. Ramos, and A. P. López-Jiménez, "An overview of leaks and intrusion for different pipe materials and failures," *Urban Water J.*, vol. 11, no. 1, pp. 1–10, 2014.

[7] N. Merah, M. Irfan-ul-Haq, and Z. Khan, "Temperature and weld-line effects on mechanical properties of CPVC," *J. Mater. Process. Technol.*, vol. 142, no. 1, pp. 247–255, Nov. 2003.

[8] S. Folkman, "Water main break rates in the USA and Canada: A comprehensive study," 2018.

[9] H. F. Mark, N. M. Bikales, C. G. Overberger, and G. Menges, *Encyclopedia of polymer science and engineering*, Second ed. 1985.

[10] D. Priddy, "Why do PVC & CPVC pipes occasionally fail?," pp. 1–16, 2012.

[11] D. C. Wright, *Environmental stress cracking of plastics*. iSmithers Rapra Publishing, 1996.

[12] Lubrizol, "Other compatibility topics," *FG/BM/CZ System Compatible Program*, 2017. [Online]. Available: https://www.lubrizol.com/CPVC/FBC-System-Compatible-Program/Other-Compatibility-Topics#Acetone. [Accessed: 10-Jan-2018].

[13] E. B. Rabinovitch and J. W. Summers, "The effect of physical aging on properties

of rigid polyvinyl chloride," vol. 14, no. 3, 1992.

[14] L. Laiarinandrasana, E. Gaudichet, S. Oberti, and C. Devilliers, "Effects of aging on the creep behaviour and residual lifetime assessment of polyvinyl chloride (PVC) pipes," *Int. J. Press. Vessel. Pip.*, vol. 88, no. 2–3, pp. 99–108, 2011.

[15] P. J. Withers and H. K. D. H. Bhadeshia, "Residual stress. Part 1 – measurement techniques," *Mater. Sci. Technol.*, vol. 17, no. 4, pp. 355–365, 2001.

[16] A. Guevara-Morales and U. Figueroa-López, "Residual stresses in injection molded products," *J. Mater. Sci.*, vol. 49, no. 13, pp. 4399–4415, 2014.

[17] M. Perl and R. Arone, "An axisymmetric stress release method for measuring the autofrettage level in thick-walled cylinders – Part I: Basic concept and numerical simulation," *J. Press. Vessel Technol.*, vol. 116, no. 4, pp. 384–388, 1994.

[18] A. J. Whittle, R. P. Burford, and M. J. Hoffman, "Influence of residual stress on the relationship between pipe pressure and C-Ring tests," *Polym. Eng. Sci.*, vol. 40, no. 11, pp. 2311–2316, 2000.

[19] J. Poduška, P. Hutař, J. Kučera, J. S. Andreas Frank, G. Pinter, and L. Náhlík, "Residual stress in polyethylene pipes," *Polym. Test.*, vol. 54, pp. 288–295, 2016.

[20] P. Hutař, M. Ševčík, A. Frank, L. Náhlík, J. Kučera, and G. Pinter, "The effect of residual stress on polymer pipe lifetime," *Eng. Fract. Mech.*, vol. 108, pp. 98–108, 2013.

[21] R. K. Krishnaswamy, "Influence of wall thickness on the creep rupture performance of polyethylene pipe," *Polym. Eng. Sci.*, vol. 47, no. 4, pp. 516–521, 2007.

[22] K. Chaoui, A. Chudnovsky, and A. Moet, "Effect of residual stress on crack propagation in MDPE pipes," *J. Mater. Sci.*, vol. 22, no. 11, pp. 3873–3879, 1987.

[23] P. Davis, S. Burn, M. Moglia, and S. Gould, "A physical probabilistic model to predict failure rates in buried PVC pipelines," *Reliab. Eng. Syst. Saf.*, vol. 92, no. 9, pp. 1258–1266, 2007.

[24] Shao Yu, Tuqiao Zhang, and T. Yu, "Probabilistic model to predict longitudinal fracture of buried PVC pipes," *Eng. Mech.*, vol. 27, no. 5, pp. 199–204, 2010.

[25] D. S. Forsyth and B. Jay, "Organotin leachates in drinking water from chlorinated poly (vinyl chloride) (CPVC) pipe," *Appl. Organomet. Chem.*, vol. 11, no. 7, pp. 551–558, 1997.

[26] S. Burn, P. Davis, and T. Schiller, *Long-term performance prediction for PVC pipes*. AWWA Research Foundation, 2005.

[27] L. S. Burn, "Effect of installation damage on the lifetime of upvc pipes subjected to cyclic pressures," *Polym. Int.*, vol. 26, no. 3, pp. 147–150, 1991.

[28] Lubrizol, "Incompatible products," *FGG/BM/CZ System Compatible Program*. [Online]. Available: https://www.lubrizol.com/CPVC/FBC-System-Compatible-Program/Incompatible-Products. [Accessed: 01-Mar-2018].

[29] M. L. Knight, "Failure analysis of PVC and CPVC piping materials," *CORROSION 2003*, no. NACE-03606. NACE International, San Diego, California, 2003.

[30] N. Merah, "Natural weathering effects on some properties of CPVC pipe material," *J. Mater. Process. Technol.*, vol. 191, no. 1–3, pp. 198–201, Aug. 2007.

[31] N. Merah, A. Bazoune, and Z. Khan, "Artificial and natural weathering of chlorinated polyvinyl chloride (CPVC)," *Adv. Mater. Res.*, vol. 652, pp. 1277–1282, 2013.

[32] R. L. Hauser, "Environmental stress sracking of sommercial CPVC pipes," *J. ASTM Int.*, vol. 8, no. 7, pp. 1–7, 2011.

[33] S. J. F. Gould, P. Davis, D. J. Beale, and D. R. Marlow, "Failure analysis of a PVC sewer pipeline by fractography and materials characterization," *Eng. Fail. Anal.*, vol. 34, pp. 41–50, 2013.

[34] E. Kuliczkowska and A. Zwierzchowska, "A qualitative analysis of early defects present in PVC-U sewers but not observed in rigid pipes," *Tunn. Undergr. Sp. Technol.*, vol. 56, pp. 202–210, 2016.

[35] M. D. Hayes, M. L. Hanks, F. E. Hagan, D. Edwards, and D. Duvall, "Challenges in investigating chlorinated polyvinyl chloride pipe failures," vol. 8, no. 1, pp. 252–268, 2011.

[36] J. Hunt, "Joining Thermoplastic Pipe," *Chem. Eng.*, vol. 97, no. 2, pp. 110–114, 1990.

[37] S. Rahman and R. K. Watkins, "Longitudinal mechanics of buried thermoplastic pipe: Analysis of PVC pipes of various joint types," *Pipelines 2005: Optimizing Pipeline Design, Operations, and Maintenance in Today's Economy*. pp. 1101–1116, 2005.

[38] P. Barber and J. R. Atkinson, “The use of tensile tests to determine the optimum conditions for butt fusion welding certain grades of polyethylene, polybutene-1 and polypropylene pipes,” *J. Mater. Sci.*, vol. 9, no. 9, pp. 1456–1466, 1974.

[39] “ASTM F2620 standard practice for heat fusion joining of polyethylene pipe and fittings.” ASTM International, West Conshohocken, PA, 2013.

[40] “ASTM F656-15 standard specification for primers for use in solvent cement joints of poly (vinyl chloride) (PVC) plastic pipe and fittings.” ASTM International, West Conshohocken, PA, 2015.

[41] “ASTM F493-14 standard specification for solvent cements for chlorinated poly(vinyl chloride) (CPVC) plastic pipe and fittings.” ASTM International, West Conshohocken, PA, 2014.

[42] V. K. Stokes, “Joining methods for plastics and plastic composites: an overview,” *Polym. Eng. Sci.*, vol. 29, no. 19, pp. 1310–1324, Oct. 1989.

[43] M. J. Troughton, “Solvent welding,” in *Handbook of plastics joining: a practical guide (2nd Ed)*, M. J. Troughton, Ed. William Andrew, pp. 139–143, 2008.

[44] “ASTM D2564-12 standard specification for solvent cements for chlorinated poly (vinyl chloride).” ASTM International, West Conshohocken, PA, 2012.

[45] C. Y. Yue, “Influence of the bonding solvent on the structure and strength of solvent welded joints,” *J. Adhes.*, vol. 20, no. 2, pp. 99–116, 1986.

[46] W. V. Titow, *Adhesion-2*. London: Applied Science Publishers, 1978.

[47] W. V. Titow, M. Braden, B. R. Currell, and R. J. Loneragan, “Diffusion and some structural effects of two chlorinated hydrocarbon solvents in bisphenol A polycarbonate,” *J. Appl. Polym. Sci.*, vol. 18, no. 3, pp. 867–886, 1974.

[48] U.-B. P. P. Association, *Handbook of PVC pipe design and construction (5th edition)*. Industrial Press., 2013.

[49] W. V. Titow, *PVC technology (forth edition)*. 1986.

[50] M. Moghri, H. Garmabi, and M. Akbarian, “Effect of processing parameters on fusion and mechanical properties of a twin-screw extruded rigid PVC pipe,” *J. Vinyl Addit. Technol.*, vol. 9, no. 2, pp. 81–89, 2003.

[51] H. A. Visser, T. A. P. Engels, L. E. Govaert, and T. C. Bor, “A new engineering approach to predict the hydrostatic strength of uPVC pipes,” pp. 1–10, 2007.

[52] J. W. Summers, E. B. Rabinovitch, and P. C. Booth, “Measurement of PVC fusion (gelation),” *J. Vinyl Technol.*, vol. 8, no. 1, pp. 2–6, 1986.

[53] “ISO 6259-2.” International Standard, 1997.

[54] H. Jr and R. T., “Changes in strength of pressurized PVC pipe with time,” *Am. Water Work. Assoc.*, vol. 73, no. 7, pp. 384–386, 1981.

[55] AASHTO, “Standard specifications for highway bridges: section 18 soil-thermoplastic pipe interation systems.” American Association of State Highway and Transportation Officials, Washington, D. C., 2000.

[56] “ASTM D1599-14e1 standard test method for resistance to short-time hydraulic pressure of plastic pipe, tubing, and fittings.” ASTM International, West Conshohocken, PA, 2014.

[57] “ASTM D1598-15a standard test method for time-to-failure of plastic pipe under constant internal pressure.” ASTM International, West Conshohocken, PA, 2015.

[58] “ASTM D2837-13e1 standard test method for obtaining hydrostatic design basis for thermoplastic pipe materials or pressure design basis for thermoplastic pipe products.” ASTM International, West Conshohocken, PA, 2013.

[59] “EN ISO 9080 Plastics piping and ducting systems-determination of the long-term hydrostatic strength of thermoplastics materials in pipe form by extrapolation.” 2003.

[60] A. S. Dinovitzer and R. J. Smith, “Strain-based pipeline design criteria review,” *2nd International Pipeline Conference*, vol. 2. American Society of Mechanical Engineers., pp. 763–770, 1998.

[61] B. Ma and J. Shuai, “Influence of plastic deformation capacity on failure behavior of pipelines,” *J. Fail. Anal. Prev.*, vol. 18, no. 3, pp. 508–518, 2018.

[62] A. Liessem, G. Knauf, and S. Zimmermann, “Strain based design - What the contribution of a pipe manufacturer can do,” in *The Seventeenth International Offshore and Polar Engineering Conference*, no. 3, pp. 3156–3163, 2007.

[63] L. Laiarinandrasana, C. Devilliers, S. Oberti, E. Gaudichet, B. Fayolle, and J. M. Lucatelli, “Ring tests on high density polyethylene: Full investigation assisted by finite element modeling,” *Int. J. Press. Vessel. Pip.*, vol. 88, no. 1, pp. 1–10, 2011.

[64] “ASTM D2290-16 standard test method for apparent hoop tensile strength of plastic or reinforced plastic pipe.” ASTM International, West Conshohocken, PA, 2016.

[65] N. S. Rossini, M. Dassisti, K. Y. Benyounis, and A. G. Olabi, "Methods of measuring residual stresses in components," *Mater. Des.*, vol. 35, pp. 572–588, 2012.

[66] J. G. Williams, J. M. Hodgkinson, and A. Gray, "The determination of residual stresses in plastic pipe and their role in fracture," *Polym. Eng. Sci.*, vol. 21, no. 13, pp. 822–828, 1981.

[67] A. Siegmann, A. Buchman, and S. Kenig, "Residual stresses in polymers I: The effect of thermal history," *Polym. Eng. Sci.*, vol. 22, no. 1, pp. 40–47, 1982.

[68] A. Siegmann, A. Buchman, and S. Kenig, "Residual stresses in polymers. II. Their effect on mechanical behavior," *Polym. Eng. Sci.*, vol. 21, no. 15, pp. 997–1002, 1981.

[69] G. J. Sandilands and J. R. White, "Effect of injection pressure and crazing on internal stresses in injection-moulded polystyrene," *Polymer (Guildf).*, vol. 21, no. 3, pp. 338–343, 1980.

[70] J. Poduška, J. Kučera, P. Hutař, M. Ševčík, J. Křivánek, J. Sadílek and L. Náhlík, "Residual stress distribution in extruded polypropylene pipes," *Polym. Test.*, vol. 40, pp. 88–98, 2014.

[71] W. Cheng and A. Finnie, *Residual stress measurement and the slitting method*. Springer Science & Business Media, 2007.

[72] "ASTM E837-13a standard test method for determining residual stresses by the hole-drilling strain-gage method." ASTM International, West Conshohocken, PA, 2013.

[73] A. Turnbull, A. S. Maxwell, and S. Pillai, "Residual stress in polymers – evaluation of measurement techniques," *J. Mater. Sci.*, vol. 34, no. 3, pp. 451–459, 1999.

[74] "ASTM E1928-13 standard practice for estimating the approximate residual circumferential stress in straight thin-walled tubing." ASTM International, West Conshohocken, PA, 2013.

[75] F. A. Kandil, J. D. Lord, A. T. Fry, and P. V. Grant, "A review of residual stress measurement methods – A guide to technical selection," *NPL Mater. Cent.*, no. Report MATC(A)04, pp. 1–42, 2001.

[76] A. Niku-Lari, J. Lu, and J. F. Flavenot, "Measurement of residual-stress distribution by the incremental hole-drilling method," *J. Mech. Work. Technol.*, vol. 25, no. 2,

pp. 175–185, 1985.

[77] A. Magnier, B. Scholtes, and T. Niendorf, “Analysis of residual stress profiles in plastic materials using the hole drilling method – Influence factors and practical aspects,” *Polym. Test.*, vol. 59, pp. 29–37, 2017.

[78] R. G. Treuting and W. T. Read, “A mechanical determination of biaxial residual stress in sheet materials,” *J. Appl. Phys.*, vol. 22, no. 2, pp. 130–134, 1951.

[79] W. Cheng and L. Finnie, “The single slice method for measurement of axisymmetric residual stresses in solid rods or hollow cylinders in the region of plane strain,” *J. Eng. Mater. Technol.*, vol. 120, no. 2, pp. 170–176, 1998.

[80] W. Cheng, I. Finnie, and O. Vardar, “Estimation of axisymmetric residual stresses in a long cylinder,” *J. Eng. Mater. Technol.*, vol. 114, no. 2, pp. 137–140, 1992.

[81] G. V. Shimov, “Rapid method for determining the distribution of residual stresses in pipes,” *Mater. Perform. Charact.*, vol. 7, no. 4, 2018.

[82] S. Vaidyanathan and I. Finnie, “Determination of residual stresses from stress intensity factor measurements,” *J. Basic Eng.*, vol. 93, no. 2, pp. 242–246, 1971.

[83] W. Cheng and I. Finnie, “A method for measurement of axisymmetric axial residual stresses in circumferentially welded thin-walled cylinders,” *J. Eng. Mater. Technol.*, vol. 107, no. 3, pp. 181–185, 1985.

[84] W. Cheng and I. Finnie, “Measurement of residual hoop stresses in cylinders using the compliance method,” *J. Eng. Mater. Technol.*, vol. 108, no. 2, pp. 87–92, 1986.

[85] M. B. Prime, “Residual stress measurement by successive extension of a slot: The crack compliance method,” *Appl. Mech. Rev.*, vol. 52, no. 2, pp. 75–96, 1999.

[86] E. Q. Clutton and J. G. Williams, “On the measurement of residual stress in plastic pipes,” *Polym. Eng. Sci.*, vol. 35, no. 17, pp. 1381–1386, 1995.

[87] J. Poduška, J. Kučera , P. Hutař, M. Ševčík, , J. Křivánek, J. Sadílek, and L. Náhlík, “The effect of specimen size on the determination of residual stress in polymer pipe wall,” *Key Eng. Mater.*, vol. 627, pp. 141–144, 2015.

[88] J. Poduška, P. Hutař, A. Frank, , J. Kučera, , J. Sadílek, , G. Pinter, and L. Náhlík, “Numerical simulations of cracked round bar test: Effect of residual stresses and crack asymmetry,” *Eng. Fract. Mech.*, 2018.

[89] A. R. Berens, J. P. Pfau, D. E. Crum, and K. E. Carns, “Prediction of organic

chemical permeation through PVC pipe [with discussions]," *Journal (American Water Works Association)*, vol. 77. American Water Works Association, pp. 57–65.

[90] S. Rehab-Bekkouche, W. Ghabeche, M. Kaddeche, N. Kiass, and K. Chaoui, "Mechanical behaviour of machined polyethylene filaments subjected to aggressive chemical environments," *Mechanika*, vol. 77, no. 3, pp. 40–46, 2009.

[91] C. B. Lin, L.-C. Wu, and Y.-C. Chou, "Effect of solvent and cosolvent on friction welding properties between part of PMMA with PVC," *J. Mater. Sci.*, vol. 38, no. 12, pp. 2563–2570, 2003.

[92] K. S. Casteloes, G. P. Mendis, H. K. Avins, J. A. Howarter, and A. J. Whelton, "The interaction of surfactants with plastic and copper plumbing materials during decontamination," *J. Hazard. Mater.*, vol. 325, pp. 8–16, 2017.

[93] T. H. Heim and A. M. Dietrich, "Sensory aspects and water quality impacts of chlorinated and chlorminated drinking water in contact with HDPE and cPVC pipe," *Water Res.*, vol. 41, no. 4, pp. 757–764, Feb. 2007.

[94] E. A. Boettner, G. L. Bell, Z. Hollingsworth, and R. Aquino, "Organic and organotin compounds leached from PVC and CPVC pipe." 1981.

[95] B. R. Stern and G. Lagos, "Are there health risks from the migration of chemical substances from plastic pipes into drinking water?," *Hum. Ecol. Risk Assess. An Int. J.*, vol. 14, no. 4, pp. 753–779, Jul. 2008.

[96] D. G. Desrosiers and P. C. Dunnigan, "The diffusion of chloroform and carbon tetrachloride from rigid PVC pipe and rigid CPVC pipe into water," *J. Vinyl Addit. Technol.*, vol. 5, no. 4, pp. 187–191, Dec. 1983.

[97] L. Zhang and S. Liu, "Investigation of organic compounds migration from polymeric pipes into drinking water under long retention times," *Procedia Eng.*, vol. 70, pp. 1753–1761, Jan. 2014.

[98] J. A. Smith, J. Saunders, and P. G. Koehler, "Combined effects of termiticides and mechanical stress on chlorinated polyvinyl chloride (CPVC) pipe," *Pest Manag. Sci.*, vol. 64, no. 2, pp. 147–155, Feb. 2008.

[99] R. Fleischhauer, H. Dal, M. Kaliske, and K. Schneider, "A constitutive model for finite deformation of amorphous polymers," *Int. J. Mech. Sci.*, vol. 65, no. 1, pp. 48–63, Dec. 2012.

[100] A. S. Ognedal, A. H. Clausen, A. Dahlen, and O. S. Hopperstad, "Behavior of PVC and HDPE under highly triaxial stress states: An experimental and numerical study," *Mech. Mater.*, vol. 72, pp. 94–108, May 2014.

[101] Y. Zhang and P. Y. Ben Jar, "Quantitative assessment of deformation-induced damage in polyethylene pressure pipe," *Polym. Test.*, vol. 47, pp. 42–50, 2015.

[102] "ASTM D2855-15 standard practice for the two-step (primer and solvent cement) method of joining poly(vinyl chloride) (PVC) or chlorinated poly(vinyl chloride) (CPVC) pipe and piping components with tapered sockets." ASTM International, West Conshohocken, PA, 2015.

[103] "ASTM F402-05(2012) standard practice for safe handling of solvent cements, primers, and cleaners used for joining thermoplastic pipe and fittings." ASTM International, West Conshohocken, PA, 2012.

[104] L. F. Henry, "Prediction and evaluation of the susceptibilities of glassy thermoplastics to environmental stress cracking," *Polym. Eng. Sci.*, vol. 14, no. 3, pp. 167–176, 1974.

[105] "ASTM D2672-14 standard specification for joints for IPS PVC pipe using solvent cement." ASTM International, West Conshohocken, PA, 2014.

[106] C. Y. Yue and C. M. Chui, "On the structure and strength of solvent-welded joints: The intrinsic joint strength and the effect of dissolved polymer in the solvent cement," *J. Adhes.*, vol. 24, no. 2–4, pp. 155–171, 1987.

[107] C. Y. Yue and B. W. Cherry, "The differential displacements and the failure in solvent-welded lap joints," *J. Adhes.*, vol. 24, no. 2–4, pp. 127–137, 1987.

[108] B. Chen, P.-Y. Ben Jar, P. Mertiny, and R. Prybysh, "Effects of primer on mechanical behavior of CPVC pipe," *SPE, ANTEC, Tech. Paper ID211*. 2018.

[109] E. Crawford and A. J. Lesser, "Mechanics of rubber particle cavitation in toughened polyvinylchloride (PVC)," *Polymer (Guildf).*, vol. 41, no. 15, pp. 5865–5870, 2000.

[110] A. S. Ognedal, A. H. Clausen, T. Berstad, Thomas Seelig, and O. S. Hopperstad, "Void nucleation and growth in mineral-filled PVC – An experimental and numerical study," *Int. J. Solids Struct.*, vol. 51, no. 7–8, pp. 1494–1506, 2014.

[111] R. W. Hertzberg, "Fracture surface micromorphology in engineering solids," in *Fractography of Modern Engineering Materials: Composites and Metals*, ASTM

International, 1987.

[112] J. Chen and Y. Qiao, “Interaction of cleavage ridges with grain boundaries in polysilicon films,” *Appl. Phys. A Mater. Sci. Process.*, vol. 91, no. 1, pp. 127–130, 2008.

[113] W. Cheng and I. Finnie, “An overview of the crack compliance method for residual stress measurement.” In Proc. 4th Int. Conf. on Residual Stress, pp. 449–458, 1994.

[114] M. A. Seif and H. A. Kishawy, “Determining residual stresses in thin-walled ceramic/ceramic composite pipes,” *J. Am. Ceram. Soc.*, vol. 82, no. 4, pp. 977–980, 1999.

[115] B. Chen, P.-Y. Ben Jar, P. Mertiny, and R. Prybysh, “Ductility loss of CPVC pipe material due to exposure to primer.” *Journal of Pressure Vessl Technology* (under review), 2018.

[116] F. P. Beer, E. R. Johnston, and J. DeWolf, *Mechanics of materials*, Fourth edi. New York: McGraw Hill Eduacation, 2006.

[117] Z. W. Guan and J. C. Boot, “A method to predict triaxial residual stresses in plastic pipes,” *Polym. Eng. Sci.*, vol. 44, no. 10, pp. 1828–1838, 2004.

[118] P. Hutař, M. Ševčík, Z. M, L. Náhlík, and J. Kučera, “The effct of residual stresses on crack shape in polymer pipes,” *Crack Paths*, pp. 489–496, 2012.

[119] A. Kazakov, “An automated method for the measurement of residual stress in melt-extruded plastic pipes,” *Polym. Test.*, vol. 17, no. 6, pp. 443–450, 1998.

[120] M. Nie, Q. Wang, and S. Bai, “The effect of cooling mode on slow crack growth resistance of polyethylene pipe,” *J. Macromol. Sci. Part B Phys.*, vol. 49, no. 4, pp. 640–651, 2010.

[121] B. Chen, P.-Y. Ben Jar, P. Mertiny, and R. Prybysh, “A refined one slit-ring method to quantify residual hoop stress in CPVC pipe – applicatoin to specimens after immersion in primer.” (Ready for submission), 2018.

[122] “ASTM F441/F441M-15 standard specification for chlorinated poly (vinyl chloride) (CPVC) plastic pipe, schedule 40 and 80.” ASTM International, West Conshohocken,PA, 2015.

[123] S. Muhammad and P. Y. B. Jar, “Effect of aspect ratio on large deformation and necking of polyethylene,” *J. Mater. Sci.*, vol. 46, no. 4, pp. 1110–1123, 2011.